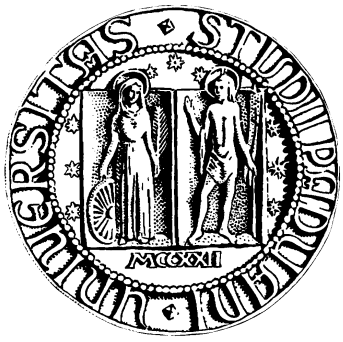

UNIVERSITÀ DEGLI STUDI DI PADOVA

Facoltà di Ingegneria

Corso di laurea in Ingegneria Chimica e dei Processi Industriali
Dipartimento di Ingegneria Industriale

Tesi di Laurea Magistrale

Rheology and wall friction in confined granular flows

Relatore

Prof. **Andrea Claudio Santomaso**

Università di Padova

Correlatore

Dott. **Riccardo Artoni**

IFSTTAR- Site de Nantes

Laureando

Alberto Soligo

Anno Accademico 2016-2017

Contents

Abstract

In this work, the first steps of an experimental campaign are moved. The rheology and the force network in the flow of a confined granular material are studied. The experimental apparatus is an annular configuration where the granular material is placed over a rotating rough surface, whereas the upper rough surface is static. In this frame, the effect of rotational velocity, load on the top surface, height of the granular material and roughness of the surfaces on the velocity profiles are studied, both solely and combined. Starting from the vertical profiles of the horizontal velocity, the width of the shear band on the granular material is calculated, and so the effect of each parameter on the shear band width is described. The velocity profiles are worked out by using a PIV (*Particle Image Velocimetry*) code on the images of the granular material while it is flowing at steady state. Successively, the effective wall friction coefficient is calculated. This coefficient is calculated as the ratio between the tangential stress and the normal stress, while the granular material is flowing. A force sensor, installed on the experimental apparatus, measures these stresses. Since the width of the shear band are known, the effect of this physical quantity on the coefficient is analyzed. In the same way, the variation of the effective wall friction coefficient over the height of the granular material is determined. In the final section, the experimental apparatus is tested in the analysis of the density-driven segregation. A segregation model is worked out and the experimental results are compared with this model.

Keywords: Granular flow; Rheology; Wall Friction; Effective Wall Friction Coefficient; Density-driven segregation; Particle Image Velocimetry

Introduction

The rheology of granular materials is relevant to many industrial applications, like grain transport and storage, or feeding of granular materials along a process chain. Also, the interpretation of some natural events, like avalanches and mudslides, concern the mechanic of the granular materials. About this topic, one of the most relevant and still unsolved problem is the interaction of the granular material with a solid boundary and its implication in the rheology of the system. In fact, such interactions are crucial to understand shear banding, that is a widespread phenomenon in slow granular flows. This problem is faced in many works by simplifying the wall friction as a constant boundary condition, disregarding its dependence on the rheology of the granular flow. Indeed, the existence of cooperative effects in the force network prevents the simple relation of the local stresses to the local shear rate. In recent works, by the use of the discrete element simulations, it is shown that at flat frictional walls the effective wall friction coefficient scales with a sliding parameter. Nevertheless, still no experimental work has been carried out in order to verify these results. In this frame, an experimental campaign is started. The experimental apparatus consists in two coaxial transparent cylinders with flat but frictional surfaces: in this annular space, some monodispersed glass spheres are poured. The bottom and the top surfaces are rough, the bottom surface can rotate while the upper surface is static: using an electric motor, the rotation of the bottom surface induce a shear stress on the granular material. The shear stress affects the glass beads differently, depending on the distance from the bottom surface. It is possible to capture this difference at the wall of the transparent experimental apparatus. In particular, the flow of the

beads at the wall is recorder with a high-speed camera. Successively, the Particle Image Velocimetry is applied to these sequence of images, in order to determine the velocity profiles of the particles. From the velocity profiles, it is possible to represent the shear bands on the granular material: in particular, it is determined the effect of some operative conditions on the width of the shear bands. The operative conditions that are varied in this thesis are the rotational velocity of the bottom surface, the load on the top surface, the height of the granular bed and the roughness of the surfaces. Once the rheology of the confined flow is characterized, the effective wall friction coefficient is calculated. To do this, a force sensor is fixed to the wall of the experimental apparatus: the operative conditions vary through the tests as well as the position of the force sensor. The values of the tangential and the normal forces are measured and it is possible to determine the effective wall friction coefficient. It is defined how the rotational velocity and the load on the granular material affect this coefficient. Most importantly, it is verified that this coefficient varies with the position of the measurement, therefore the assumption that the wall friction cannot be assumed as constant is verified. In the last part, the experimental apparatus is applied to a segregation problem: ceramic beads with a different density are distributed on the top surface of the glassy granular bed, which is sheared in the same way of the previous tests. These beads are made distinguishable by a surface treatment and the external surface of the experimental apparatus is photographed every minute, for 6 hours. The concentration profile of the ceramic beads during time is calculated and the segregation and diffusion phenomena are modelized.

In Chapter 1, the state of art is rapidly resumed; in the second chapter, the whole experimental apparatus and all the equipments used in this experimental campaign are accurately described; in the third chapter, the basic of the image analysis and its implementation are outlined; in the fourth chapter, the setting up of the acquisition system of the velocity profiles and the forces is explained; in the fifth chapter, the results concerning the effect on the velocity profiles of the operative conditions and the measurements of the boundary stress state of the granular material are illustrated; in the sixth chapter, the segregation application is fully described; in the last chapter, the conclusions and the perspectives of this thesis are reported.

CHAPTER 1

State of art

1.1 Bulk properties

The term *granular material* concerns a conglomeration of discrete solid macroscopic particles. Size and shape of these particles can vary. The constituents that compose the granular material are large enough that they are not subjected to thermal motion fluctuations. Particulate materials, powders or bulk solids are widely used in all areas of the process industries, for example in food processing, pharmaceutical, biotechnology and plastics. In many powder handling and processing operations, particle shape and size distribution play a key role in determining the bulk properties of the powder. In fact, these two aspects strongly affect the interactions between the particles, and summing up they influence the behaviour of the bulk. The population of particles can be described by a particle size distribution, which is usually displayed graphically as histograms or continuous curves. PSD may be expressed as frequency distribution curves or cumulative curves and the base of the distribution can be by number, mass, surface of volume. Which is the base of distribution chosen depends on the final use of this information, and it is possible to change the base using appropriate shape coefficients under simplifiyng conditions (i.e. constant particle shape or density). Basically, considering the PSD by mass (or volume, since they are equivalent), the

distribution classifies the particles in different size ranges according to their mass (or volume). These distributions can be measured with different techniques : sieving, settling time, laser counters,etc. . Successively, it is possible to normalize the masses over the representative size of the category and to display the relative frequency of the particles presence in that size range (frequency size distribution) or the sum of the weight in all the lower ranges (cumulative undersize distribution). Concerning the bulk properties, due to the interstitial spaces between the particles, the density of the material can be expressed in different ways, since it is represented by the intrinsic density multiplied by a solid fraction. This solid fraction varies depending on the particles arrangement in the granular solid; therefore different values can be identified: the poured density, the tap density and the compacted density.

1.2 Flow regimes and characterization

The rheology of granular materials is relevant to many industrial applications, like powder transport and storage, or feeding of granular materials along a process chain. Also the interpretation of some natural events, like avalanches and mudslides, concern the mechanic of the granular materials. Several geometries have been used to probe the rheology of granular systems, similarly to the different equipment used in all the processes where these systems are implicated. Nevertheless, the full description of 3D flows remains an open challenge. Granular materials are very sensitive to various parameters: geometry of the flow, wall roughness, flow rate, shape of the grains, granulometry and coupling with interstitial fluids. Since the forces between the particles interact with their flow, it is interesting to understand how these parameters affect the interparticle forces. [14] The behaviour of assemblies of grains can be very complex even in the simple case of dry cohesionless particles. When the grains are large enough (d > 100 μm) and the surrounding liquid is not too viscous, contact interactions dominate the particle interactions. [14] Van der Waals forces or viscous interactions can be neglected and the mechanical properties of the material are only controlled by the momentum transfer during collision or frictional contacts between grains. Still, the flows of these dry granular materials are not easy to describe. They are usually divided in three classes depending on

the flow velocity. When the rates of deformation are slow, many direct shear tests give good indication of the behaviour of granular material. In this case, the material behaves more like a solid and its quasi-static limit is described in terms of plasticity. Basically, the strength of the material in this regime is characterized by an angle of internal friction (ϕ) : the material yields along slip planes, also called shear bands, when the ratio of tangential and normal stress reaches $\tan(\phi)$. In these bands, the velocity of the granular solid varies and the shear rate is different than 0. Secondly, a *gaseous-like* regime exists when the medium is intensely agitated or sheared and the grains are far apart one from another. In this regime particles interact through binary collisions and a kinetic theory has been developed by analogy with the kinetic theory of gases. In between these two regimes there exists the dense flow regime where grain inertia becomes important but where a contact network still exists that percolates through particles. Up to now no constitutive equations are available in this *liquid-like* regime and no uniformed framework allows to describe the whole dynamics from quasi-static to gaseous regime. [11] [8] In particular, this kind of flow dilates when flowing, since the distance between the particles increase, even if the grains are still in contact with each other. Shear bands are characteristic of this of this flowing regime : their typical width is 10/15 particle layers [13] far from the source of motion and in these zones the shear is notable ; in the rest of the granular solid, the velocity profile is flat. Different flow configurations have been used in order to describe the granular solid flows in equipment similar to corresponding practical applications. For any of these, the flow of the granular solid has been described by some physical models and successively verified by proper experiments. In the case of the annular configuration, in particular, several tests underlined the importance of the boundary conditions, like the roughness of the surfaces used to apply the shear. [13] In order to identify the flowability of the granular material, several methods are available: these methods can be divided in Direct and Indirect methods. The indirect methods characterize the flowability by measuring one property of the powder which can be assumed as representative of its flowability: for example, the angle of repose and the ratios between different densities. The direct methods, instead, observe the material during flow and work out the flow function: then, comparing with standard curves indicating the flowability, the property of powder is assessed. In these second

methods, different shear cells can be used and the measure take into account also of the compaction of the powder.

1.3 Mechanics

When a confined bulk solid element is loaded with a vertical stress σ_v, an horizontal stress σ_h can be also regitered. In the active state the horzontal stress is lower than the vertical one. The ratio of the two stresses (horizontal to vertical) is the stress ratio, K, whose values are typically between 0.3 and 0.6. It follows that - in analogy to solids - in a bulk solid a stress distribution (anisotropy) can be found in different cutting planes. Using a simple equilibrium of forces at a volume element cut from the bulk solid element, the normal stress, σ_α, and the shear stress, τ_α, acting on a plane inclined by an arbitrary angle α, can be calculated. After some mathematical transformations, it follows that:

$$\begin{aligned} \sigma_\alpha &= \frac{\sigma_v + \sigma_h}{2} + \frac{(\sigma_v - \sigma_h)}{2}\cos(\phi) \\ \tau_\alpha &= \frac{\sigma_v - \sigma_h}{2}\sin(\phi) \end{aligned} \tag{1.3.1}$$

The interested reader can find a detailed derivation of equation in Nedderman [12]. The pair of values (σ_α,τ_α), which are to be calculated according to equations (1.3.1) for all possible angles α (inclination of planes), can be plotted in a σ,τ-diagram (normal stress, shear stress diagram). Joining all the possible angles, the Mohr stress circle is obtained. It is located at. $\sigma_m = \frac{\sigma_v+\sigma_h}{2}$ and $\tau_m = 0$. The radius of the circle is $\sigma_r = \frac{\sigma_v-\sigma_h}{2}$. Since the centre of the Mohr stress circle is always located on the σ-axis, each Mohr stress circle has two points of intersection with the σ-axis. The normal stresses defined through these points of intersection are called the major principal stress and the minor principal stress. If both principal stresses are given, the Mohr stress circle is fully defined. From the explanation above it follows that the state of stress in a bulk solid cannot be completely described by only a single numerical value. Depending on the consolidation load acting on a bulk solid element, the corresponding Mohr stress circle can have a smaller or a larger radius, a centre at a lesser or greater normal stress, and hence also different principal stresses, σ_1 and σ_2. In conclusion, it is possible

to state that a bulk solid can transmit shear stresses even if it is at rest and that in different cutting planes different stresses can be measured. [18]

The Mohr stress circle is generally worked out by the application of a shear cell. Flowability is defined as plastic deformation of a consolidated bulk solid sample, due to the application of a force. In order to measure this property objectively, the magnitude of the necessary force is measured. The flow function test starts by the application of a normal consolidation load (pre-shear test). Then, the material is sheared until a steady flow is reached. Afterwards a normal stress, smaller than the initial one, is applied to the material, which is successively sheared up to its failure. Between each new test, the consolidation part of the test is repeated. Carrying out this procedure for a certain number of times, different (σ,τ) points are obtained. These points represent the internal yield locus (YL or IYL) for that state of consolidation. For each YL two circle of Mohr can be drawn, the smaller passing through (0,0) and tangent to the yield locus and the larger passing through (σ_{pre},τ_{pre}) and again tangent to the yield locus. From these circles, a couple of principal stresses can be determined and represented in the f_c,σ_1-diagram. If the test is repeated at a larger pre-shear stress, another yield locus is obtained. Therefore, plotting each couple of principal stresses in the f_c,σ_1-diagram, the flow function of the material is obtained. [16]

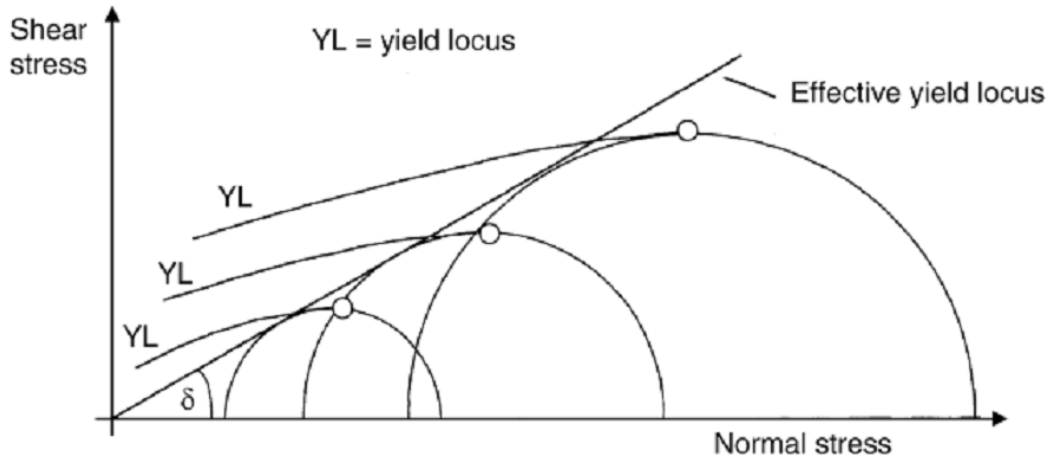

Figure 1.1: Definition of effective yield locus and effective angle of internal friction,ϕ [16].

This curve depends on time of consolidation and on the conditions of the powder that affect the forces between the particles (temperature, humidity,..). It is possible to apply a similar procedure to the wall friction, which represents the friction between

the granular material and the walls. The IYL curve usually can be approximated to a straight line. The linear case reperesents an ideal material and its constitutive law is called Coulomb's law (1.3.2).

$$\tau = \sigma\mu + c \tag{1.3.2}$$

where μ is the tangent of the angle of internal friction ϕ and c represents the cohesivity of the powder. It means that the failure of the material occurs when the shear stress reaches a critical value which is linearly related to the normal stress.

Depending on the height of the confined granular material, two different approaches can be used to calculate the vertical stress. In shallow granular beds, the most suitable approach is considering the profile of vertical stress as hydrostatic, where the stress linearly increase with the height. On the other hand, if in thick granunlar bed, the vertical stress can be calculated with the Janssen equation and the profile is exponential and shows a vertical asymptote. At large depth the stress is therefore independent of the height of the granular material.

1.4 Frame of reference

Recent progress has been made in the theoretical description of the rheology of granular materials. However, a scientific bottleneck still prevents the use of those theories in real configurations: the modelling of the interaction of the granular material with a solid boundary and its implication on the rheology of the system. Yet, such interactions are crucial to understand shear banding that is a widespread phenomenon in slow granular flows. The aforementioned difficulty originates from experimental and numerical evidence that questions the modelling of a solid interface as a simple boundary condition. Indeed, the existence of cooperative effects in the force network and in the velocity field prevents the use of a purely local approach, i.e., an approach in which the local stresses are simply related to the local shear rate. An important source of cooperative effects and thus of nonlocality is the mechanical noise of the flow itself. Thus, the effective friction coefficient of a granular material flowing on a flat but frictional interface and the corresponding slip velocity are partially con-

trolled by the shearinduced fluctuations of the force network, and their prediction remains a challenge. In previous works, by the use of discrete element simulations, the effective friction of a dense granular material confined in a shear cell is studied. It is shown that at flat frictional walls, even if the system is globally below the slip threshold, force fluctuations trigger slip events, leading to a nonzero slip velocity and an effective wall friction scaling with a sliding parameter. Nevertheless, still no experimental work has been carried out in order to verify these results. [1]

CHAPTER 2

Materials

In this section, all the equipment used for the tests are presented, dwelling on the mode of operation of some of them.

2.1 Experimental apparatus

The common part of all the tests is the experimental apparatus. Two coaxial Plexiglas cylinders, whose diameters are respectively 18 cm and 9 cm, are fixed on an aluminum structure. This structure is made by four aluminum rods and two plates of the same material: the first, lower plate sustain the electric motor, whereas the cylinder are arranged over the second upper plate. The structure is on a desk, it is stable in order to minimize the effect of possible vibrations coming from the flowing system but it is light enough to be handled if required. An aluminum rod is the crankshaft, connecting the motor to the bottom surface which is free to rotate in the space between the two cylinders. This surface is 3D printed and is made by Polylactic Acid and it will be successively described. Over this surface, the granular solid is poured. The granular solid is made by mono dispersed glass spheres, whose diameter is 4 mm. The homogeneity of the spheres is guaranteed by sieving them before pouring. Different spheres are used in the tests, since they be damaged during

the flow, due to the collisions between spheres and with the surface of the cylinder. A second plastic surface is positioned on the top of the bed of spheres: its roughness is the same of the bottom surface and it is produced in the same way. This surface is fixed on a plastic structure which makes the surface to be static during the flow. In fact, it comes across to a barrel of aluminum, sustained by two other rods, which is situated over the cylinders. This barrel fixes the structures printed over the top surface and, at the same time, fixes the internal cylinder, integrating it to the bottom structure. The barrel can be removed if the top surface has to be moved from its position: this is the case, for example, of the filling and discharging of the spheres between the cylinders. It is possible to position some iron cubes over the top surface, in order to increase the normal stress on the granular material. This operation will be carried out in some of the presented tests. Each iron cube weighs 0.21 Kg and its side measures 4 cm. The cubes are positioned in the most uniform possible way, in order to build a uniform profile of normal stress.

Figure 2.1: Experimental apparatus

2.2 Electric motor

The electric motor that makes the bottom surface rotate is provided by Schneider Electrics and it is integrated to a driver. It is placed on an aluminum plate with four screws, and it is connected to the surface by an aluminum crankshaft. It is controlled by an external CPU unit, which allows to control the rotational velocity of the crankshaft: the accuracy is 0.01 rpm. It is possible to chose between four rotation velocities; 1.17 rpm, 5.9 rpm, 23.4 rpm and 117 rpm. The motor is a stepper motor: it is easy to notice this mode of operation when the slowest velocity is chosen, since the steps are easily distinguishable. On the other hand, it is possible to assume the rotation of the surface as continuous for the higher velocities. In addition, the slowest velocity is not used in any test. The important characteristic of this motor is that its rotation is not affected by the conditions of the flow. In fact, due to the phenomenon of jamming (section 4.5), the lower layer of the granular solid becomes more compacted if some forces cause the compaction of the particles. This causes an increase of the friction between the particles and the bottom surface: at the same time, this means that the torque required to the motor increases, in order to keep the angular velocity constant (*constant velocity mode*). This motor is able to act in the desired way up to a limit, which corresponds to the maximum required voltage. When that limit is overcome, the motor immediately stops the rotation of the crankshaft. This problem is mentioned in the section 4.

2.3 Lights and Camera

In order to study the flow of granular materials the image analysis is widely used in academic and industrial fields. The first requirement is the high quality of the images: image analysis can be carried out on images whose clarity and resolution are good enough to distinguish the particles. With this purpose, two LED lights enlighten the surface that is recorded by the High Speed Camera. The position of the lights is decided in order to reduce reflection problems on the external plastic surface, but provide sufficient lightening. The effect of the LED lights is to create two little white spots on the particle surface, which help the identification of the particles made by

the post-processing software. On the other hand, videos are registered by Phantom Miro 320S. It is a high speed camera, whose available frequency of shooting depends on the resolution of the image, the available memory is fixed. The resolution changes according to the dimension of the object that has to be recorded: in this work, the height of the granular material. The camera is connected to a PC where the video can be seen on real time and the setting of the camera is set up. The exposure time is 2 μs, in order to freeze motion and avoid blurry images. Each video is successively saved in a hard disk and post-processed by using ImageJ Software. In this software, the image sequence is cut, in order to eliminate the static part from each frame of the video. Moreover, the number of bit per pixels is decreased to the number required by the PIV software, which is the final user of these videos.

Figure 2.2: LED lights and High Speed Camera

2.4 3D printer

The plastic surfaces of the the experimental apparatus are obtained from a 3D printer, the Ultimaker 2+, sold by Ultimaker. This printer is good for small project, which complexity is medium. Different nozzles are available, but in this case just

the 0.8 mm one is used. Several materials can be fed to the printer, in particular the surfaces are made of Polylactic Acid. It is possible to set the temperature of the base surface and the velocity of the deposition of plastic, which will affect the time required for the printing. The velocity of deposition should be a compromise between the time required for the whole project and the quality of the final result, since a higher velocity increase the presence of flaws. 3D printing consists in melting the fed polymer and deposing it in different layers, following the geometry designed with some appropriate programs. Therefore, it split the objects in many layers and for any layer the right quantity of polymer in the right coordinates of a 2D space is deposed. Possible problems are represented by smears due to the displacement of the nozzle while the polymer is still melted: it is needed to eliminate these manually. The designed object is uploaded to the 3D printer by a SD card, where the project is saved in a readable format (gcode). The files are converted in this format by Cura, which is a software provided by the 3D printer vendors that converts CAD projects into meshes that can be read by the printer. The CAD project was built by SALOME software, which is an open software for CAD modeling. This software is able to read the python codes, as it is for these surfaces. In Python script, the annular surface is created, then the disposition of the asperities is casually obtained. In particular, this placement is dependent on the parameter s, which is adapted from the by Jenkins and Richman definition of Θ, where $sin(\Theta) = (d + s)/(d + \sigma)$ [9] . In this case, s is defined as the ratio between the distance between the asperities and the diameter of the asperities. The asperities consist in some hemisphere which have the same diameter of the spheres inside the cylinder, in order to represent a sort of continuity condition. If the smooth space is equal or larger than the diameter of the asperities, the roughness can be said to be heterogeneous, while if the distance is smaller the roughness is homogeneous. The other case of homogeneous roughness is a completely smooth surface. The roughness are classified in this way depending on the kind of contact they can have with the particle. In case of a homogeneous surface, just the hemispheres (or the smooth surface) would contact the particles; in the other case, both the asperities and the flat surface could contact the spheres.

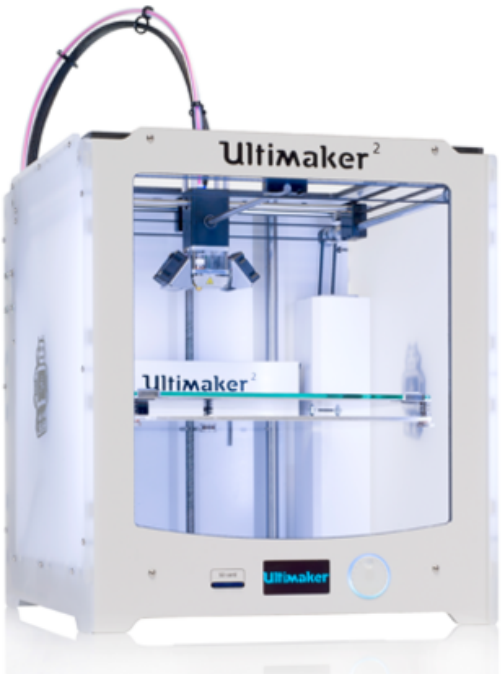

Figure 2.3: 3D printer

2.5 Force sensor

The most important result of this thesis is worked out from the measurement of the forces at the wall of the experimental apparatus. With this purpose, the sensor FT Mini 040 distributed by Schunk is used. The sensor is fixed on the external surface of the cylinder by using three screws that penetrate the plastic cylinder. Glued in front of the sensor there is the analysis window, which it a cut out of the external surface of the cylinder itself. That cut out is made with a laser cutter by an external company. The sensor is linked to a DAQ, provided by the same enterprise. The sensor registers continuously 5000 signals of voltage each second: strain gauges (DMS) measure the strains applied in all six degrees of freedom: two tangential and one normal forces and three torques. The DMS signals are amplified in the sensor. The interface board located in the power supply box converts the strain gauge into a signal which can be used by the DAQ card. The DAQ card, eventually, converts the sensor's analog DMS signals into digital signals, which are immediately displayed by Dasylab, a block diagram environment. The displayed values are calculated by passing through a converter. The converter consists in a conversion matrix, provided by the vendor of the sensors: by the application of this matrix, each signals of voltage is converted into

a value of force. The sensor is based on the variation of the extension of a metallic foil which is located in an electrode. This causes the variation of the electric resistance, which is measured by a Wheathstone bridge, which eventually outputs the voltage signal that is caught by the DAQ system.

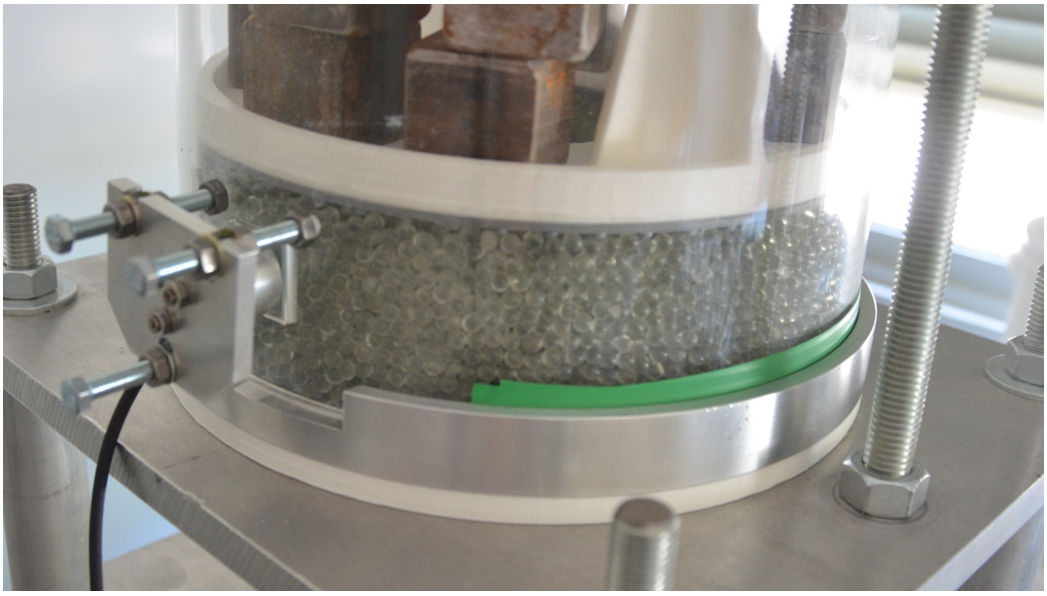

Figure 2.4: Force sensor

2.6 Equipment for segregation test

For the segregation tests, the same experimental apparatus described above is used. Additionally, to the glass spheres, some ceramic spheres are used, whose density is slightly higher than the glass ones. The shape is the same, as well as the volume of the spheres. In order to make them notable during the tests, they are colored with fuchsia spray. In addition, the enlightening of the particles is improved by placing a LED lights ribbon inside the internal cylinder. In addition, some photos of one face of the experimental apparatus are taken: with this purpose, a GoPro Hero4 is used. It is collocated in front of the cylinder, using the suitable support, and it remains in this position for the whole lasting of the test. The time lapse function is used for this test: one photo is taken each minute, for 6 hours from the beginning of the test. Successively, all the images are processed by using ImageJ, as it is described in the dedicated section (6).

CHAPTER 3

Introduction to PIV and application

The visual nature of granular materials makes image analysis a key part of many experimental techniques. Furthermore, programming languages developed image analysis software and libraries, which are expressly made for the analysis of particle ensembles.

3.1 Operative procedure

In order to describe the velocity of the particles during the flow of the system, the video shot must be handled. The videos are processed using ImageJ, specific software for analysis and adjustment of images. Videos are cropped, in order to exclude the static parts, and converted in a format suitable to the postprocessing software. It is also possible to adjust the balance of the colors, as the brightness, but this is useful just to a human operator, whereas the software is not affected by this adjustments. This conversion constitutes a loss of information, since the format of the images is split in half (from 16 bit per pixel to 8). Anyway, all the required information are still available. Eventually, they are saved as a sequence of images. The number of images taken is dependent on the resolution, since a limitation on the size of the video is imposed by the camera. In addition, videos are taken in an amount of time

which depends on the amount of images that are taken in each second (frame per second), whereas the number of shot is fixed. The resolution changes according to the dimension of the shot, and this is adapted by the operator to the size of the area which has to be analyzed. Therefore, resolution decrease as shorter the particle layer is, so the number of shot increases. It is also required an accurate positioning of the camera, where the bottom border must be parallel to the bottom surface of the cylinder. In this way, the positions of particles will be assessed accurately, where the reference is the cylinder internal surface. The image shot by the camera is made clearer by using two LED lamps, which are headed to the same surface the camera is recording.

3.2 Manual Particle Tracking

Several methods can be applied for the particles tracking: one of these is doing it manually. The operator identifies a particle, records its position and the number of the initial image; subsequently, he follows this particle through all the images, until it is possible to him to see the same particle. Recorded positions are just the initial and the final ones, and the same is for the registered image numbers. In this way, it is possible to identify an average displacement and the corresponding time interval. From these measurements, it is possible to determine an average velocity of the particles. It is necessary to consider particles that are moving in different layers throughout the image: in this way, the velocities of granules depending on x and y positions are worked out. Collecting velocity values of many different particles, the horizontal velocity profile depending on y is obtained. This technique has been used in this work and it is cited in chapter 4.

The limit of this technique is its dependence on the work of the operator. In fact, it is required that the operator identifies one light point on a particle and then follows this light point as the particle moves. And this procedure is applied to different points, so to different particles. But the problem is that the light point is not fixed on the spheres, because of the relative motion between the lightning points (fixed) and the spheres (in motion). This means that, in this measure, rotation of particles is disregarded. Therefore, it is possible to assume that the identification of particles is

acceptable, even if the trajectory of the points is not the one of the particles. Another issue is that, in this procedure, the starting image is the first one, at time 0: since the identified displacement should occur in a certain number of images, it is possible to consider just the particles in the left side of the initial image. In fact, the particles on the right side of the image appear on the recording area just for a little number of frames, therefore they are less representative and therefore disregarded. This means that a limited number of particles can be considered in each test. Eventually, another problem is that if the displacement of the particle in two consecutive images it excessive, identifying the same particle can be a complicated task. Images are rather unclear to the human eye; therefore the operator could commit some error. This problem is particularly present if particles are fast and frame rate is low. In order to solve this problem, the procedure described above should be carried out on different videos, where the frame rate varies. Increasing the number of frames per second, the displacement of the particles will occur in a higher number of images and the relative displacement between two images will be smaller. In this way, the tracking of the particles will be easier.

In conclusion, in order to describe the velocity profile of the particles, the manual tracking is not a valid technique. In addition to the many problems cited above, it is particularly stressing for the operator, who need to spend much time just following particles through different images, and the results obtained are not particularly relaiable. Instead, it could result helpful in a rough verification of the results obtained by different automated techniques.

3.3 Automated Particle Tracking

The particle tracking techniques have been applied in the past in different areas of interest. In particular, it has been applied widely in fluid dynamics, by the use of tracers. In fact, using some particles easily traceable, it is possible to describe the flows by using these techniques. Images of the system under consideration are taken at fixed time interval between them. These techniques, mostly based on cross correlation, are able to identify the same areas in two consecutive images, even if this area is displaced. Applying this procedure to the whole image, it is possible

to obtain a discrete field of displacement for each couple of images. Therefore, it is possible to assess a velocity field in a chosen interval of time, by averaging the values of displacement in the same interval.

One of the most relevant parameters in the application of these techniques is the density of traceable particles in the images. In fact, if the density is low and the single particles are easily distinguishable, it is possible to describe the motion of each particle. In this case, a *Particle Tracking Velocimetry* can be applied. If the density is medium, so that it is still possible to identify the particles, but the operator is no more able to distinguish the particle after they displaced, the *Particle Image Velocimetry* (PIV) should be applied. This technique, in fact, is able to locate the particles at different times in specified portion of the images, which are called interrogation areas. In the third case, where the identification of the particle is further complicated for the operator, the *Laser Speckle Metrology* is the right option. In fact, this technique is able to identify all the single particles in each image and to correlate them. [15]

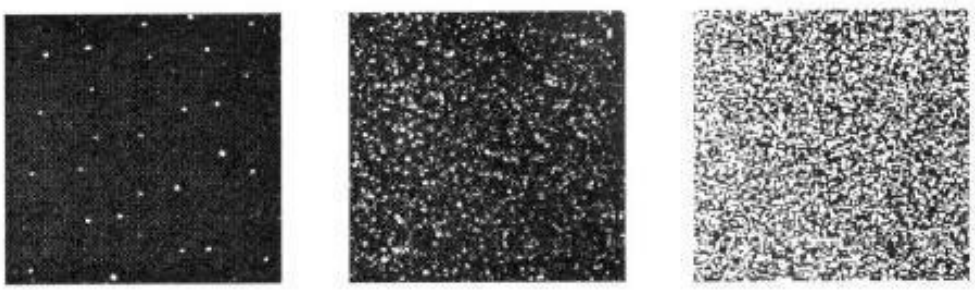

Figure 3.1: Different densities of particle: at left, first case; in the middle, second case; at right, third case.

3.4 Bases of Particle Tracking techniques

In this thesis, the PIV technique is used. Conceptual bases are in common with particle trackiing. The task of particle tracking breaks into two parts: locating the particles in a particular image frame (location) and determining where a particle has moved from one frame to the next (connection). This latter task consists of finding the permutation of particle indices in two consecutive images, which minimizes the maximum distance traveled by a particle. Regarding the location, instead, many

techniques exist to locate particles and other objects in images. Since digital images represent light intensity near discrete grid points or pixels, the spatial accuracy of the information obtained from the image depends on the pixel size or resolution. Most techniques can determine an object's position to pixel resolution: however, to measure many important quantities sub-pixel accuracy is needed. This accuracy is obtained by using a technique based on least square fitting (LSQ). The basic idea of LSQ fitting is to compare the actual image to a calculated image based on a particle shape function and find the positions and parameters that minimize the difference. In that way, the LSQ determines the most likely position of a particle, the position that minimizes the weighted squared difference between the actual image and the calculated ideal particle image. In particular, the minimum of the weighted squared difference can be expressed in terms of convolution and cross-correlation. These can be evaluated quickly using Fourier transforms and are implemented in hardware on the graphics processing unit of most of computers. The cross-correlation will be maximum near particle centers and 0 outside the borders of the particles, therefore it works well when the contours are well defined. The LSQ technique, as well as other techniques, gives particle centers to approximately one pixel accuracy. One method to get sub-pixel accuracy is to interpolate the peaks found by different techniques.

3.4.1 Bases of PIV

Based on this method, a particular technique is used in this work. It is called PIV, which means Particle Image Velocimetry. This technique is a useful method for extracting motion information from images in which individual particles are hardly distinguishable. The idea of PIV is to find the most likely location of a small area from an image at time t in a later image at time t+Δt. This location will be an approximation of the displacement Δx for the center of the small area. In the LSQ framework, the "ideal particle" becomes a small patch from the frame at t and the "image" becomes the frame at t+Δt. The spatial parameters of the small area should be chosen such that they are small enough that the velocity is approximately constant over the region, but large enough that there are distinct features in the region. They are indicated along the code as the dimension of the window size, which is exactly the size of the

area whose displacement in successive images is analyzed. An example is shown in figure 3.2, where the arrow represents the approximate displacement of the patch at time t+Δt. By adjusting the value of Δt, the sensitivity can be retrospectively adjusted. Large Δt are used for slow moving regions and small Δt for fast moving regions. Using PIV, the entire flow field can be mapped for each point. Further, since the flow is steady a temporal average can also be performed. [7]

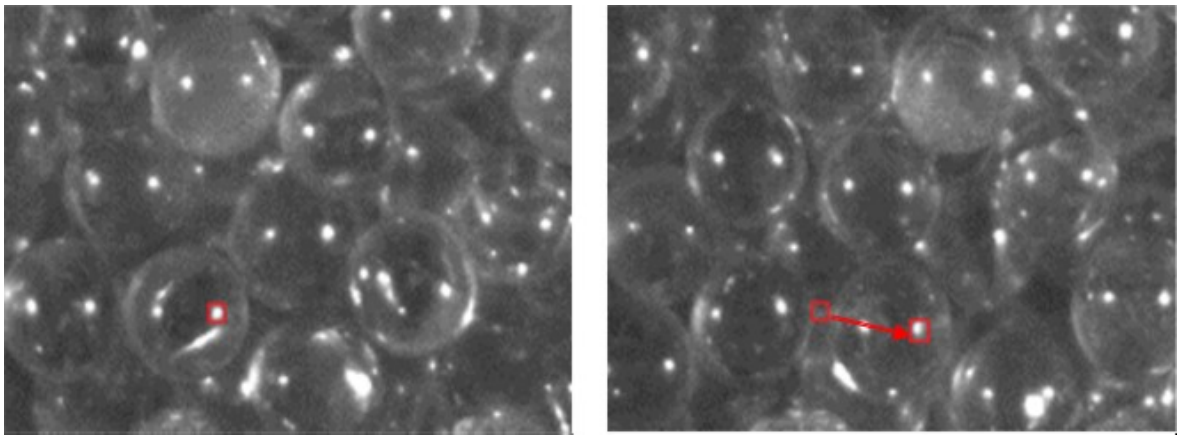

Figure 3.2: Located point at time t (right) and t+Δt (left). The vector represents the identified displacement of that point.

3.5 PIV application

PIV code can be applied to sequences of images, which are for example different frames of a video. In the sequence of images, particles are in different positions in any image: in particular, as the faster the particle is, as the higher will be its displacement between two consecutive images. Since this displacement depends on the velocity, it involves differently the particles at different heights (y). Calculating the velocity of a particle means registering the position of the same point in all the different images, calculating the distance run by this point and dividing the displacement for the time passed between the first and the last analyzed image. Initial assumption is that the registered points are a suitable representation of the particles. This assumption is supported by how all the tests are set up: lights head to the shot surface cause two points appearing over the spheres. These points are particularly distinguishable; therefore they are exploited during the tracking operation. In particular, these points

represent a peak of the intensity of light in the image; therefore the software will recognize them as a peak, so as a representative area. If the displacement of the particle is not excessive, the light points will look like similarly in two consecutive images, so the location of the area will be easy.

In this work, PIV is taken from an open library available in Python, which is called *Openpiv*. In the implementation of this method, (script Appendix A), several indications are required. First of all, it is necessary to choose the size of the small area considered by the method, the one where the peak is identified. This value is called "window size" in this work. This means that n small areas are identified on the loaded images and each of them has the chosen size. The shape of these areas is a square, and the chosen value is the side of these squares (unit of measurement is pixel). The quantity of these small areas depends on the resolutions of the loaded images, since it is the number of pixels for each side of this image. There are indications in literature about the size of the interrogation window: the areas should be small enough that displacement gradients should be neglected. In addition, only linear displacements should be present inside the window and the particle should be still located inside the shifted window in the later time considered. Summing up, the window size should be small enough to have a uniform motion. Due to considerations and tests on how the obtained result varies changing the window size, it is possible to assume that the size of the window should be close to the size of the particle. In this way, it is also possible to make the collocation of particles easier, since that likely a small number of particles will be contained in the interrogation windows. In this way, the identified area, compared among the two consecutive images, will be similar. In the section 4, tests for the choice of this measure are illustrated. Another value which is strictly related to the window size is the overlap, which represents the superposition of subsequent windows. In fact, during the partition of the image in small areas, the successive areas are superposed to the previous one. The amount of shared area is determined by the value of the overlap. The superposition of successive windows identifies the number of values calculated by the code. In fact, the choice of the dimensions of the interrogation area is led by the necessity that the displacement of the particles in two consecutive images is smaller than the window size.

These values define how PIV computes the analysis of images. Initially, two

images are implemented to the program (line 4, Appendix A). The called method is a zero order displacement predictor cross-correlation algorithm, which cope with the problem of loss of pairs when the interrogation window is small by increasing the search area on the second image. In addition, the values of window size and the overlap are indicated. Subsequently, the program scans the interrogation area to detect the correlation peak: comparing the two different images, the program determines where the same identified area is most likely located. In fact, in the comparison of the interrogation area from the two images, the presence of the same area will result in a peak of correlation. The interrogation area is shifted in the two images and the sum of the product of overlapping pixels results into a peak, which produces a cross-correlation function. The number of calculations increases if the window size decrease and if the overlap decrease. Several methods can be used to determine the correlation peak: usually, the functions are fitted by using three adjoining value to estimate one component of displacement. The same procedure is carried out for the other component of the displacement. Gaussian peak fitting is the utilized method, since generally the Airy intensity functions of the images are well described by the Gaussian intensity distributions. In addition, the cross correlation of two Gaussian distribution is still a Gaussian distribution. [7]

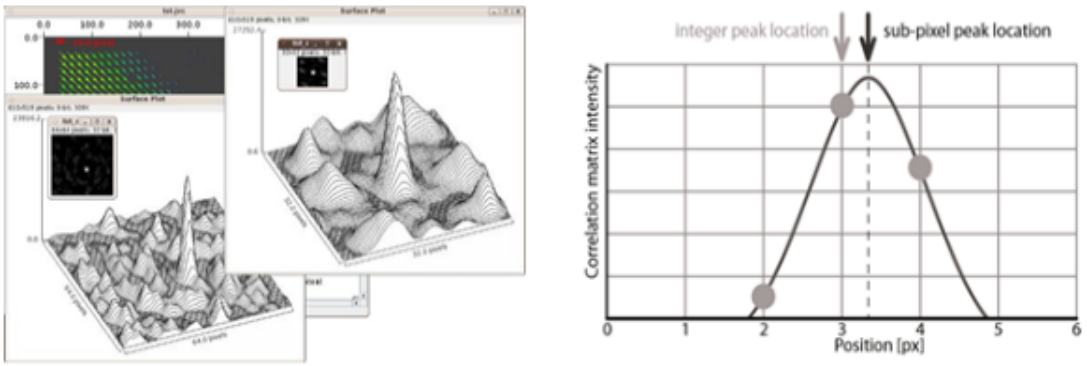

Figure 3.3: Right, peak detection; left, Gaussian fitting

In this way, it is possible as well to obtain sub-pixel accuracy. If more peaks are present on a window, just the highest peaks are considered, in a comparison among the local values in proximity, therefore it is not required that just one particle is included in the window size. In this way, in fact, different particles can be located

in the same interrogation area, resulting as different peaks. After the correlation procedure, where two different peaks, belonging to the same particle, are identified, the displacement is estimated. In fact, if the particle moves, also the detected peaks move in the subsequent images, since they represent two different times: t and t+Δt. The interval of time between the two images depends on the frequency of camera recording (frame rate). In this way, since displacement and time are estimated, it is possible to calculate the instantaneous velocity of the particles.

Secondly, some instructions about the filtering of images are provided (line 8, Appendix A). Filtering of images indicate how the detection of the peaks occur: one criterion and one threshold are required. The chosen criterion is the *signal to noise* method, which specifies which method is used for the evaluation of the *signal/noise* ratio. In particular, different methods can be applied for the identification of the peaks, but the one used in this case is the *peak to peak* one. This means that the calculation is accepted in the event that the ratio of the velocity of that point over the second fastest velocity among the nearby points is lower than the threshold. Other possible criteria can be chosen, but results do not vary, as described in section 4. Decreasing the threshold value, it is less likely that the value will be accepted. On the other hand, increasing the threshold it is possible that an outlier value will be considered as reliable. In fact, in the case of a really disturbed image, the level of noise on the image could be really high, so that the calculated displacement of the particles could be unrealistic. Disturbs on the images can be linked to the conditions of the system or to the quality of the recording. For this reason, some errors in the location of the peaks and so in the calculation of the displacement could occur. In general, these errors could take place whereas the software is not able to work out a proper velocity value. Therefore, the code calculates a value that is much higher than the nearby value. In these cases, the filtering procedure used in this code (line 10, Appendix A) replaces the calculated value with a *NaN* value, for the specific coordinates of that interrogation window. Successively, this filter replaces the NaN values calculating the velocity for that coordinates. This calculation is carried out by considering an average built on the closest values. How many values are considered depends on the dimension of kernel. In addition, this local average relies also on further values, since this averaging procedure occurs for a decided number of iterations, which means that

kernel is extended to as many values as this number indicates. This extension occurs just in case that the nearby velocity values are NaN as well. Lately, these are the values that will be considered in the calculation of the velocity profiles. Depending on the size of the neighborhood considered in this averaging, the accuracy of the replacement of the outliers varies. Different tests were carried out, in order to estimate the influence of these parameters, as reported in section 4. Eventually, it is indicated the interval of time between the shot of the different images and a scaling factor is applied, in order to convert the image coordinates from pixels to millimeters. For this reason, a plastic strip is glued on the cylinder surface and partially shot by the camera: since this strip is squared, during the processing of the video the pixel size of a centimeter is measured. In this way, it is possible to assess the scaling factor. This procedure is applied to any couple of images, for any shot video. Successively, since all the velocity values are calculated for any different moment in any coordinate, a simple average is applied to the values (line 16, Appendix A). All the velocity calculated values are summed up and divided for the number of values considered. If one of the calculated values is NaN, the whole calculation results as NaN, therefore it is particularly important to avoid the presence of undetermined values. Otherwise, as reported in section 4, a different averaging code can be implemented: averaging is carried out by adding to an array just the values different to NaN, then dividing for the numbers of values effectively considered. In this way, NaN values are simply disregarded, whereas in the first case they were worked out by local averaging, resulting in a sort of approximation. In any case, results seem to be similar, so the approximation does not affect the velocity profiles. When this code is run, the results are a text file, where all the coordinates and the related velocities are reported, and the graphical representation of these velocities.

CHAPTER 4

Calibration of the analysis system

4.1 Choice of the criterion

The aim of these tests is to define the setting of videos recorded for the decription of dense granular flow under application of a shear stress. In fact, studying the particular configuration of flowing solid particles, where motion is originated by the rotation of a rough surface, particles velocity values can be considerally different. As described in the section about PIV(3), in the studied configuration just one surface is rotating, while the other surface is static, so velocity of particles varies depending on the distance from the source of motion (the bottom surface). Furthermore, the variation of velocity depends on configurational factors that will be studied in the following tests. High spatial velocity gradients could be present in the vertical direction, therefore it is needed to analyse particles in different conditions at the same time. The aim of this test is to identify how the horizontal velocity profiles can be worked out in a proper way and how it varies depending on the height of the particles. Velocity profiles of particles worked out in these tests are calculated considering the motion of the particles in contact with the surface of the external cylinder, disregarding all the particles behind them. A particular portion of the external surface is considered, since in this portion it is possible to record the whole height of cylinder and so the

particles in direct contact with the surface. The size of this area depends on the mass of the spheres poured between the two cylinders, which determines the height of the particle bed. Since the flow is assumed to be steady, according to the regularity of the two cylinders, the surfaces and the spheres, the shot area can be assumed as representative of the whole external surface of the cylinder. Depending on the fps, videos last for different times, but the number of images depends only on the resolution of the image, which is constant since the mass of particles is the same. In particular, for this resolution of the camera (640x1200), images are nearly 5000; fps can be 3400, 1000, 100 and 24 according to the different cases. 3400 and 24 are the maximum and the minimum fps allowed by the camera. Subsequently, videos are processed with ImageJ software: they are cropped, in order to eliminate the static parts of the shot; their brightness is regulated, in order to make them clearer; eventually, they are converted to a format readable for the postprocessing software (Python). Using ImageJ, the scaling factor is identified by measuring pixel distance on a strip of a squared paper glued on the external cylinder. Eventually, Python library *Openpiv* calculates some correlations from the images and works out the average horizontal velocity profiles for the particles in the shot.

In all the tests reported in this section, the rotational velocity of the bottom surface is 23.4 rpm. All the four fps mentioned above are used: In addition, 1 fps case is artificially created by skipping a proper number of frames during the analysis of images. Starting from the video taken at 24 fps, every time that a couple of images is considered, the successive couple of images is 24 images forward from it. For example, since there is a counting variable for the ith image considered, first couple of images is composed by the first and 25^{th}; the second couple is composed by the 26^{th} and 50^{th} images. This means also that between first and second analysis 24 intervals of time dt are passed. In this way, it is possible to simulate a video which framerate is 1 fps. This procedure is carried out in order to increase the quality of the description of the particles motion far from the bottom, which was unsatisfying also with the lowest fps possible. The reason for the application of this procedure will be clearer later.

Results in figure 4.1 are reported using a logarithmic scale for the horizontal velocity (u), whose unit of measure is mm/s, since values vary several order of

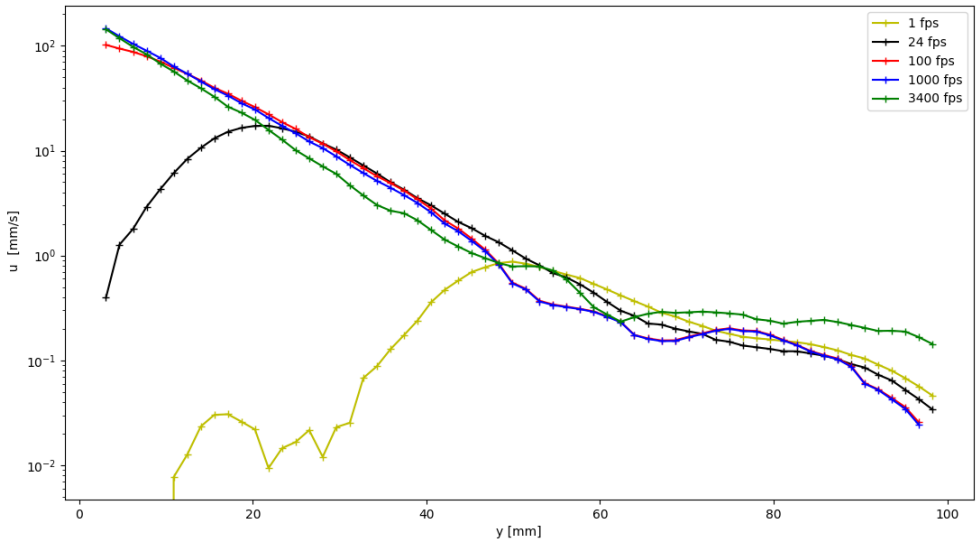

Figure 4.1: Particle velocity profiles calculated on different videos

magnitude. y values represent the distance of particles from the bottom, where 0 represents the bottom surface: their unit of measurement is mm. Logarithmic scale for velocity is the most appropriate choice also because profiles are assumed to be exponential and so linear in this representation: in figure 4.1, this assumption is confirmed, even if in the righter part of the figure, for higher and so slower particles, the slope of the curves changes. Increasing the number of fps, it is noticed that linearity of curves starts from lower values of y. This fact creates some doubts regarding the reliability of the results obtained. This problem is made clearer by the figure 4.2, which shows this particular behaviour for the intermediates values of fps. In fact, it is possible to notice that, at certain y specific for each fps, the curve at lower fps decays whereas the curve at higher fps show higher velocity values. This is true going from the left towards the right part of the figure: vice versa, the trend is the opposite.

Therefore, it is possible to suppose that each curve shows velocity values higher than the others in a certain interval of y coordinates. By this, it seems possible to describe the whole profile of velocity by considering the videos taken at different fps according to different y, height positions, and so to different horizontal velocities. In this way, each level of particles will be assessed with its most reliable velocity value, whereas the remaining part of the curve will be disregarded. Since the trend seems

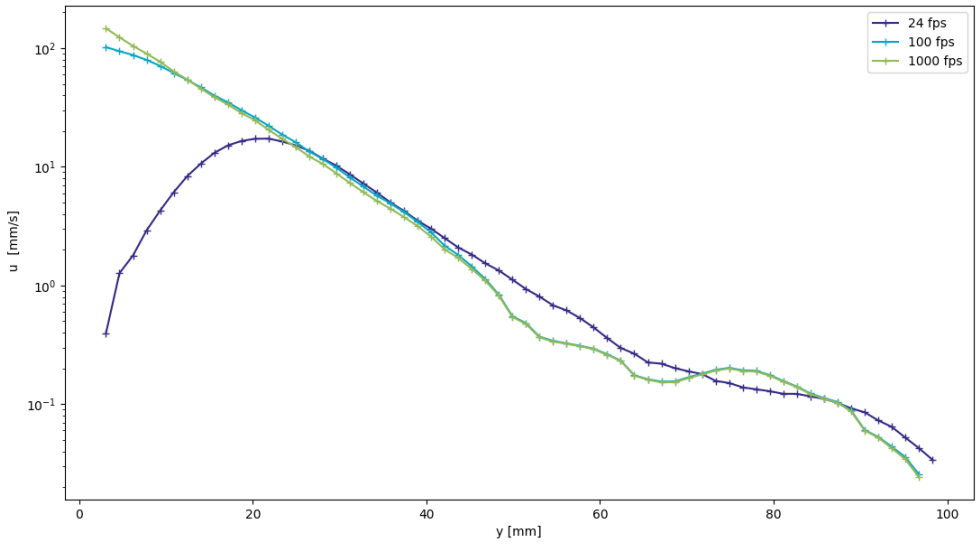

Figure 4.2: Particle velocity profiles in logarithmic scale, of 24 fps, 100 fps and 1000 fps videos

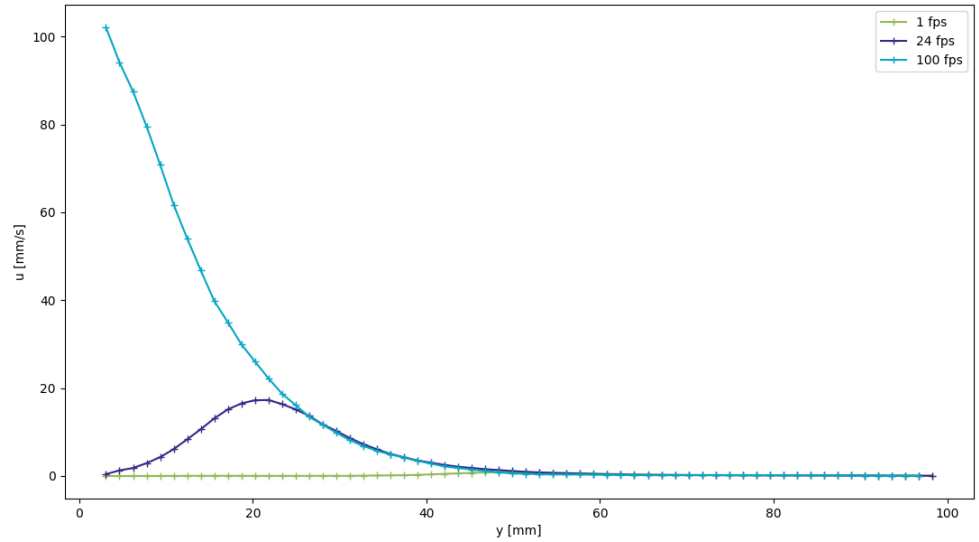

Figure 4.3: Particle velocity profiles of 1 fps, 24 fps and 100 fps videos

to be this, it is necessary to define a criterion able to correlate in an accurate way reliable values of particles velocity with a variable that varies with the y coordinate. For example, since getting far from the bottom surface the velocity decreases, the displacement of the particles in two consecutive images will vary, so it could be possible to define the minimum and maximum displacements that the software is able to describe properly. Nevertheless, this procedure does not take care of the closeness

of these measures to the real velocities of the particles. In fact, this assessment assumes that the results worked out by the PIV software are reliable at least in the identified interval of y coordinates. Then, at a later time, it will be necessary to validate the results. The problem is that curves are really similar in the central part of logarithmic scaled figures, and a reliable criterion to establish which one is the most representative is not univocally determined (overcoming criterion is just a supposition). In fact, the decay of the velocity profile does not univocally prove that the result is not acceptable. Profiles from the slowest fps are presented in figure 4.3, whereas the velocity profile obtained with 1 fps is showed in figure 4.4 : all the others profiles, if properly scaled, look like this. In this figure, the velocity is reported in linear scale.

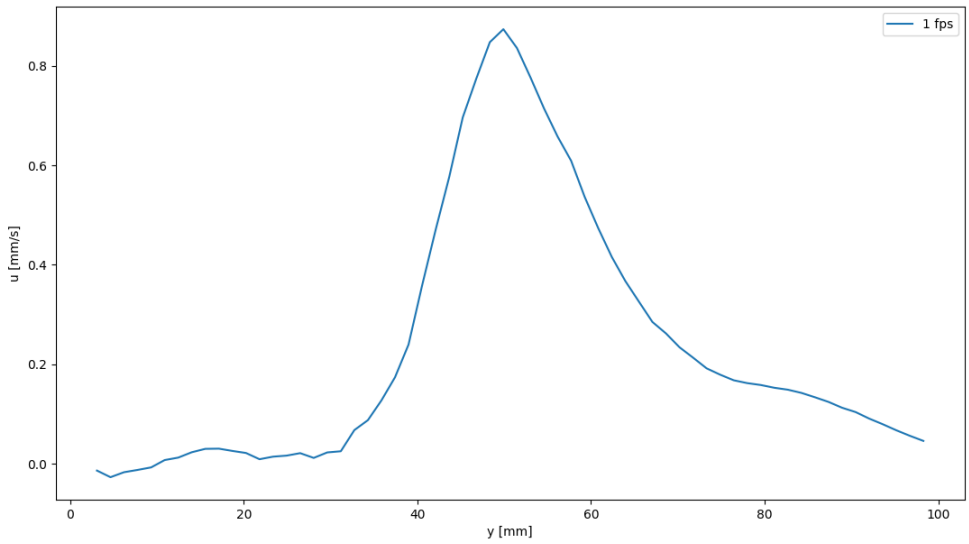

Figure 4.4: Particle velocity profiles of 1fps

As just mentioned above, this clarifies the initial assumption: in order to describe different velocities, different fps should be used. In fact, positive slope parts of the curves are meaningless, as it is known that for smaller y values the velocity of particles increases. These means that the values of the curves, for y smaller than the point of maximum, must be neglected. This problem is due to the analysing software: the difference among two consecutive images is the base for establishing correlations between images that allow identifying a displacement and so a velocity of the particles. If the displacement of the particles between two consecutive images

is excessive, the software is not able to identify it, so it is not able to work out a correlation. Eventually, the software assume that the particles are static, or at least slower than how they really are, making some mistakes in the correlation procedure described in section 3. This behaviour can be noticed in particular by plotting velocity vectors worked out by considering a couple of images. Velocities calculated in this way are instantaneous values of velocity, since the considered time interval is just the variation of time between the two shots. In figure 4.5, it is possible to notice how just the vectors in the central part of the images have a reasonable size and direction, representing in this way a reasonable velocity of the particles. Instead, in the lowest and highest parts of the image, the size of the vectors is unrealistic. It is possible to notice as well that, plotting the velocity vectors on a video with different fps, this zone of reliability is displaced. Especially in the lower part of the image (figure 4.5,left), it is well known that the particles will be faster, but the values of velocity worked out by the program are smaller or even null. It is also possible to notice, in this lower zone, that some vectors represent particles that are not following the flow. This problem seems to be fixed up by plotting the vectors on the right image (figure 4.5,right), where the vectors are worked out on a video shot at 1000 fps.

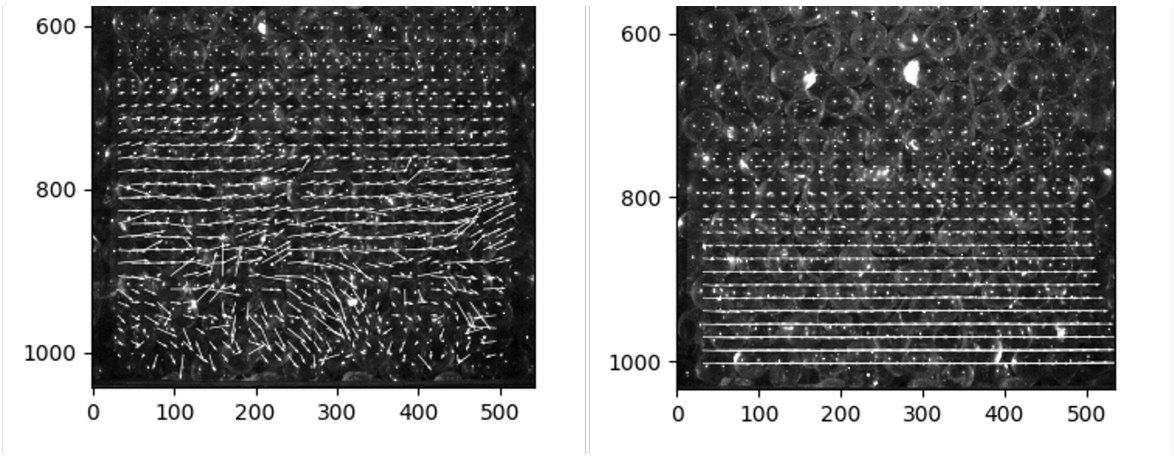

Figure 4.5: Left: Vectors on 24 fps video; Right: Vectors on 1000 fps video

In conclusion, from these figures it emerges the necessity of finding a criterion for deciding which part of the curves are reliable and so, in similar tests, which fps should be used, depending on the bottom velocity, to obtain the real velocity profiles of particles. At this point, it can be assumed that recording and postprocessing videos

with less fps are representative for the slowest particles; vice versa, more fps are required to represent the fastest particles. Furthermore, curves of less fps videos (as can be noticed in figure 4.3) are meaningful just for values of y higher than their point of maximum. Probably, also the right part of curves is representative up to a certain value of y, as can be noticed by the vectors plot. Therefore, wide part of the values of the curves has to be excluded. The same considerations are valid for the tests at higher fps, which are not able to describe the motion of the slowest particles.

4.2 Comparison with Manual Tracking

In a second time, in order to validate the results shown by *Openpiv* software, particles are manually tracked using ImageJ tools. Using coordinates of particles in different slices, it is possible to establish their velocity profiles by averaging displacement in time variation. The operator has to ensure that the particle tracked through the images is the same one. Assuming that this requirement is respected, this procedure tests the correlations identified by the software.

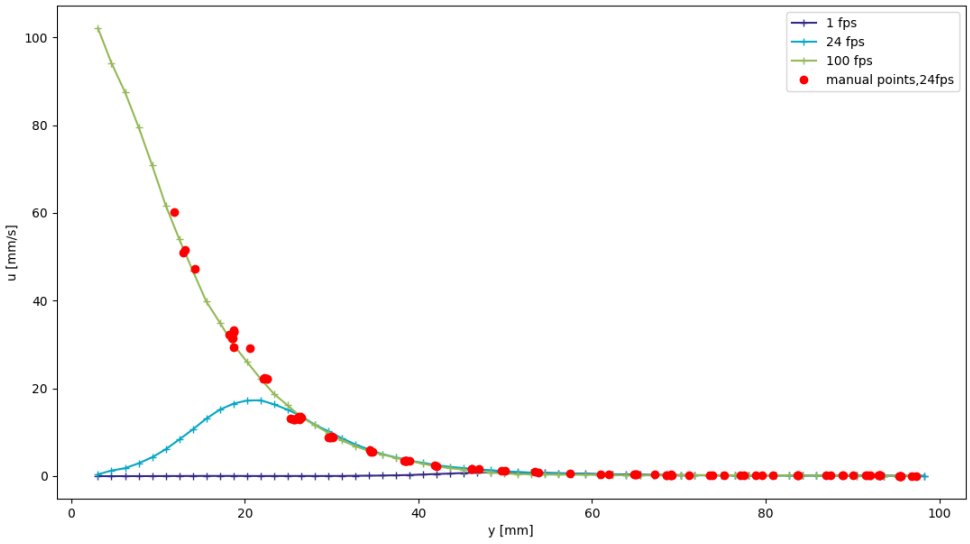

Figure 4.6: Particle velocity profiles of 1fps, 24 fps, 100 fps videos and manual points worked out on the 24 fps video

Firstly, manual tracking is applied to the 24 fps video. As it was explained in figure 4.2, this video is more reliable for slower particles. In fact, it is possible to

track a smaller number of particles when they are faster. This is due to the fact that just the particles on the left side of the image at t=0 are considered, as explained in section 3. For this case, comparing results in figure 4.6, it is possible to see that the results coming from the manual tracking follow the higher values of the curves, as previously supposed. Therefore, it is possible to assert that results worked out by the software are reliable for the slower particles. On the other hand, it is complicated to work out values for faster particles with this procedure on this video. In fact, for the highest values of velocity even the visual identification becomes complicated, since the difference between two consecutive images in that area becomes really consistent. Therefore, it seems preferable to apply the same procedure to the 1000 fps video. In this second case, as shown in figure 4.7, results show some small differences. In fact, data of manual tracking show some values different from the ones coming from software analysis. Trend in not well defined, but generally, manual data are higher than *Openpiv* values. Anyway, differences among velocity values are small, so the velocity profiles can be assumed as representative and will be accepted.

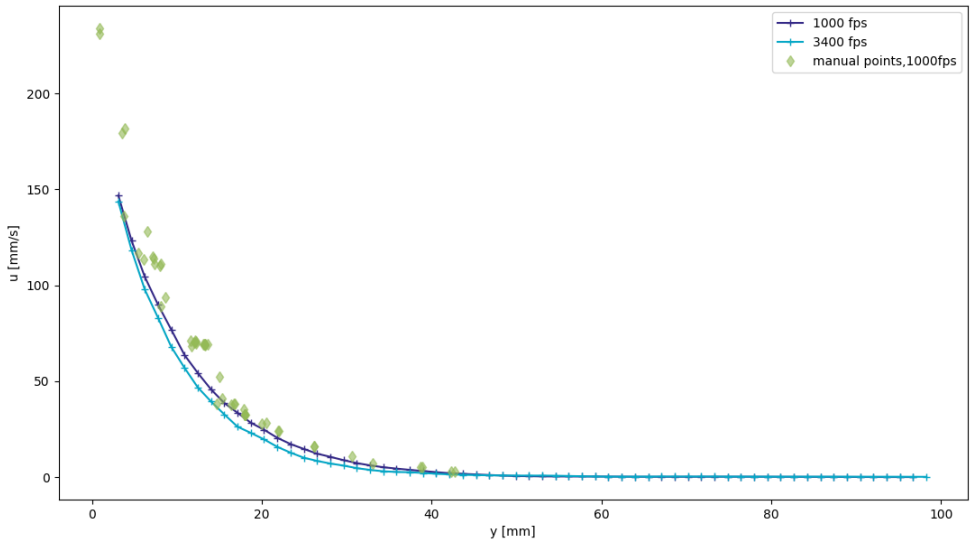

Figure 4.7: Particle velocity profiles of 1000 fps and 3400 fps videos and manual points worked out on the 1000 fps video

For these particles, manual analysis is restricted to the particles closer to the left edge of the image because their movement can evolve in time. Whereas, if particles are on the right part, it is not possible to follow them through a substantial number

of shots. Also particles closer to the bottom are individually taken into accounts with manual tracking, so their velocity values are close to the velocity of the bottom. Highest values are exactly the ones of the bottom roughness. Differently, *Openpiv* software works out an average value of the particles velocity, which depends on the window size, so they could result slightly lower. In addition, particles in direct contact with the bottom surface slip; therefore a difference between particles and surface velocity is expected. Figure 4.8 presents all the results together.

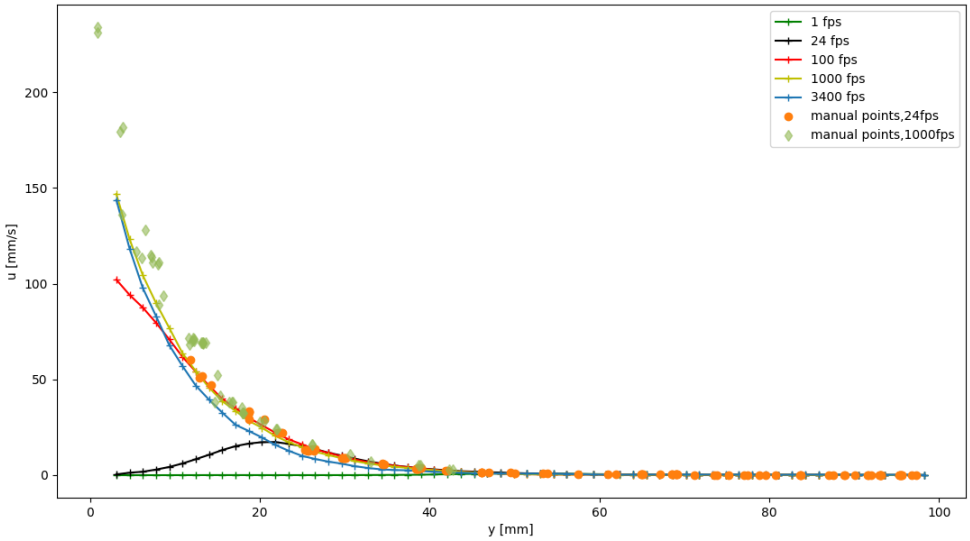

Figure 4.8: Particle velocity profiles of all the videos and manual points worked out on both 24 fps and 1000 fps video

4.3 Velocity profile

As already mentioned, some criteria are applied to make figures more clear, as presented in figure 4.9. Left and right parts of the curves are omitted, since they represent velocity profiles that are better described by the other curves. This omission is obtained by limiting the displacement considered in the building up of the curve: if particles displacement is lower than 0.5 px or higher than 10 px, it is assumed that *Openpiv* is not able to describe the velocity profiles properly. This supposition is due to the fact that, the code identify the displacemente of the particles only in a certain range of values. If the displacement is too small or too large, compared

to the displacement of the interrogation areas, this possibility is not guaranteed. This means that the results worked out by the code will be probably affected by a huge error, as previously described, so they are not reliable. As the displacement of the particles between two different images depends on the fps of the video, it is a meaningful parameter. It is able to distinguish the reliable part of the curves in a homogeneous way for all the curves. Since the important parameter is the relation among the displacement of the particles and the one of the interrogation windows, this criterion affects all the curves in the same way. Second criterion is applied to exclude the rising part of the curves. In this case, the reason is physical: it is known that decreasing y coordinate, the velocity is exponentially increasing, so the values of velocity for y lower than the maximum point of parabolas are not feasible. Therefore, any part of the curves which slope is positive cannot be accepted. In this way, it is possible to obtain an exponential profile, as initially supposed, where particles velocity profiles at different heights are represented by videos at different fps.

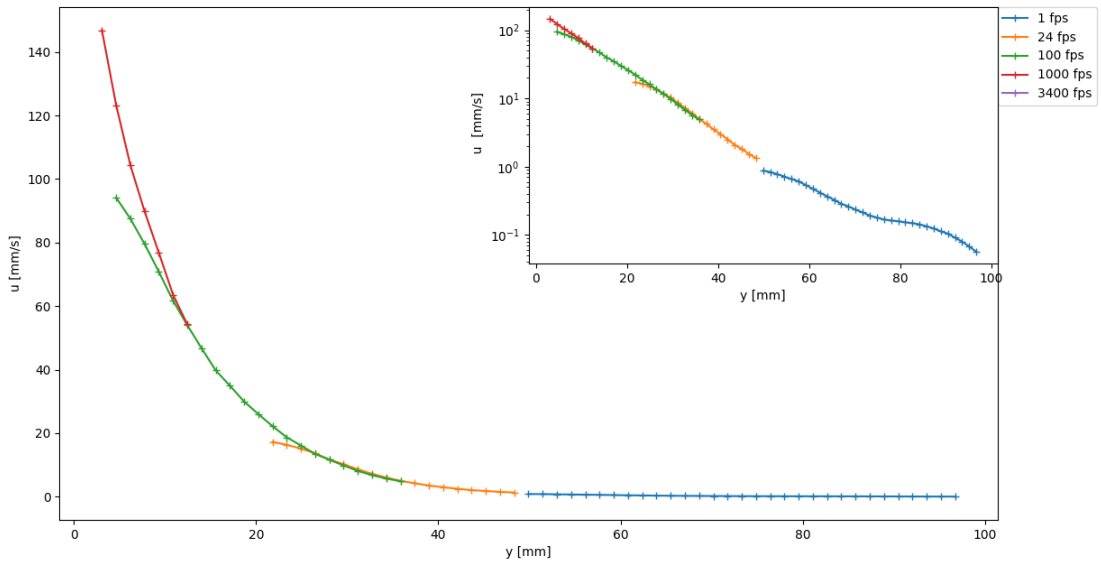

Figure 4.9: Particle velocity profiles of all the videos with the selection criteria applied

The considered parts of the curves are the most reliable ones, so the representativeness is guaranteed. In particular, according to these criteria, it is possible to notice that the contribution of the video shot at 3400 fps is negligible. This is valid only for this experimental setup, but this result suggests that for each different test, depending on the maximum velocity of the system, it will be possible to avoid the

recording at highest or lowest fps, since these videos will not be representative of any layer of particles in the system. The range of values accepted is 0.5 - 10 pixels: filtering the data with this range, the meaningless parts of the curves are disregarded.

4.4 PIV parameters

In the implementation of PIV code, some parameters can be varied by the operator. Therefore, it is required to determine how these parameters affect the results and determine how to set them up. Compiling the code, in fact, it is necessary to choose the size of the interrogation windows; in addiction, the method for the calculation of the signal to noise ratio can vary, as it is for the dimension of the kernel in the filtering procedure. Eventually, the averaging of the values worked out by PIV is coded in a way different than the original one. All these cases are reported below, in this same order. The size of the interrogation window is the first parameters that can be set by the operator. According to the dimension of the interrogation area, the number of particles taken into account will vary. If the window is too big, many particles will be considered and so the velocity vector worked out will be the average of the velocity of all these particles. In this case, the measure will lose representativeness. In the other hand, if the considered area is too little, the displacement of a particle in the time interval could be so long that it gets off the interrogation area, preventing the location of the particle. In this case, the results worked out by the code are not reliable, since the location of the particles in the two consecutive images could be prevented. General indications suggest using power of 2 values, so in this test window sizes are 32, 64 and 128. The scaling factor in this case 10.25, which means that 1 mm correspond in the images to 10.25 pixels. It is know that the particles used in these tests are glass spheres and their diameter is 4 mm. Therefore, if the window size is 32, the interrogation area is not being able to contain at least one particle, while this is possible if the window size is 64. In the case of 128, instead, the number of particles in the window is surely higher than one. This means that the average velocity value considers more than one layer of particles; therefore the calculated velocity is lower than expected. In addition, the representativeness is lower, since the images are split in a smaller number of interrogation areas. Therefore, the curve is shifted to lower

values of y coordinate and velocities are lower as well. On the other hand, the smaller window size shows a bad-looking result, since the curve is irregular and shows really low values. This case is similar to the case previously analysed in this chapter, where the unreliability of the results in case of excessive particle displacements was shown. As in those cases, since the displacement of the particles is bigger than the size of the interrogation window, a lower value of velocity is calculated. Therefore, this value is not correct and it is not reliable. Another fact that deals with these considerations is that the small window leads to unreliable results in particular for the fastest particles, where the displacement is longer. It is possible to notice all these considerations in figure 4.10. In conclusion, it is possible to say that 64 is the best value for the window size. In addition, increasing the size of the interrogation window the time required for running the code decreases, since the images are split in less interrogation areas. As well, fewer calculations are needed, since the fewer collected data. Therefore, assessing the right window size save up time required for the processing of the images.

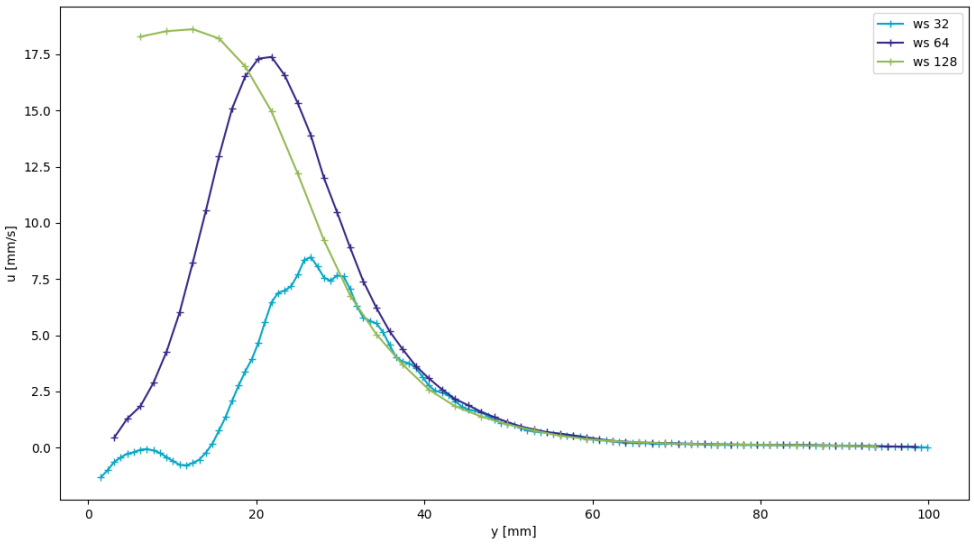

Figure 4.10: Particle velocity profiles varying the window size

The second choice is the method for the calculation of the *signal to noise* ratio. As it is explained in section 3, the software attributes a value for the displacement of each repeating area located on an interrogation area. This procedure is repeated for any considered image. In order to identify the outliers, the ratio between the values of the nearby displacements is calculated. This procedure is required since that likely some outliers will be present, and if they are considered on the averaging they will affect the results. Therefore, applying a *mask*, the code identifies these outliers by calculating their ratio with the nearby values of displacement. In particular, two methods can be applied for this calculation. The peak to peak method calculates the ratio between the first and second highest peaks recorded. Instead, the peak to mean method identifies the representative peaks by their ratio with a mean value of the nearby displacements. The peaks are considered if the values of their ratio are higher than a threshold value, which is 1.3. Decreasing this threshold value cause the omission of variations on velocity higher than that, and so in a loss of information. In opposition, if this value is too high, some outliers could be not filtered. In figure 4.11 it is possible to notice that there is no difference between the two different methods. Curves are slightly different, but the variation is so minimal that the choice of the method can be assumed as irrelevant.

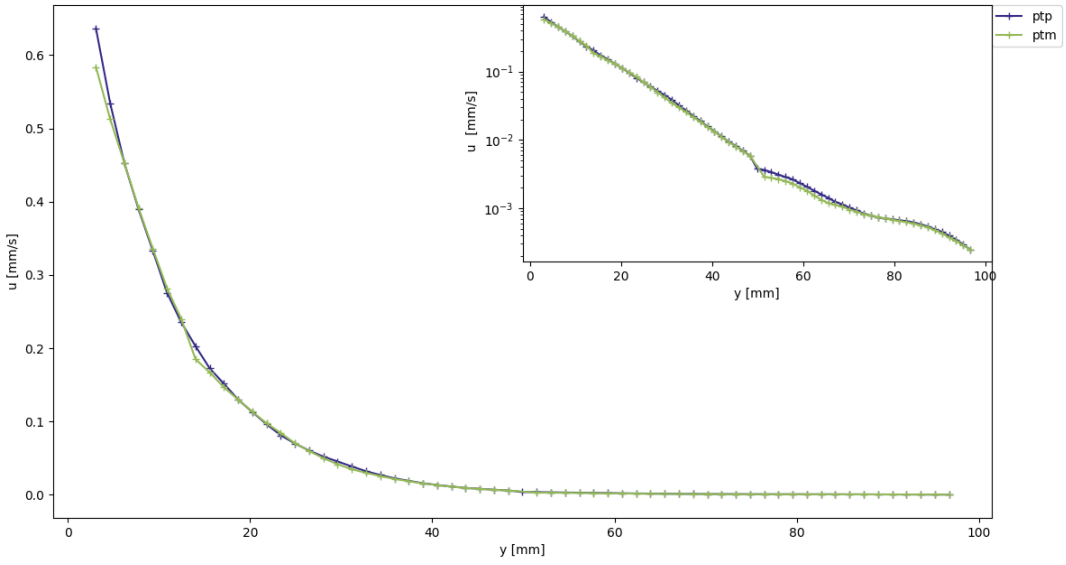

Figure 4.11: Particle velocity profiles varying the *signal to noise* calculation method ; Ω = 23.4 rpm

This calculation is linked to the one mentioned above and allows the software to obtain a smooth field of velocity, improving the PIV results. As it is explained in section 3, the calculation of the outliers values depends on the neighbour values that are considered, i.e. the kernel size. In order to determine how the number of iterations and the kernel size affect the results, the code is run using different values. In figure 4.12 the results are reported: as the legend indicates, three different tests are carried out. In the legend, the number on the left is the maximum number of iterations, while the number on the right is the size of the kernel. It is possible to notice that the curves are nearly perfectly overlapped, which means that a number of iterations higher than 4 in the process of smoothing of the velocity field is rarely reached. This testifies that the approximation in the smoothing procedure is equivalent in the two cases. In addition, it is possible to notice that reducing further the parameters, as in case of curve *ker 2 1*, the representation of the curve is no more possible, since all the values for y lower than 30 are missing.

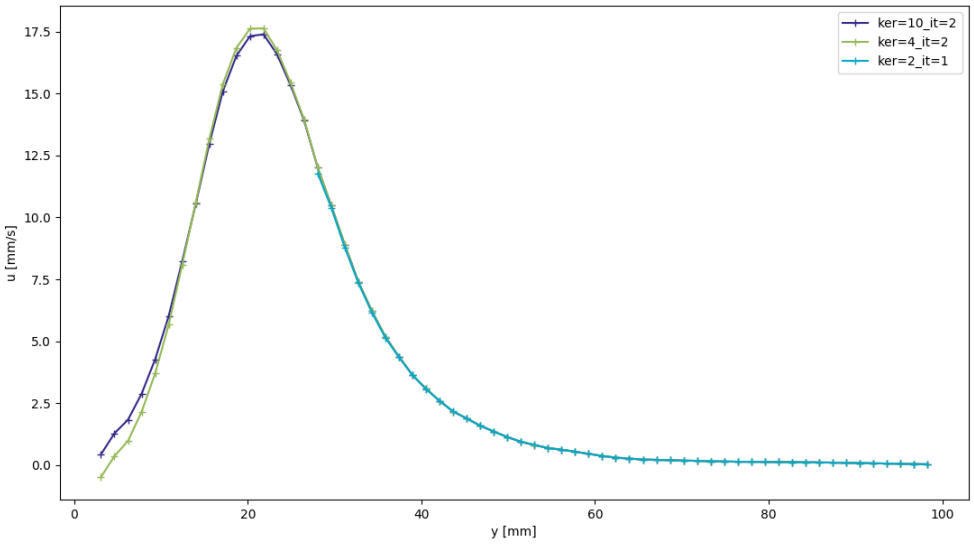

Figure 4.12: Particle velocity profiles varying the dimension of the kernel

As already cited above, this problem depends on how the final averaging is coded. In fact, reducing the possibility of the software in the smoothing procedure, it could be impossible to assess a velocity value. In this case, this means that at least in an i^{th} image for the point whose y coordinate is lower than 30 the contiguous points are NaN and their immediately contiguous points are NaN as well. Therefore, since the

final averaging ads all the values calculated for each image and applies the average, adding a NaN makes all the average to be a NaN. It is possible to fix this problem by modifying the averaging procedure: all the results coming from the different images are collected in a matrix, then the average is carried out disregarding the NaN values. Eventually, the results are obtained and displayed as curves in figure 4.13. As it is indicated in the legend, the new averaging method is applied by reducing the smooth parameters. In fact, in this way it is possible to understand the approximation that the system applies when replacing the outliers. In this way, all the y coordinates of the curve with the smallest parameters are coupled with a velocity value. This means that the applied approximation is less influencing. Nevertheless, comparing the results it is noticed that there is a little difference among the curves. Plotting the curves in a logarithmic scale for the velocity values shows that this difference is negligible, since that the curves are perfectly overlapped. As explained in the previous figures of this chapter, the logarithmic scale is the one used for the representation of the profiles. Therefore, it is possible to state that the averaging procedure does not relevantly influence the results and that the approximation deriving from the smooth procedure is acceptable.

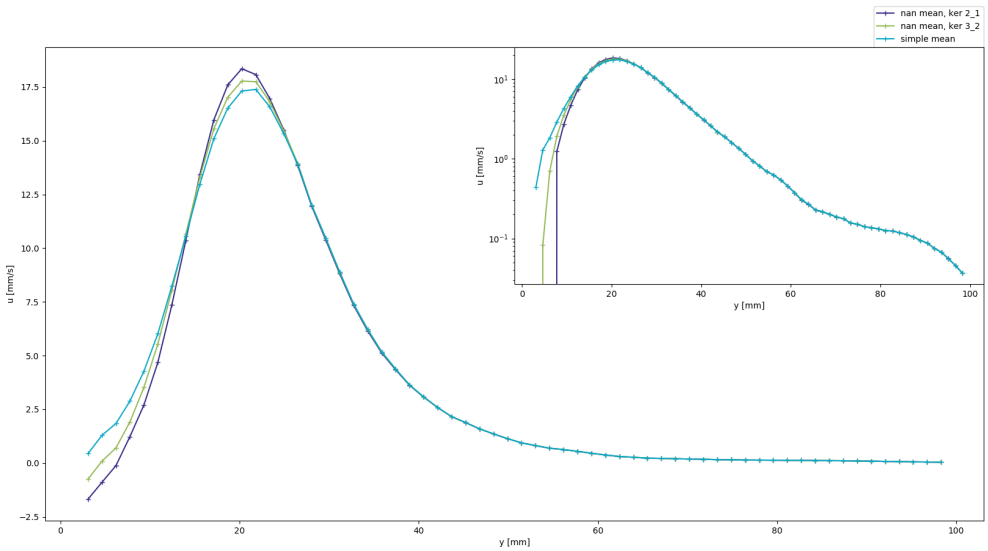

Figure 4.13: Particle velocity profiles varying the method of averaging on the velocity values

4.5 Jamming

A particular problem occurring when rotational velocity is particularly high is that particles tend to compact, since the shearing and the vibrations of the system cause a spatial rearrangement that decrease the free volume among the particles. For this reason, friction is more effective in its distribution between layers of particles and so generally it increases. This causes an increase to the power provided to the engine for keeping the rotational velocity constant, up to a maximum value: when that value is reached, the bottom surface does not rotate anymore and the engine stops. Generally, this problem is defined on the studies about the granular materials as Jamming. This phenomenon occurs when the bulk density is increased, causing the granular material to behave like a solid. Basically, this is due to the reduction of the free space between the particles, which increases the force network between the grains. In addition, it is also linked to the application of a stress, which could be normal but also tangential, as in the case of these tests, but also to the intensity of the stress. The density at which systems jam is determined by many factors, including the shape of their components, the deformability of the particles, frictional interparticle forces, and the degree of polydispersity of the system. [5] Initially, this problem occurred also during these tests: for this reason, it was necessary to expand the particles by lifting up the top surface and moving the particles, in order to modify their settling. This problem is even worse when the weight over the top surface increase, as in test 4: in fact, it occurs also for slower rotational velocities. In addition, also increasing the roughness of surfaces, the problem occurs.

To assume the flow as steady, it is needed that jamming does not cause the stop of the motor. In order to have a rough evaluation of the phenomenon action on the analysed system, it is possible to check the position of the top surface on the videos. In fact, the camera and the experimental apparatus are fixed, therefore the only thing present in the videos that can move on this axe is the top surface (except of the particles). Using the processing image software or by a visual inspection of the experimental apparatus, it is possible to assess a rough approximation of compaction of the flow. It is noticed that the compaction is time dependent, since it increases during time: this behaviour was expected, since jamming is due to rearrangement

of the particles. Increasing angular velocity, load and surface roughness, the same trend is observed, since the reduction of the height of the granular solid is faster by the increasing of these parameters. In particular, increasing the roughness of the surface, the compaction of the granular solid occurs rapidly and the variation of height is roughly the 10%. Furthermore, the load effect is particularly notable when the maximum load is applied, whereas the difference between the minimum and the medium loads is neglectable. Eventually, the effect of the rotational velocity is appreciable just for the case with the higher Ω. Nevertheless, for any configuration of the experimental apparatus the stability of the system is tested, since the rotating surface is run for several minutes before taking the videos. In addition, the system is run at different velocities, verifying that the flow is not affected by any friction internal to the experimental apparatus. In this way, the same compaction is obtained for any test as well. Since the problem is particularly complex, it is not properly faced in this work: just the condition of steady flow is verified. Successive tests will be necessary for deepen the analysis of this phenomenon.

4.6 Forces analysis

In a second time, the analysis turns to the measurement of the forces at the wall, with the aim to identify the effective wall friction and how it changes by the variation of the shear stress. This analysis is carried out by using the force sensors described in section 2. The first step is the implementation of the calibration matrix and the scheme of sensors on the software for the elaboration of the signals. The sensors provide their measurement with a frequency of 5000 values per second. This signal is acquired by the DAQ illustrated in section 2, then the software Dasylab is used for its elaboration, which is a block diagram environment. On the software, a scheme of work is represented: the acquisition of the signal in 6 channels sends the data to a converter, which transfers the data to the display. The converter consists in a conversion matrix, provided by the vendor of the sensors: by the application of this matrix, each signals of voltage is converted into a value of force. Therefore, on the display the values of the forces during the measurement are shown on real time. It is possible to notice that the signal is oscillating, since it is affected by several variables. Since the sensibility of the force sensors is extremely high, it is needed to measure their offset before any test. It is noticed, during the tests, that the offset is not constant: it is affected, for example, by the screw used for the setting up of the experimental apparatus. In fact, depending on how much the fixing screw penetrates into the wall (see figure 2.4), the forces measured by the sensor change. For this reason, it is needed to measure an offset before running each test. In order to do this, the sensors measure the forces when the experimental apparatus is set up and completely empty for 30 seconds. Secondly, when the data are post-processed, the offset is subtracted to the measurement, to get the absolute value of the measured forces. The offset value of the forces is calculated by averaging the measured forces in each direction over the whole duration of the test. In order to test how the forces evolve by changing the angular velocity, the sensor works while the spheres are sheared by the annular surface. The tested velocities are all the ones that can be provided by the electric motor. The test runs continuously and the operator changes the rotational velocity approximately every minute. Successively, it is needed to separate the interval of measurements of each velocity, since the recorder file is unique. With this purpose,

the spectrogram of the data is worked out.

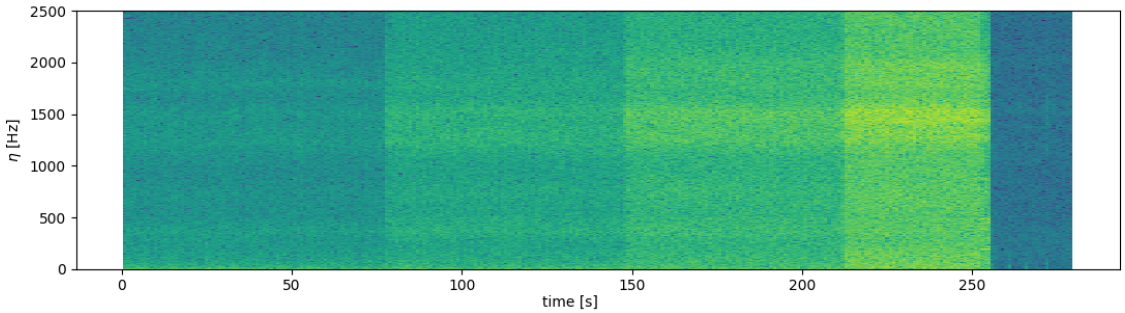

Figure 4.14: Frequency of the signal in time: different colors correspond to different velocities

By this spectrogram (figure 4.14) it is possible to notice that each velocity cause a force signal with many different frequencies, even if just the tangential horizontal force is considered. It is noticed that the energy of the signal in a fixed interval of time increases with the force measured by the sensor. At the same time, the signal energy increases with the velocity and averaging the values in each interval of time, the ratio of the frequencies at different velocities is similar to the ratio of the rotational velocities. The choice of the length of the running interval for each velocity, instead, is influenced by the autocorrelation of the signal. The autocorrelation is the analysis of a signal in time. In fact, since a signal can be very oscillatory in its time evolution, it is required to identify a sampling frequency able to represent the information that is in the signal. It is not possible to consider each point of the signal as representative of the system, since otherwise working on the raw signal would be computationally costly and because the oscillations of the signal are due to the effect of different phenomena. Applying the autocorrelation function consists in verifying if two successive points of the signal in time are related. This is determined by the application of equation 4.6.1, which is function of l, the interval of time between the two points.

$$\phi(l) =< x(t) * x(t+l) > \tag{4.6.1}$$

This average is calculated on the whole duration of the signal, until the conditions of the system are the same. The correlation of two signals is identified by the calculation of the moving average on the signal, where the number of values involved in this calculation depends on l.

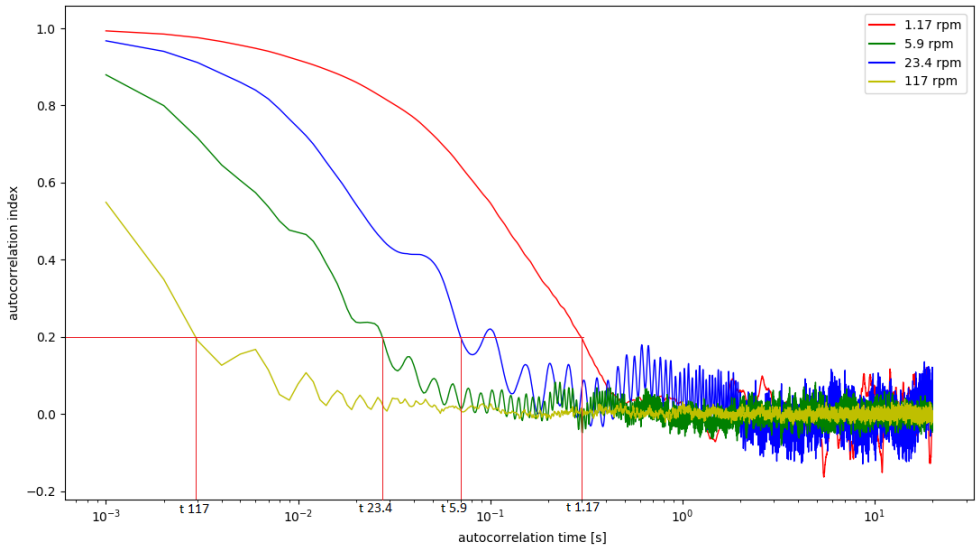

Figure 4.15: Autocorrelation of the signal for different velocities

Curves in figure 4.15 represent the different rotational velocities of the system. The calculated autocorrelation index is based on the force normal to the analysis window. By this calculation, it is possible to identify the periodic part of the signal, since the autocorrelation is positive just for a verified interval of time, which is representative of the characteristic time of the system. After that interval of time, the autocorrelation function decays, since the values of the signal are no more correlated. Assuming that the autocorrelation is ensured when the *autocorrelation index* is 0.2, the code for the calculation of that index is applied to any test. The *autocorrelation index* is the ratio between the autocorrelation calculated on an initial part of the signal, representing the initial time, ad a generic part of it, of a fixed length, measured in subsequent times. It can be seen by figures 4.15 and 4.16 that the autocorrelation time increases when the rotational velocity decreases, whereas for the height of the window analysis the trend is the opposite. Comparing with the velocity profiles of the tests, autocorrelation times increase when the velocity of the particles decreases. Anyway, it can be noticed that the increase of the correlation time in y is slightly smaller than the decrease of the velocity in that coordinate. Therefore, it is possible to assume that there is dependence between the two variables, and this confirms the assumption that the variation of the signals is mainly due to the flowing of the particles in front of the analysis window. The correlation time is mainly affected by the velocity of the particles: other effects,

like some probable modification in the force chains during the flowing of particles, are less relevant. In any case, the most important fact that is verified by the analysis of the autocorrelation time is that this time is smaller than the time of measurements (1 minute): in this way, it is possible to be sure that the signal is not correlated and so that the identified phenomenon is occurring more than once. For this reason, the measurements can be assumed as reliable (from this point of view). Nevertheless, it is possible to notice in figure 4.15 that the autocorrelation time for the slowest rotational velocity measurements is notably higher than the ones of the other cases. In particular, considering the highest window, it is noticed that the correlation of the signal lasts for a long time, comparable to the time of measurement. Therefore, in the successive tests, this velocity will not be analysed, whereas in future tests will be carried out in a longer interval of time.

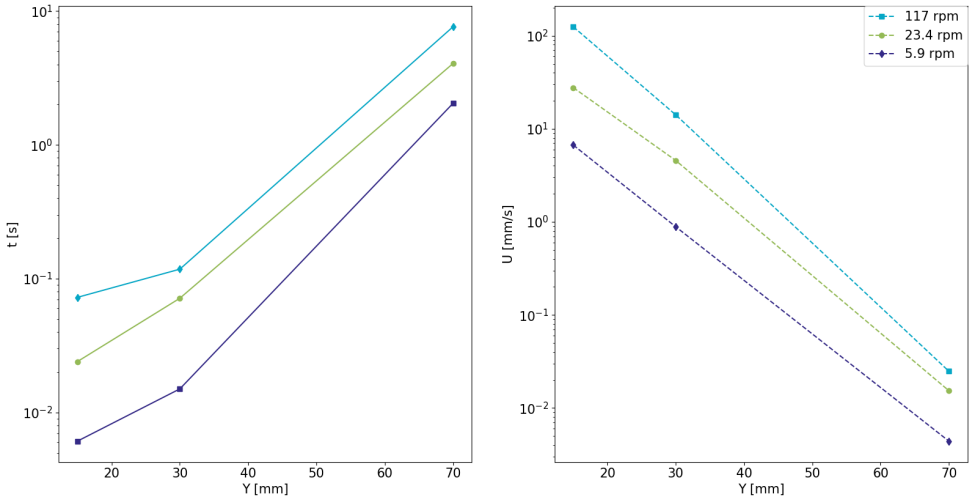

Figure 4.16: Evolution of autocorrelation time (left) and velocity of particles (right) varying the height of analysis windows and of the particles, respectively.

Once the intervals of the signal at constant velocity are identified, all the forces are calculated as the average of the force in that interval. Then, subtracting to this value the offset previously calculated, the measurement of the average force on the 3 directions for each rotational velocity is worked out. In conclusion, the averaged values of the force are used for calculating the effective wall friction coefficient in each inteerval, as the ratio between the values of tangential horizontal force and normal force 4.6.2.

$$\mu_{wf} = < F_x > / < F_y > \tag{4.6.2}$$

It is possible to calculate an error on this measure, according to the averaging procedure applied. In fact, since the huge amount of data is sampled in many intervals and averaged, it is possible to calculate the dispersion of sample means around the population means. Therefore, the standard error will be defined as the ratio of the standard deviation of the sample means and square root of the numbers of samples. The entire procedure is run by the appropriate script in Python.

4.7 Calibration of the force sensor

Using the sensors described in the section 2, the network of forces in the flowing granular material is described. In particular, the effect of the wall on the particles flowing is quantified by measuring their interaction. The sensors report the forces in the three axes: F_x are the horizontal forces, F_y are the vertical forces and F_z are the normal forces, referring to the window of analysis. Then, the measurements are averaged in time intervals: this procedure is carried out for any different velocity tested. Several tests are carried out (Table 4.1) in order to examine how the flow of the particles is affected by the friction. The variables that characterize the tests are the angular velocity of the bottom surface, the load on the top surface and the position of the analysis window in vertical coordinate. Referring to the analysis window described in the section 2, some tests are carried out in order to define which is the most appropriate shape. For each condition, 3 different masses are loaded on the top surface, so that the load are, respectively 0.2 Kg, 1.1 Kg and 5.5 Kg. Moreover, in all the case the tested velocities are 4: 1.17 rpm, 5.9 rpm, 23.4 rpm, 117 rpm. The height of the granular solid in the first two tests is just 5 cm, whereas the height in the last two tests is 10 cm : nevertheless, concerning the aim of these tests, this difference is not relevant. In Table 4.1 the tests carried out are rapidly resumed.

There is no difference on the setting procedure for the different windows: the laser cutting is applied in the same way. Therefore, the quality of the work does not affect the choice of the window shape. At the same time, the cutting is realized in the same

Table 4.1: Different conditions of the calibration tests.

Height of window (mm)	*Window size* (mm)	*Shape*
30	20x20	Square
30	20 (d)	Circular
15	20x20	Square
15	20x40	Rectangular

time (a specialized enterprise is charged of the work) and also the fixing of the sensor apparatus follows the same procedure. In this frame, it is possible to define which is the best shape for the window only by considering the quality of the measurements. Three different shapes are considered: circle, square and rectangle. The reason of these choices is to adapt the windows to the shape of the experimental apparatus (in particular, to the cylinder) and, at the same time, to obtain a uniform flow while the particle is in contact with the wall. Based on this same purpose, also the size of the windows is set as 20 mm for the first comparison, whereas in the second case the length of the window is increased, in order to increase the area. Since the shape of the velocity profile is well known, if the area of the window is too extended it would represent layers of particles which velocity is notably different. Therefore, the quality of averaging and of the successive comparison with the velocity profiles would be poor. The first comparison concerns the square and the circular windows. Three tests are carried out for any window, since the load on the top surface is increased along the tests. The data are collected and processed as described in section 4.6.

Since the aim of this test is the choice of the most suitable shape for the window analysis, the effect of the other variables on the measurement is set aside, at the moment. In the left side of figure 4.17 it is noticed that the magnitude of F_z, which represents the forces normal to the wall, is higher for the squared window. This trend is confirmed in each case, so it is possible to assume that it is due only to the different shape of the analysis window. This result agrees with the expectations: since the surface of the squared window is larger, more particles interact with the window and so the measured force is higher. In fact, in the right side of figure 4.17, the magnitudes of the force are scaled by the surface of the window. The profiles are nearly the same: only in the case where the load is 5.5 Kg, the forces are not properly scaled by the

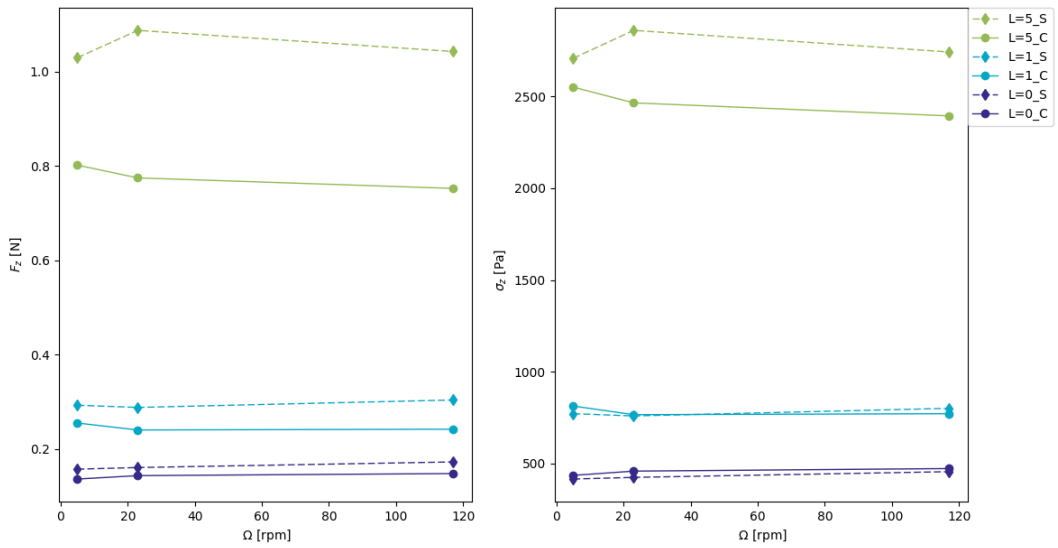

Figure 4.17: Normal Forces (left) and stresses (right) with square window (dashed lines) and circular window (solid lines). 3 different loads (L)

area. Therefore, the squared window is the most proper analysis window compared to the circular one, since the aim is to obtain the highest value of the force. In this way, the instrumental error on the measure, which is a fixed percentage of the measure, would affect the result in a slighter way. The same test is carried out by changing the size and the shape of the window. In this test, in fact, the squared window is compared with a rectangular window, whose longest side is 40 mm. In this way, the surface of the window is doubled, therefore it is expected that the measures of the forces double as well.

The results agree with the expectations. In fact, considering the left side of figure 4.18, the measurements of the forces using the rectangular window are roughly two times the measurement with the square window. Also in this case, scaling the forces by the surface of the windows, the results overlap, as it is reported in the right side of figure 4.18. Therefore, it is possible to assume that using the rectangular window the measured forces are higher and so less sensitive to instrumental error. Nevertheless, since the successive analysis concern the effective wall friction, it is necessary to compare this physical quantity as well. Since the effective vertical wall friction is calculated as the ratio between the vertical tangent stress and the normal stress, it is expected that its value is independent off the size of the analysis window.

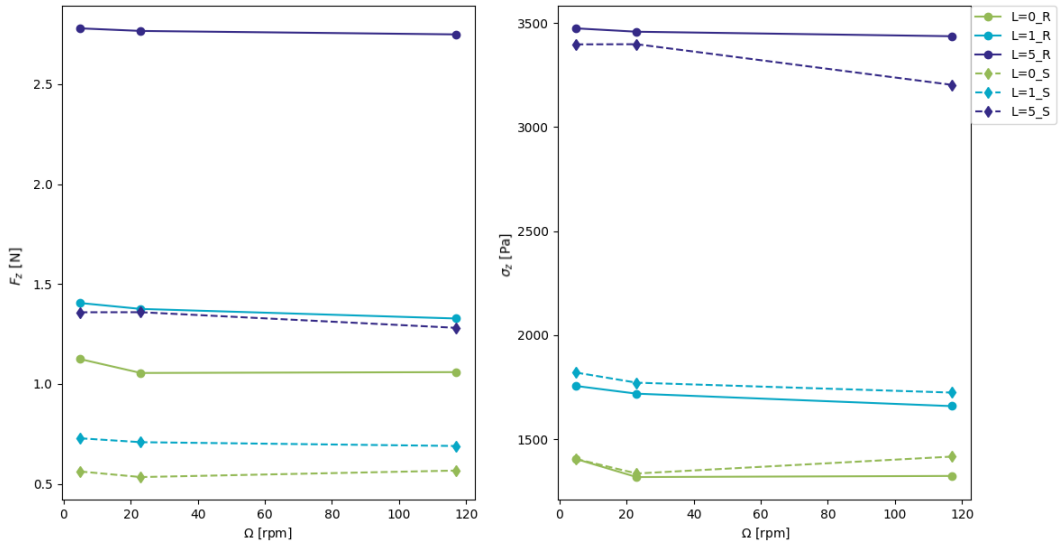

Figure 4.18: Normal Forces (left) and stresses (right) with square window (dashed lines) and rectangular window (solid lines)3 different loads (L).

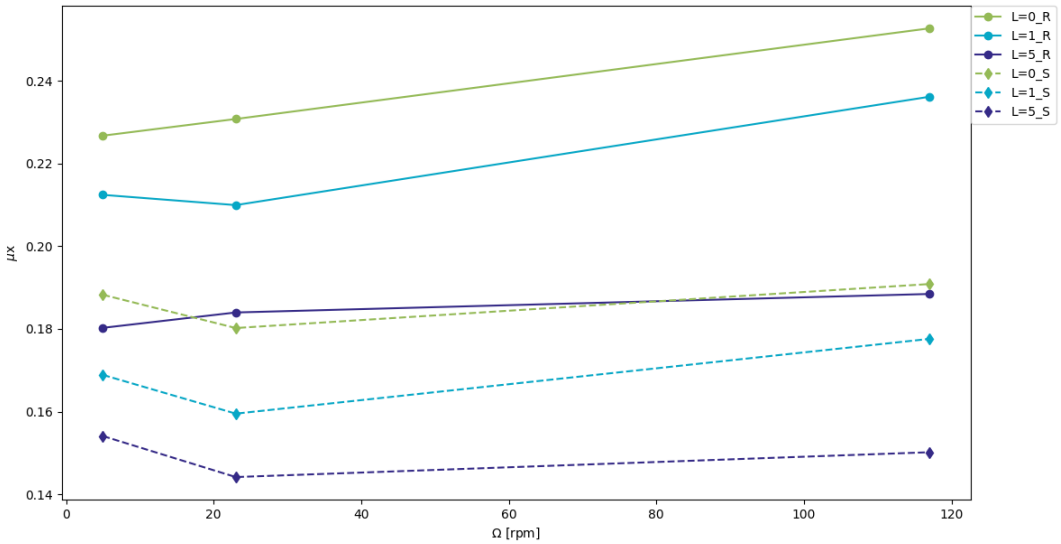

Figure 4.19: Effective horizontal wall friction coefficient with square window (dashed lines) and rectangular window (solid lines).3 different loads (L)

In figure 4.19, it is noticed that the ratio between the forces on x and y directions does not scale with the area of the analysis window; therefore, this result is surprising. In particular, analysing the data, the curves are nearly overlapped by scaling the force on x of the rectangular window by a factor of 1.3. This factor is constant for any condition, since it has the same effect for each curve. Therefore, the tangential

horizontal forces do not scale with the surface size, but they are overestimated of 30%. This means that the measurement of the effective wall friction calculated with the rectangular windows is different than the one calculated with the square windows. This particular behaviour can be ascribed to the trend of the rectangular window to straighten: in fact, since it is longer, it tends to relax the internal forces that make it to be curve. This causes a slight difference between the cylinder and the window, so the regularity of the surface is not respected. Moreover, if the surface is not smooth as normal, some particles could bump into the emerging part of the window, causing an irregularity on the measurements. Since other tests would be necessary in order to establish the correlation between the shape of the window and the overestimation of F_x, the square window is chosen. In fact, in the calculation of the effective wall friction coefficient with the square and the circular windows, the same values are obtained; therefore, the square window seems more reliable.

CHAPTER 5

Results

5.1 Velocity profiles

In this chapter, the results coming from the all the tests are discussed. The topic of these tests is the description of the horizontal velocity profiles of a granular solid flowing in a cylinder, where a torsional shear stress is applied. From these profiles, it is possible to describe the shear band of the granular solid. In particular, the effect of the operative parameters on the shear band width is studied, where the shear band width is the section of the granular solid where the shear rate is different than 0. In that band, the velocity profile varies over the spatial coordinate. The shear stress is applied by a rotational bottom surface, whereas is top surface is static. Both the surfaces are rough, so that particles motion is due to the friction between the surface and the particles. Starting from previous studies carried out on similar configurations [2], some parameters that influence the flow of the granular solid in this configuration are identified. In these tests, four of them are considered: rotational velocity of the bottom surface; normal stress on the granular solid layers; height of the granular solid; roughness of top and bottom surfaces. The particles of the granular solid are glass spheres: their diameter is 4 mm and, in order to ensure this, they were sieved before the tests. Frictions between particles and between particles and walls

are considered as similar, even if the particles are made of glass and the cylinders are made of PMMA. These beads are used since they are spherical: it could be possible in a second time to extend the obtained results to particles with a different shape, using suitable correlations. For simplicity, the motion of the bottom surface is considered as continuous and so the flow of the granular solid is steady. The problem about this consideration is discussed in the final part of the chapter 4. During the tests the flow is never interrupted and the operative conditions are unchanged; therefore the consolidation problem is verified at steady state.

Table 5.1: Configurations of the experimental apparatus for the tests

Test	*Height* (cm)	*Load* (Kg)
1 to 3	10	1.1
4 to 6	10	5.5
7 to 9	10	0.2
10 to 12	7	1.1
13 to 15	7	5.5
16 to 18	7	0.2
19 to 21	4	1.1
22 to 24	4	5.5
25 to 27	4	0.2

5.1.1 Rotational velocity

In Table 5.1 all the tests carried out are reported. For each condition of height and load, 3 velocities are tested. This set of tests considers all the influencing parameters. The units of measurement are reported: rotational velocities of bottom surface correspond to tangential velocities of particles at the cylinder surface which are, respectively, 57.7, 230.6 and 1153 mm/s. These are the highest velocities that can be measured in the systems in each test, since even the velocities of the particles in direct contact with the surface will be lower, due to the slip, as it will be successively described. In the first 3 figures, velocity profiles are compared: these profiles are obtained by varying the rotational velocity of the bottom surface. The difference among the pictures is the mass of the load over the top surface. The mass over the top surface is represented by some iron cubes of known mass that are added

over the surface, taking care that a uniform distribution is obtained. The velocity profiles are represented in a scaled form: the height of the granular solid is scaled over the diameter of the particles (y/d), while the horizontal velocity is scaled over the tangential velocity of the bottom surface at the wall ($u/\Omega R$) (in the left part of the figures) and over the highest velocity among the particles in the right part of the figures ($u/u0$). In addition, the so scaled velocity is additively scaled as logarithmic in the bottom right part of figures. The first aim is to understand the effect of the rotational velocity on the velocity profile of the particles, verifying the uniformity of the identified behavior among different pressures on the particles. Initially, the height of the granular solid is kept constant, therefore only those two parameters are studied. The calculations on these tests concern the horizontal tangential velocities of the particles on the cylinders surface.

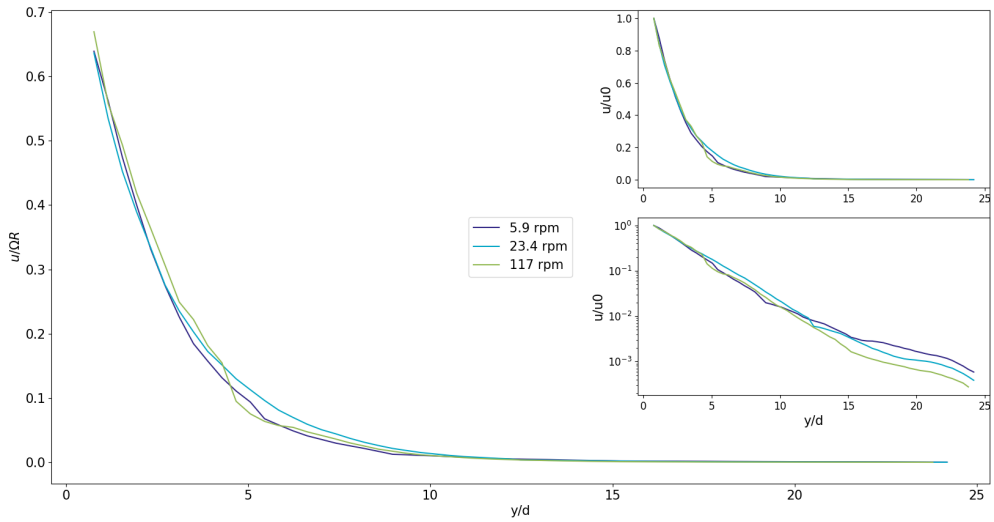

Figure 5.1: Particle velocity profiles varying the rotational velocity ; Load = 1.1 kg ; Particle Height = 10 cm

In figure 5.1, it is possible to notice that the values of scaled velocities are similar. From previous suppositions, the velocity profile is assumed to be exponential, which means that they look linear in a logarithmic scale. It is also true that velocities of particles vary among a broad interval, so the representation in a linear scale hides the differences between the relatively slowest particles, and this is an additional reason to show the logarithmic plot. The exponential decay of the velocity is confirmed and this is valid for all the tested rotational velocities. It is possible to assume that the

shape of velocity profiles is independent on the velocity of the bottom surface, since they look similar. Similarity is assumed since the exponential decays are the same: the velocity decreases exponentially getting further from the bottom surface. All the three profiles have a similar slope of decay, comparing the figures 5.1. It is possible to define this behavior as an exponential decay since the difference of the orders of magnitude between fastest and lowest particles is at least 2. In addition, it is possible to say that the profiles are nearly overlapped for heights lower than 12 particle diameters, then they show some difference. In fact, it is noticed that, when the fastest velocity is applied, the particles are slower compared to the other profiles, taking into account that they are scaled by the highest velocity in their system. Therefore, it seems that the decay of the velocity is slightly increased as higher the rotational velocity is. Anyway, the difference among the profiles is small. Another thing that is noticed is that the exponential decay could be split in two different parts: where *y/d* is larger than a certain value, the exponential decay of the profiles flattens. From that coordinate on, the slope of the decay decreases, and this particular behavior is noticed in all the curves. In addition, since the profiles diverge, increasing the rotational velocity decrease the velocity of the particles when the exponential velocity profile change its slope. In fact, the flattening for the first curve occurs when scaled velocity *u/u0* is nearly 0.01, while in the fastest cases the scaled velocity is about 0.001. In the same way, the *y/d* coordinate where this flattening occurs varies in all the cases, in particular the vertical point of flattening is lower for the lowest rotational velocity. The flattening point is defined by approximating the profiles with two exponential curves: each one is suitable to the different part of the profile. Nevertheless, the analysis is qualitative and this particular behaviour will not be deeply analysed in this thesis. In conclusion, the shape of the velocity profiles is similar by changing the rotational velocity of the bottom surface. Some differences are noticed, therefore it is needed to compare if the velocity profiles vary similarly in different conditions. In order to do this, other tests are carried out by adding over the top surfaces other iron cubes. In this way, it is possible to increase the pressure on the particles. The influence of this parameter will be successively studied, indeed. At the moment, figures 5.2 and 5.3 are considered in order to confirm the suppositions concerning the effect of rotational velocity. In the second test, all the three velocities are applied:

the difference is that in this case the load over the particles is 5.5 Kg, while in the first case the load was 1.1 Kg: this weight considers also the mass of the top surface and the structure above it. In the third case, no masses are loaded over the top, then the only load is the one of the top surface's structure (0.2 Kg). The masses over the top surface are distributed as more equally as possible.

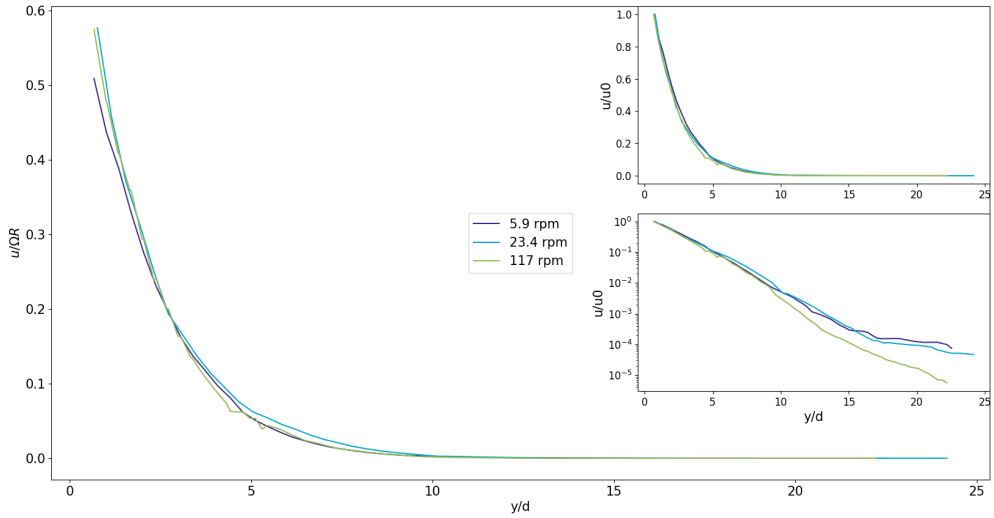

Figure 5.2: Particle velocity profiles varying the rotational velocity ; Load = 5.5 Kg ; Particle Height = 10 cm

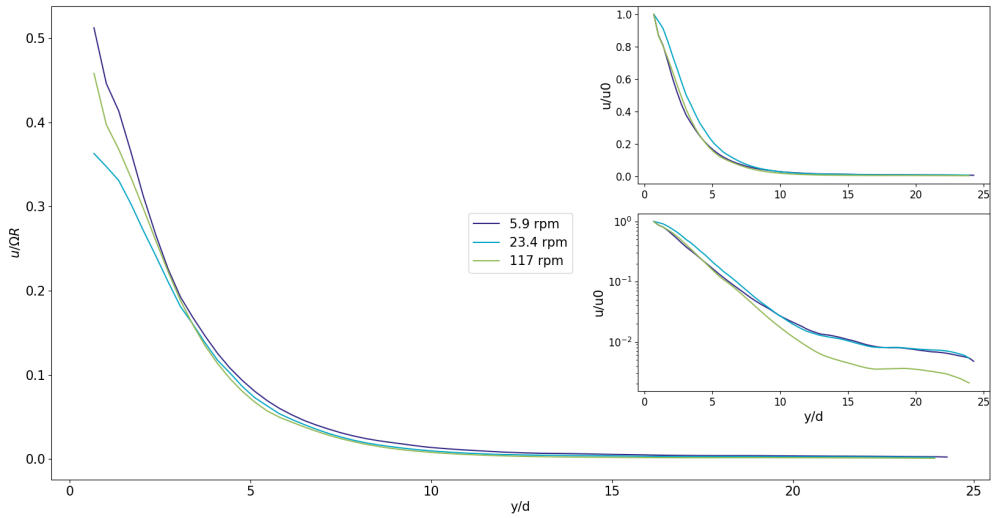

Figure 5.3: Particle velocity profiles varying the rotational velocity ; Load = 0.2 Kg ; Particle Height = 10 cm

Also in these cases, velocity profiles are nearly overlapped for *y/d* values up to 10/12, then they diverge and the higher velocity profile keeps on decreasing, while the other profiles start flattening. In addition, it is verified that the variation of the slope of the velocity profiles occur at a smaller scaled velocity for the fastest case profile. One difference is that the velocity profiles of the slowest cases for the lowest load are perfectly overlapped, whereas in the other case they are slightly different, but that difference is negligible. In conclusion, it is possible to say that the shape of the profiles is basically the same for any value of velocity tested. The assumption of an exponential profile is verified, independently on the velocity of the bottom surface. The only notable difference between the profiles is the scaled velocity value the curves reach when they start flattening. About this problem, it seems that increasing the velocity of the bottom surface the velocity profile is lower, which corresponds to lower values of scaled velocity. This means that increasing the rotational velocity, the width of the shear band is smaller. From the figures it is possible to notice that the main difference between the velocity profiles concern the slowest particles, the ones further to the bottom. In fact, these differences are notable just on the logarithmic representation, whereas the linear representations are similar for any velocity. In conclusion, it is possible to say that the velocity profiles slightly vary with the variation of the rotational velocity, but their shape is independent on this operative parameter.

5.1.2 Load on the top surface

In the figures 5.4, 5.5 and 5.6, bottom velocity is constant, whereas the load on the top surface varies. Similarly to the first analysis, the velocities are scaled with the tangential velocity of the bottom surface (on the left side) and with the fastest velocity identified among the particles, in the bottom interrogation area (on the right side). The loads over the particles are the ones cited above. Since the particles'weight is in this case is 3.28 Kg, the analyzed cases can be related to the mass of the granular solid: calculating the ratio between the added mass and the total weight of the system (sum of masses and spheres weight), the cases result to be roughly 1/20, 1/5 and 1/3. In the figures 5.4, 5.5 and 5.6 the bottom velocities tested are respectively 5.9,

23.4 and 117 rpm. The first thing is noticed from the figure 5.4 is that, increasing the load, the exponential decay is steeper. Scaling the velocity over the bottom tangential velocity and plotting the same curves, this is not particularly clear, since in the left part of the curves this behavior is absent. On the other side, in the logarithmic curves, for y/d values lower than 5, the curves are overlapped; but from that value on the curves have different trajectories. Increasing the load over the top surface, the curve is steeper and reaches lower velocity values. Also in this case, at 13/17 y/d the slope of the curve changes and the curve flattens. In that zone, in particular, it is possible to notice the difference between the curves. In addition, it is possible to notice that there is a higher difference among the curves representing 1.1 and 5.5 Kg loads than between the 0.2 and 1.1 Kg loads. The last case is much lower compared to the second cased, whereas the difference among first and second curves is smaller. This difference was expected, since there is a relevant difference among the masses added in the different cases and the effect on the velocity profiles depends on that parameter.

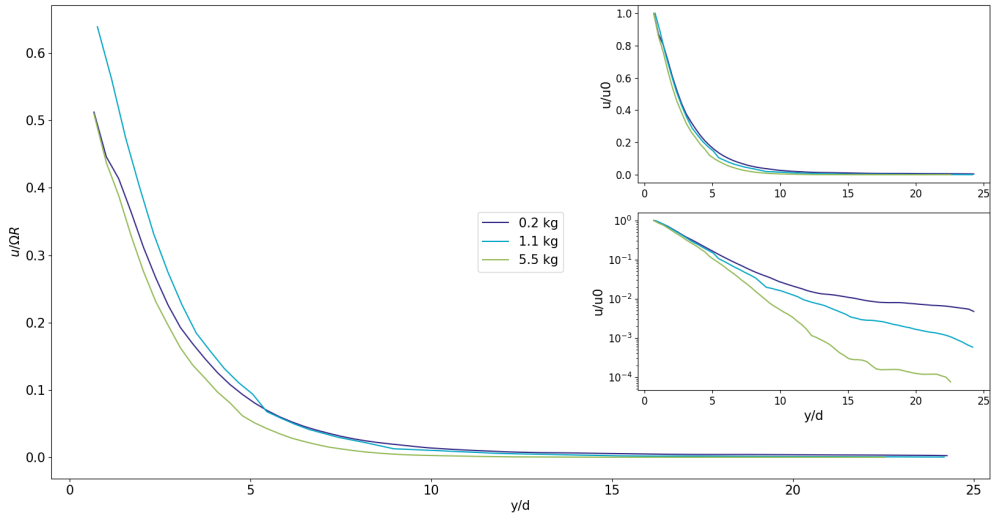

Figure 5.4: Particle velocity profiles varying the load over the top ; Ω = 5.9 rpm ; Particle Height = 10 cm

From the steepness of the curves comes the most relevant observation: increasing the load, the velocities of the furthest particles from the bottom becomes lower. Therefore, since the driven force for the motion is exactly the same, this means that the load increase the difficulty of the system to make the different layers of particles

move. Literally, the width of the shear zone is reduced by the increase of the pressure on the granular solid, since the particles slow down in a shorter distance getting far from the source of motion. This means that a higher shear rate is required in order to obtain the same motion of the particles.

Similar considerations come from the figures 5.5 and 5.6. It is possible to notice that the flattening of the curve occurs differently depending on the load: for the 0.2 load case, the slope changes at 13 y/d ; for the medium case, the flattening occurs at 15 y/d whereas in the last case the coordinate is about 17 y/d. In addition, in the three figures it is possible to notice that in the left figure, where each curve is scaled on the same number, it is particularly complicated to identify a relation between curves and loads. In fact, the 0.2 load curve is lower than the 1.1 load curve, but it is higher than the 5.5 load curve. Even, for y/d values close to 0, in second and third cases they have 0.2 load curve higher than the 5.5 load curve. Therefore, there are no trends that links load and velocity profiles. On the other hand, scaling the velocity with the maximum velocity of the particles, the trend which is notable by the linear profile is the same that is noticed by the logarithmic figures and it agrees with the previous considerations.

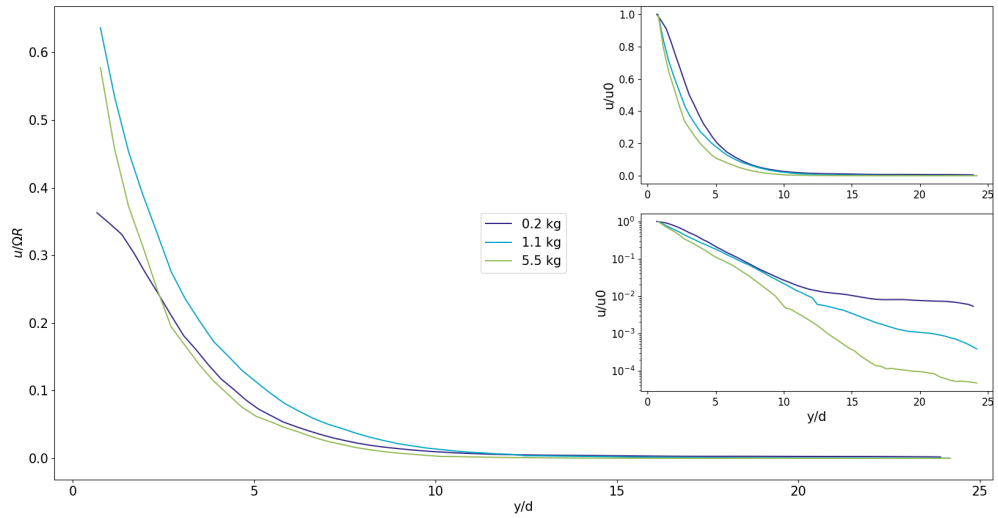

Figure 5.5: Particle velocity profiles varying the load over the top ; Ω = 23.4 rpm ; Particle Height = 10 cm

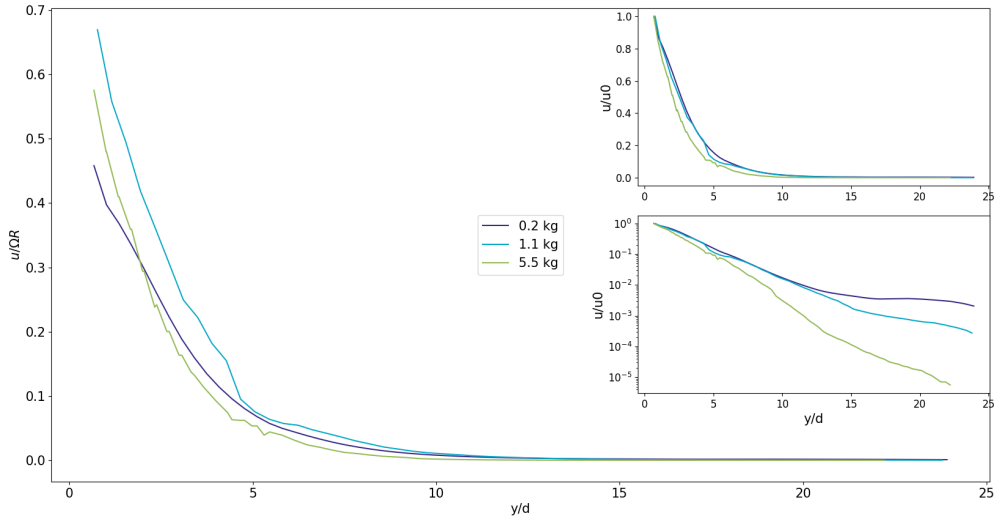

Figure 5.6: Particle velocity profiles varying the load over the top ; Ω = 117 rpm ; Particle Height = 10 cm

This particular result suggests the analysis of a further problem. This particular behavior of the highest values of particles velocity can be partially noticed also in the first three figures, in particular from the third one. The fact is that the flow of the particles is due to the friction with the bottom surface. But the particles are not integral with the surface, so they are influenced by the friction in different ways: in fact, it is known that the particles can slip. Therefore, as it is possible to notice from the left part of all the figures, scaling the velocity of the particles over the tangential velocity of the bottom surface, the obtained values are included between 0 and 1. This means that in any case the absolute velocity values are smaller than the tangential bottom velocity; therefore there is a loss of kinetic energy in this transmission. Other experiments will be carried out in order to identify how the slip velocity (u_0) is dependent on the roughness of the source of motion. On the other hand, it is possible to verify how velocity and load interact with this behavior. In fact, it is possible to describe all the velocity profiles using the equation 5.1.1

$$u = u_0 exp(\frac{-y}{\delta}) \tag{5.1.1}$$

where u is the particles horizontal velocity; u_0 is the maximum velocity of the particles; y is the height of the granular solid and δ is the coefficient of the exponential

decay. Therefore, u_0 depends on the slip mentioned above, where the slip depends on all the system variables. At the same time, the decay ratio is dependent on the variables tested in this work. In order to obtain a value for the normalized highest velocity, an interpolation is applied. In this way it is possible to obtain the trend of the curves in the logarithmic figure and the initial value for y=0, which is the u_0 indicated in the equation 5.1.1. In the same way, the value of δ is obtained by the slope of a linear interpolation carried out on the exponential scaled figures. Just the constant slope part of the curve is considered; therefore the interpolation is carried out up to 15 y/d values.The results are shown in figure 5.7, where the dependency on velocity is shown, whereas on figure 5.8 the dependency on the load is displayed. As previously described, it is possible to notice that increasing the pressure, δ increases, so the exponential decay is steeper and the velocity profile is lower. Regarding the velocity, the trend seems to be similar, even if the difference is noticed mainly between the highest mass and the lowest ones. In fact, increasing the velocity, the exponential decay coefficient seems to slightly increase. If the decay coefficient increases, the velocity of the particles decreases more rapidly by the increasing of the height. It is possible to identify the decay ratio as the steepness of the curves in the logarithmic scaled figure. Instead, concerning the slip velocity, it is not possible to identify a trend: different results come from the studied cases. In fact, studying the velocity dependence, the slip verified on the medium rotational velocity case has the slowest value. Meanwhile, the load dependence shows a clearer trend, since the maximum velocity increases if the mass increases: anyway, the difference between the increase of the velocities and the increases between the masses is not well proportionated. In fact, the higher difference is between 0.2 Kg and 1.1 Kg of added mass, whereas 1.1 Kg and 5.5 Kg of added mass show similar values. A possible interpretation to the dependence on load is that, increasing the load, the friction between the particle layers increases: at the same time, the friction between the bottom surface and the particles increases as well, so the transmission of kinetic energy is more efficient. Regarding the influence of velocity, instead, the dispersion of u_0 values could be interpreted as a lack of direct influence on this parameter of the rotational velocity. Other tests will be carried out in the next cases, where the height of particles will vary. It is expected that the load and the rotational velocity will have similar influences on

the same level tests.

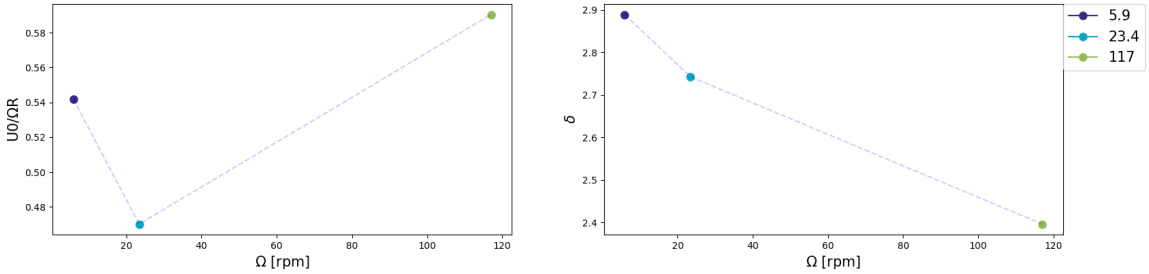

Figure 5.7: Slip velocity (left) and exponential decay coefficient (right) varying the rotational velocity ; L=1.1 Kg ; H=10 cm

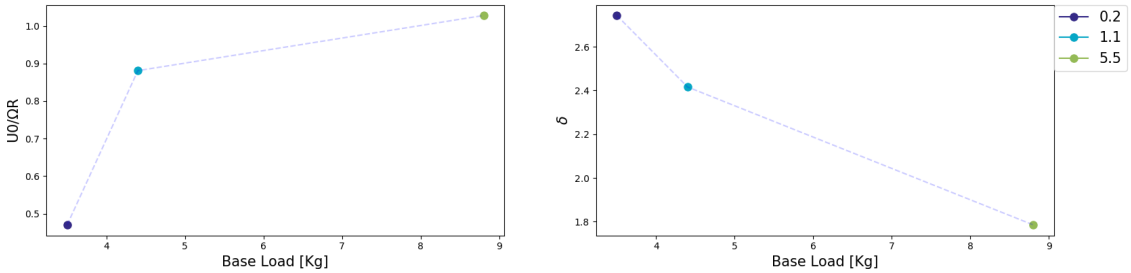

Figure 5.8: Slip velocity (left) and exponential decay coefficient (right) varying the load ; Ω = 23.4 rpm; H=10 cm

5.1.3 Height of the granular bed

In the second and third series of experiments, the height of the granular bed changes. The mass of particles between the two cylinders is reduced of about 1.1 Kg; therefore the heights are 3 cm less than the first series. In this way, it is possible to verify how the velocity profiles are influenced by the height of the granular solids, but also to identify how the other parameters affect the system in these different situations. Nevertheless, the same parameters were changed in the first series are changed in these ones. Firstly, the medium height is analyzed, corresponding to a mass of particles of 2.3 Kg. The velocity profiles for varying rotational velocities at constant load are displayed in figure 5.9.

It is possible to notice that the velocity profiles are still exponential, since the decrease is of two orders of magnitude. In fact, in the linear figures, the profiles look similar to the one displayed before. In addition, in the logarithmic scaled figure, the curves are perfectly straight. In fact, comparing with the curves obtained for the 10

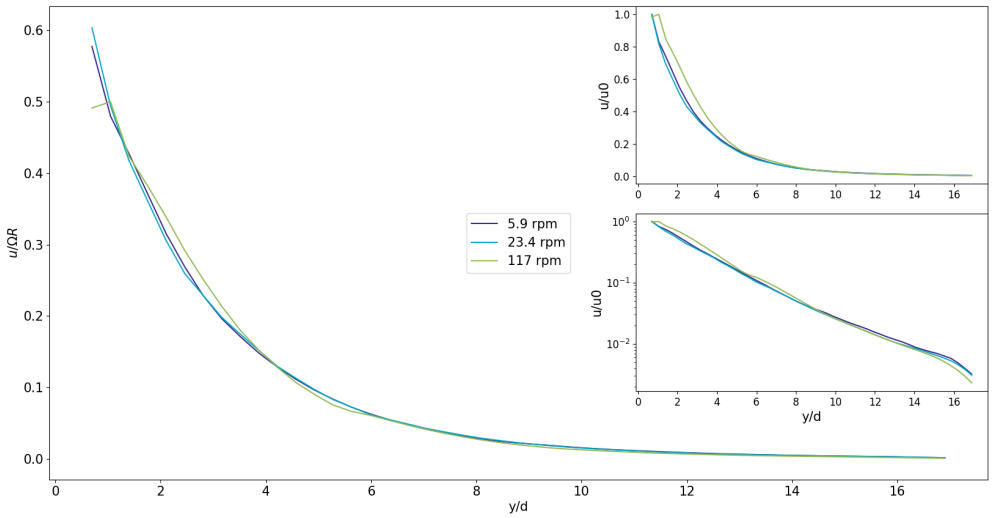

Figure 5.9: Particle velocity profiles varying the rotational velocity ; Load = 1.1 Kg ; Particle Height = 7 cm

cm height (figure 5.1) the variation of slope is absent: the curve is no more flattened. It is possible to assume that the flattening that occurs in the highest case could depend on the particles that are present above the particle layers, which influence the transmission of kinetic energy between the lower layers. In addition, the velocity profiles are exactly overlapped; therefore in this case the dependency on the rotational velocity is completely absent. The same thing could be said by the analysis of the velocity profiles changing the load on the top surface, therefore that pictures are not presented. Secondly, the masses on the top surface are varied, whereas the rotational velocity is kept as constant (23.4 rpm). The results are displayed in figure 5.10.

Also in this case, the results look similar to those obtained for in the previous tests. Increasing the weight of the masses loaded on the top, the particles slow down in a shorter distance ; therefore the decay coefficient increases. From the logarithmic figure, the difference between the different loads seems to be constant, so there is not a direct dependency among the mass of the added load and the exponential decay of the velocity profiles: it is just possible to say that, similarly to the previous case, increasing the load, the decay ratio is decreased. In conclusion, it is possible to say that increasing the load on the top surface the particles velocity decrease in shorter distance from the source of motion and that lower velocities are reached by the top particles. The profiles obtained by changing the rotational velocity of the bottom

surface look similar to these ones, so they are not reported. The same comparisons are carried out on the case where the height of the particles is 4 cm, so the mass of particles is 1.3 Kg. Comparing the velocity profiles varying the bottom surface velocity, they look similar to the 7 cm case.

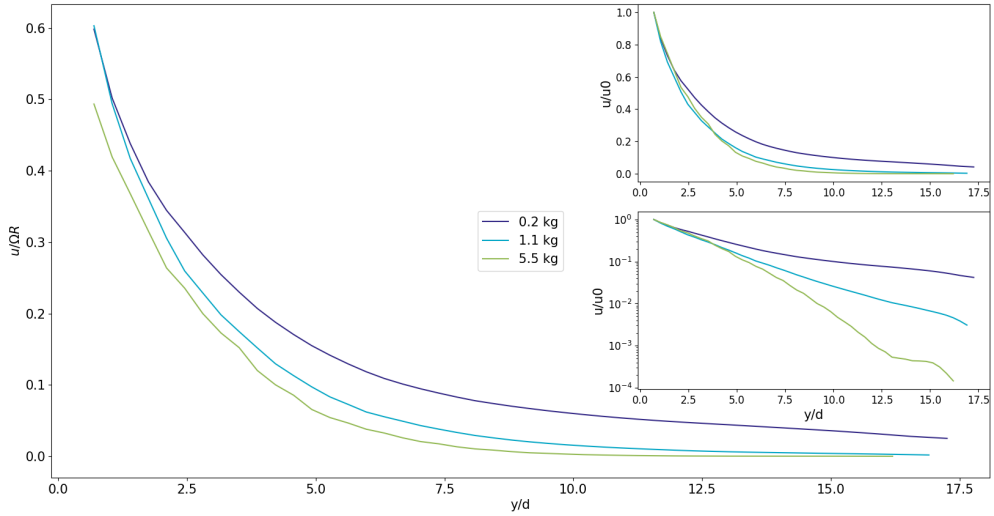

Figure 5.10: Particle velocity profiles varying the load on top ; Ω = 23.4 rpm ; Particle Height = 7 cm

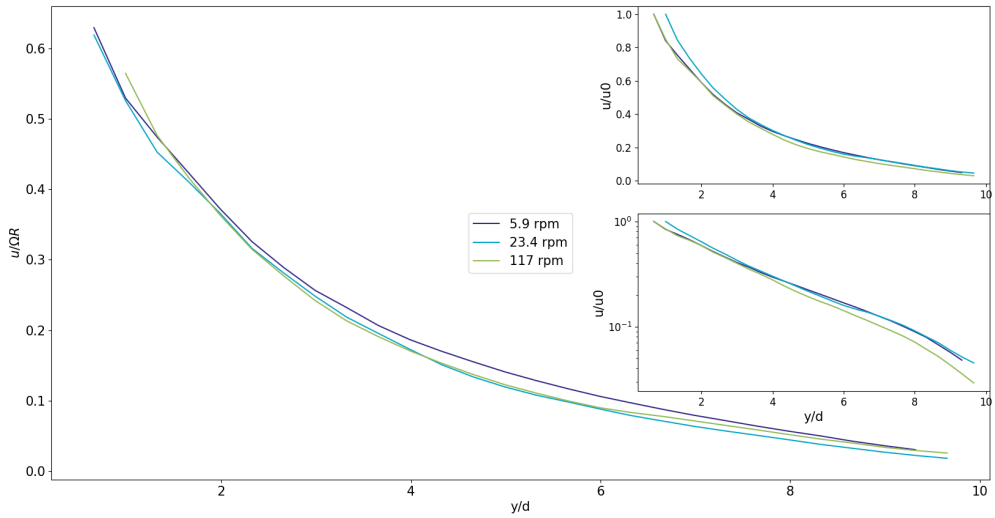

Figure 5.11: Particle velocity profiles varying the rotational velocity ; Load = 1.1 Kg ; Particle Height = 4 cm

From the figure 5.11, it is noticed that the velocity profiles are overlapped all along their length: the highest velocity case has a slightly higher decrease, but the

relative difference is so small that they can be assumed as coincident. The profiles are overlapped also in the linear scale. Profiles are shorter, as the height of the granular solid is reduced, but their progression is linear in the logarithmic scale. Nevertheless, also the linear figure shows three profiles that are closer to linearity than the ones in the other cases: in fact, the exponential decay is smaller than two orders of magnitude, so it looks more like a linear profile. In addition, similarly to the previous case, no change in the slope of the profiles in the highest y/d coordinates can be noticed; therefore the exponential decay of the profiles is constant all along their length. In conclusion, the velocity profiles can be considered nearly linear; then it is possible to say that decreasing the level of the granular solid the profiles get closer to the linearity. Varying the load, the profiles show any differences; so the other figures are not reported in this work. Eventually, also for the lowest case the dependency on the load over the top surface is analyzed. All the results are presented in figure 5.12.

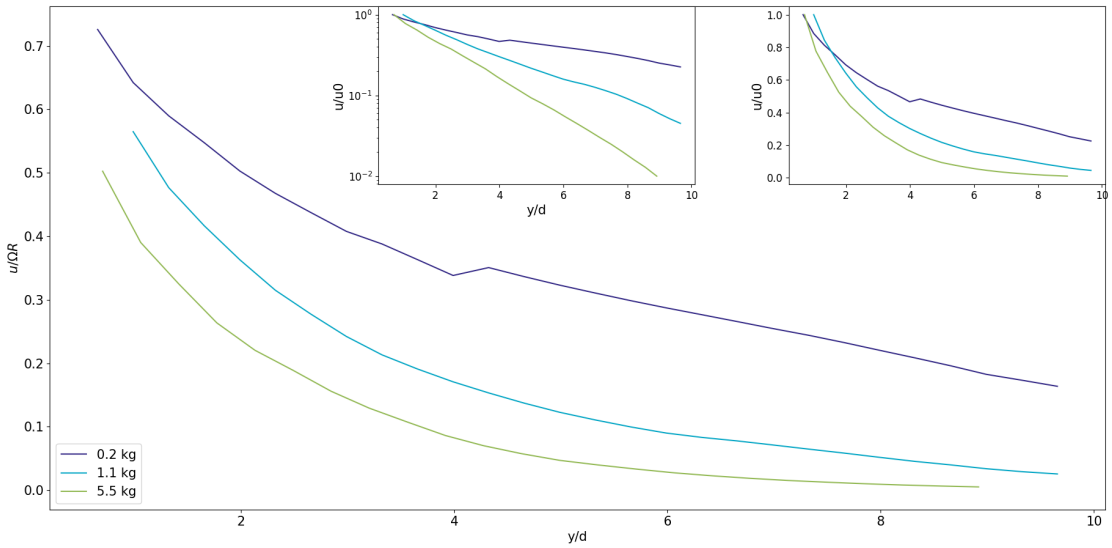

Figure 5.12: Particle velocity profiles varying the load on top ; Ω = 23.4 rpm ; Particle Height = 4 cm

The bottom velocity is the same used in the other cases for the analyses of this dependence. In this case, the profiles are closer to linearity decreasing the load on top; at the same time, the decay coefficient is increased by the increasing of load. Nevertheless, the highest profiles decrease less than two orders of magnitudes, therefore these profiles are more close to linearity. Only the highest loaded case shows a difference of at least 2 orders of magnitude between the particle velocities.

Anyway, also in this case the velocity decrease is smaller than the previous cases. The difference among the profiles is similar to the other cases and does not follow the increasing of the mass. In fact, the difference between the 0.2 Kg load test and the 1.1 Kg load test is equal to the difference between the 1.1 Kg load test and the 5.5 Kg load test. In conclusion, it is possible to say that increasing the load on the top surface the particles velocity decrease in shorter distance from the rotational surface and that lower velocities are reached by the top particles. The profiles obtained by changing the angular velocity of the bottom surface look similar to these ones, so they are not reported. In order to make more clear the influence of the height of the granular solid, the curves for different heights, keeping the velocity and the load as constant are displayed in figures 5.13 and 5.14. In the first figure height and velocity are changing, whereas the load is the same in all the reported cases (the medium one, 1.1 Kg). In the second figure, instead, the height and the load are varied and the velocity is always the same (23.4 rpm).

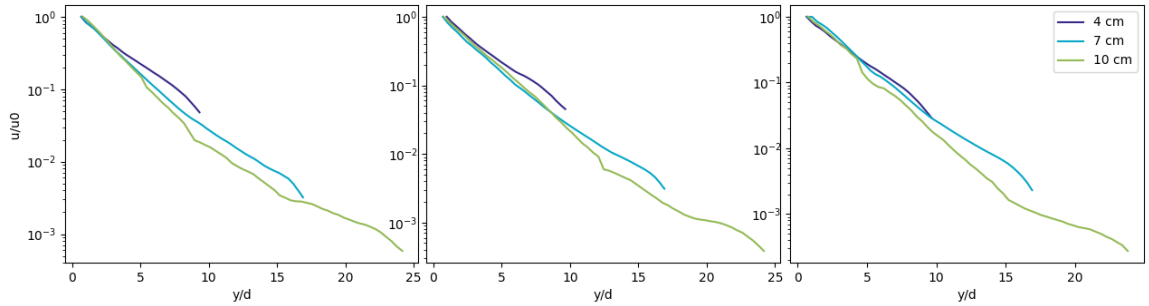

Figure 5.13: Particle velocity profiles varying the height of the granular solid at different constant rotational velocities and constant load (1.1 Kg). From left to right: 5.9, 23.4 and 117 rpm.

It is possible to notice from the logarithmic scaled figures that the exponential decay of the curves becomes slightly steeper with the decreasing of the level of granular solid. In fact, the shapes of velocity profiles in the different figures are similar: increasing the height, the velocity profile is slightly lower. Since the slowing down of the particles is caused by the loss of momentum during its transfer between layers, the greater is the number of layers, the higher will be this loss. Therefore the slowest particles will be slower compared to the slowest particles of the other cases. This means that the shear bands are smaller increasing the height of the granular

solid. Varying the rotational velocity, instead, the profiles are similar: therefore, it is possible to say that the influence of velocity is negligible, if the other two variables are constant. One difference can be noticed by the figures: the highest granular bed shows a flattened profile in its terminal part; on the other hand, the different slope of the final part of the other profiles concern a smaller part of the profiles. In addition, the difference of the magnitude of the slopes is smaller. Therefore, it seems that there is a limit condition of height for the propagation of the momentum through the layers: when the distance from the source of motion is higher than that value, the transfer of momentum changes. In addition, the three subplots of figure 5.13, it seems that the limit level is around 16 y/d, and this threshold is roughly constant with the variation rotational velocity, whereas it starts at higher layers when the load over the top surface increases. Nevertheless, other tests will be necessary to examine in depth this problem.

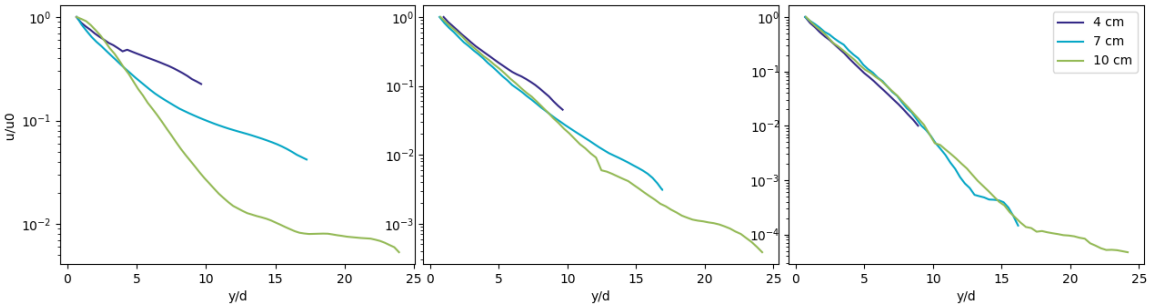

Figure 5.14: Particle velocity profiles varying the height of the granular solid at different constant loads and constant rotational velocity (23.4 rpm). From left to right: 0.2, 1.1 and 5.5 Kg.

In the figure 5.14 it is possible to notice how the effect of the granular level is overcome by the effect of the load on the top surface. In fact, it is possible to notice that in the first frame from the left of figure 5.14, where the load on top is 0.2 Kg, the velocity profiles are notably different. The decay coefficient increases as the height increases and the three profiles differentiate at roughly 3.5 y/d for the shallowest bed case and 5 y/d for the other cases. The difference is clear, and it can be noticed that, increasing the height of the particles, the velocity of the particles layers is smaller for the same y/d values. This consideration was noticed also in the analysis of figure 5.13, but in this case it is much more evident. In fact, also in the second frame of figure 5.14, the profiles diverge for some values of y/d: this diverging value increases

with the increase of the height of the spheres. In fact, for the shallowest case the curve diverges at 5 y/d, which is slightly higher than before, while the other curves diverge at 8 y/d, which is notably higher. On the other hand, the difference between the trajectories are smaller than the previous case, so the slowing effect of the particle level is diminished, and the only difference between the two frames is the load on the top. Eventually, in the third frame, the load in increased up to 5.5 Kg: in this case, disregarding the deviation of the medium curve, it is noticed that the curves are perfectly overlapped. No divergence can be noticed for any y/d value, until the curves can be traced. Therefore, the height is no more affecting the velocity profiles in the case that the load on top is a mass higher than the mass of the particles. In conclusion, it is possible to say that the load over the layers of particles are responsible of the slowing down of the particles: increasing the load added on the top surface, the load represented by the particles above the layers become less relevant, up to a limit condition when the effect of the mass of the particles is negligible. In addition, the lowest layers of particles are affected in any case by the load above them, therefore the addition of the load on the top affect only the higher layers: increasing the load, more layers are affected by that, up to a mass which is able to affect all the granular bed. Therefore, the higher is the load on the layers (taking into account both particles and added masses), the steeper is the slope of the curves, as already observed in the analysis of figures 5.4,5.5 and 5.6: the added consideration is that a certain load is required to affect all the particle layers. In addition, it is possible to assume that there is a limit value of the load on the particle layers which prevent the differentiation in the transfer of momentum. When this limit value is reached, the slowing down of the particles is constant. The effect on the height of the granular bed on the shear band, therefore, is that increasing the height the width of the shear band decreases. In fact, the effect of the height on the profiles is similar to the effect of the load, so this similarity can be extended to the effect on the shear bands.

In conclusion, it is possible to compare the results taking into account how the parameters influence the two variables of the profiles equation. The effect of velocity is weak, since the difference between the profiles is slight; furthermore, coupling the velocity with the other parameters, it does not affect the system. Moreover, the shape of the profiles is independent on the rotational velocity. The effect of the height is

similar to the effect of the load: increasing the height the layers of particles represents an adding load for the lower layers. This observation agrees with the observation worked out on the analysis of the first three figures: there is a value of y/d when the slope of the exponential decay varies, since the load on the particle layers is no more sufficient to decrease their velocity in the same way. Nevertheless, for the first two loads, 0.2 and 1.1 Kg, the y/d coordinate for the variation of slope is coherent with the load added on top. In fact, in both cases, the profiles flatten when the total mass above the layer of particles is 2.3 Kg. On the other hand, this assumption cannot be extended to the 5.5 Kg case, because this variation takes place even if load on the upper layer is 5.5 Kg (heavier than 2.3 Kg). Therefore, further tests are required to deepen this particularity. In figure 5.15, the same results obtained for the first case analyzed and reported in figure 5.8 are worked out, in the same way they were calculated in that case.

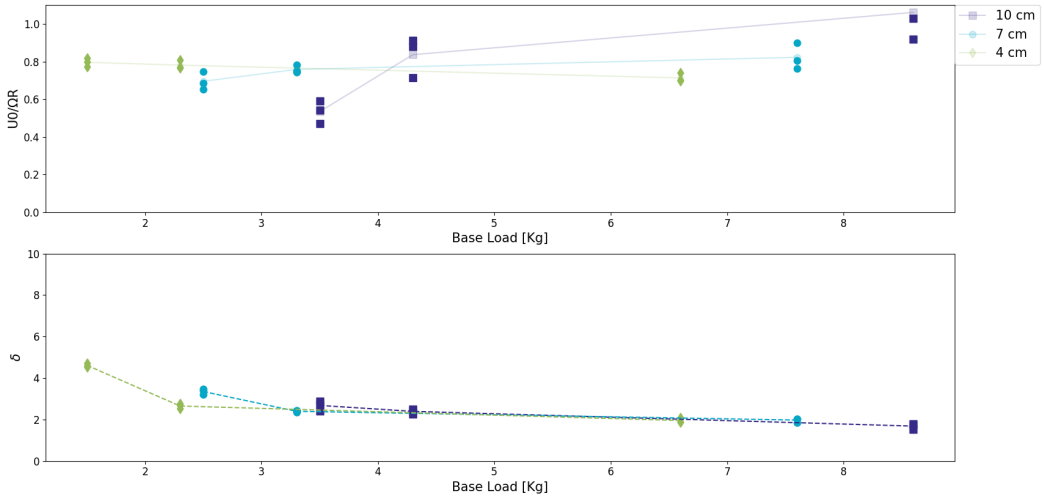

Figure 5.15: Slip velocity (above) and exponential decay coefficient (below) varying the rotational velocity, the load over the top surface and the height of the granular bed. Each point at the same *base load* corresponds to a different rotational velocity.

It is noticed that the slip velocity of the particles could be assumed as slightly dependent on the load for the two highest granular bed cases. In fact, increasing the load on top (and so the load on the base), the slip velocity increases. This trend is more clear in the case of the 10 cm height, whereas for the 7 cm case the increase is less clear. Instead, for the shallowest case, the trend is totally absent. Therefore,

it is not possible to work out a definitive consideration on the effect of the height on the slip velocity. On the other hand, it seems that increasing the load, the values of the slip velocity with the variation of the rotational velocity are more dispersed. It is possible to notice this by the distance between the markers, on the upper part of figure 5.15. But, also in this case, the medium level curve does not follow this trend. In conclusion, as in the previous analysis of the first system tests, it is not possible to assess the dependence between parameters and slip velocity. Concerning the variation of the coefficient of the exponential decay, the result of the previous test is confirmed. Increasing the load, the coefficient decrease, therefore the exponential decay increases. The same can be said for the increase of the height. This means that the velocity of the particles decreases in a shorter distance from the bottom surface and that the shear band is smaller. In addition, it is noticed that increasing the load on the top surface, the difference between the decay coefficients decrease. This means that the system is particularly affected by the increase of the base load. When the load on the top surface is lower, increasing the height of the granular bed is relevant: the base load increase the 70%. When the load in 5.5 Kg, the base load increase the 14% between the first and the second height. Therefore, it is possible to assume that the influence of the load on the exponential decay is dominant. In conclusion, it is possible to identify that the rotational velocity does not affects the flow in a relevant way. Concerning the load on the top surface and the level of the particles, they affect the system in a similar way: increasing the load, the decay coefficient decreases. This is true for the tests among granular solids with the same height, but it is true as well increasing the height of the particles. In fact, if that height increases, the total load over the bottom surface increases; the same effect is obtained by adding the masses over the top surface. Therefore, acting on these two parameters, the velocity profiles are lower and so the shear bands are smaller. Furthermore, the difference between these two parameters is that reducing the height of the particles also the shape of the profiles change: the highest profile is linear in a logarithmic scale, but its slope changes at a certain distance from the bottom. In this zone, the particles are moving slowly, therefore it can be assumed as a creep zone. In the other hand, the other cases show a more linear-like profile, which means that the shear zone, described as the zone of the granular solid where the velocity varies, are wider. Moreover, their decay

is smaller; therefore they are closer to the linearity. At this point, the effect of the surface roughness, another influencing parameter, will be analyzed. This analysis considers its influence and how it affects the others parameters, and it is carried out taking in consideration all the results obtained in these tests.

5.1.4 Surface Roughness

The variation of the surfaces roughness is obtained by printing with a 3D printer the new surfaces, as explained in section Materials (2). The choice of the s parameter leads to three different conditions of roughness, depending on the distance between two plastic spheres. The first tested surface roughness is defined as heterogeneous, since the distance between two consecutive plastic spheres is the diameter of a sphere. Therefore, it is possible to suppose that, while the bottom surface is rotational, the particles of the last layer of the granular material come in contact only with the spheres on the surface or with the flat space between the asperities as well. For this reason, two other surfaces are tested: in the first case, the distance between the spheres is equal to the half the diameter of the particles; in the second case, the surface is completely flat. Therefore, using the first surface, particles just contact the spheres while in the second case they just contact the flat surface, so in both cases the friction is homogeneous. Starting from the considerations about the previous results, in order to optimize the number of tests to carry out, just one velocity is applied when the height of the spheres is 4 cm or 7 cm. For the 10 cm height, instead, two different velocities are tested, as some differences were identified in the previous tests. Moreover, just two loads are applied in any test, since the velocity profiles of the 0.2 and 1.1 Kg load cases are usually similar. The tests carried out are resumed in Table 5.2.

The first comparison is based on the results showed in figure 5.16 : the influence of different rotational velocities on the velocity profiles when the height of the granular material is 10 cm. On the left, the results with the rough surface are reported in logarithmic scale, whereas on the right they are shown in linear scale. It is possible to see that the trend identified in the initial is less defined but confirmed: increasing the rotational velocity of the bottom surface, the velocity profile is lower and so the shear

Table 5.2: Configurations of the experimental apparatus for the tests, concerning the surface roughness

Test ()	*Height* (cm)	Ω (rpm)	*Surface* (s)
28,29	4	23.4	0.5
30,31	7	23.4	0.5
32 to 35	10	23.4,117	0.5
36,37	4	23.4	smooth
38,39	7	23.4	smooth
40 to 43	10	23.4,117	smooth

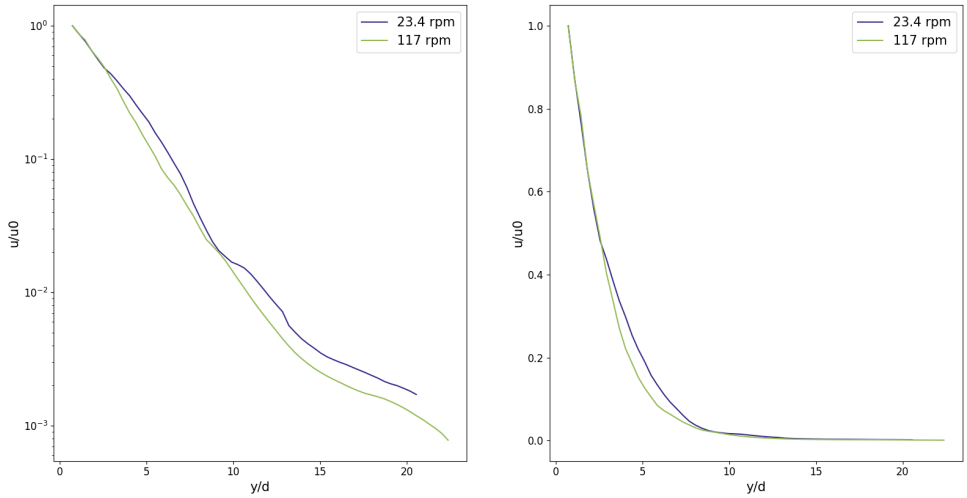

Figure 5.16: Velocity profiles with roughest surface (s=0.5), L=1.1 Kg. Logarithmic (left) and linear (right) scale

band is smaller. In the left part of figure 5.17 the results with the smooth surface are displayed. In this case, the influence on the shear band is small, since just the furthest part of the granular solid is affected. It is possible to see, in fact, that the flattening of the curve occur at higher vertical coordinate, as it is shown by the first surface. The same trend is presented by the profile of the roughest surface, even if in this case the changing point is not well defined (figure 5.16, left). As for the first surface, the velocity profiles are exponential, the exponential decay dimension is three orders of magnitude and the profile flattens at a certain distance from the rotational surface. Therefore, the shape of the velocity profiles is mainly confirmed. In particular, in the right part of figure 5.17 it is possible to see that in the case of the flat surface the flattening of the curve can be identified for lower height values, whereas for the other

surface the distance is higher, even if the flattening is not well defined. Moreover, the flat part of the curve is more consistent in the case of the smooth surface, whereas it is less developed in the first case profile and in the roughest case. The same result comes from the analysis of the velocity profiles at 117 rpm keeping all the other parameters constant, therefore they are not displayed. In conclusion, the effect of the rotational velocity on the velocity profiles is confirmed: it slightly affects the profiles and, if it is notable, the particles slow down at a lower distance from the source of motion. In addition, it is noticed that increasing the roughness the flat part of the curve is smaller and the profile is not constant as in the smooth case, but it changes its slope. Further tests will be needed to clarify this behaviour.

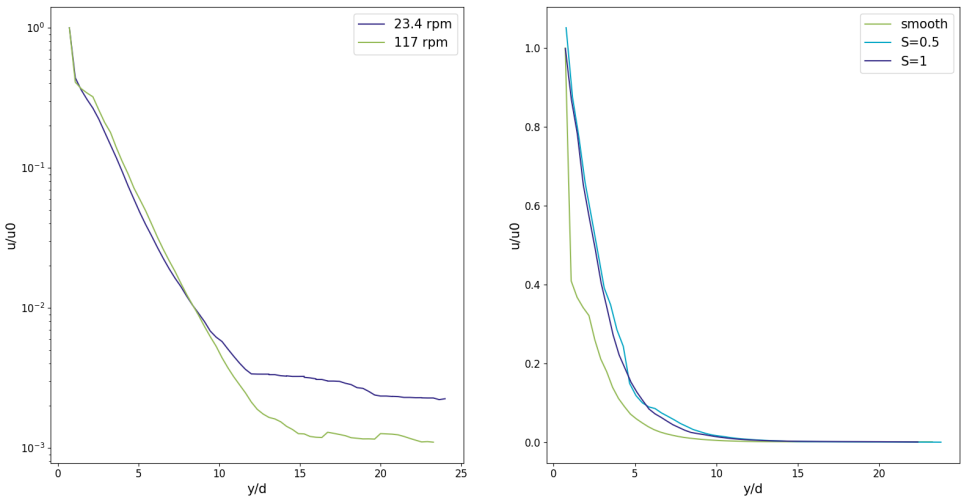

Figure 5.17: (Left) Velocity profile with smooth surface; L=1.1 Kg, H=10 cm. (Right) Velocity profiles with three surfaces; L= 1.1 Kg, H=10cm, Ω= 23.4 rpm

Concerning the effect of the load on the velocity profiles, in figure 5.18 it is possible to notice that the effect on the velocity profiles is the same. The width of the shear band is decreased by the increasing of the load over the top surface. This trend is the same for all the tested height: in order to show this fact, the highest and the smallest heights are shown in the same figure, whereas the medium height is hidden, to make the figure clearer. In figure 5.18, the profiles are shown as linear and logarithmic, in order to show their similarity: therefore, in both cases the effect of the load on the top surface is verified. In particular, the right part of the figure shows the profiles obtained by the rough surface, whereas the left part refers to the flat surface.

Regarding the flattening of the curve, instead, the y coordinate seems to be the same for the two cases, therefore it is not possible to assess univocally the effect of the load on the flattening in these two cases. As for the first tested surface, the velocity profiles are exponential and so the load does affect their shape.

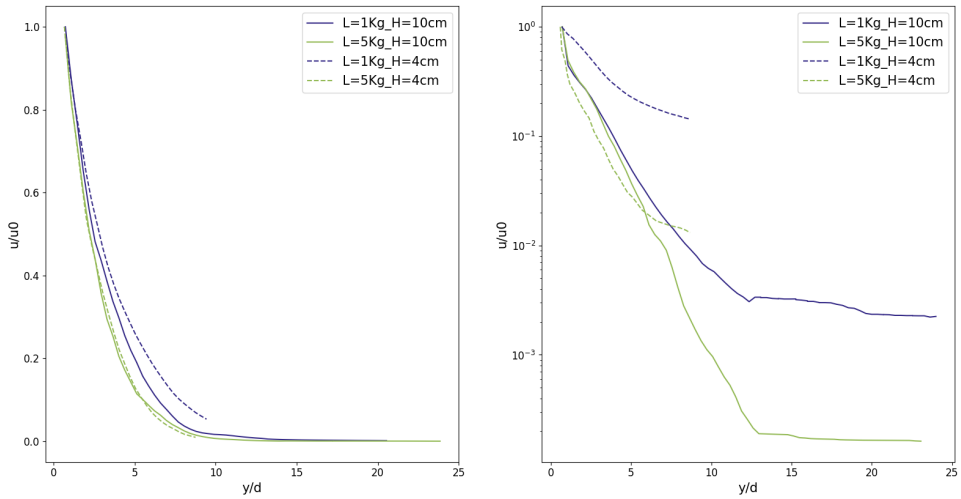

Figure 5.18: (Left) Velocity profile with roughest surface, varying the load. (Right) Velocity profiles with smooth surface, varying the load

Concerning the effect of the height of the granular material, the same considerations coming from the first test are valid: if the level of the particles inside the cylinder is higher, the shear band is reduced. In fact, increasing the height, the effect of the particles over standing the others is the same of an added load, which makes the transfer of momentum more difficult. Therefore, an higher shearing is needed in order to increase the shear stress acting on all the particles. All these considerations can be noticed by figure 5.19. Moreover, it is possible to see that, similarly to the previous case, the increase of the load over the granular material makes the profiles more similar one to the other, reducing the effect of the height. This behaviour can be assumed by the profiles showed in figure 5.20. Therefore, if the load is higher, its effect is dominant if compared to the effect of the height of the granular material. Furthermore, the level does not affect the shape of the velocity profile. Therefore, decreasing the number of layers of particles, the exponential decay becomes smaller than 2 orders of magnitude, and the profiles look more linear. This changing shape is well defined in the case of the rough surface, whereas for the smooth surface the pro-

file is still exponential. In particular, the flattening occurs in all the cases and further from the bottom surface by increasing the height of the granular solid, involving a larger part of the solid itself.

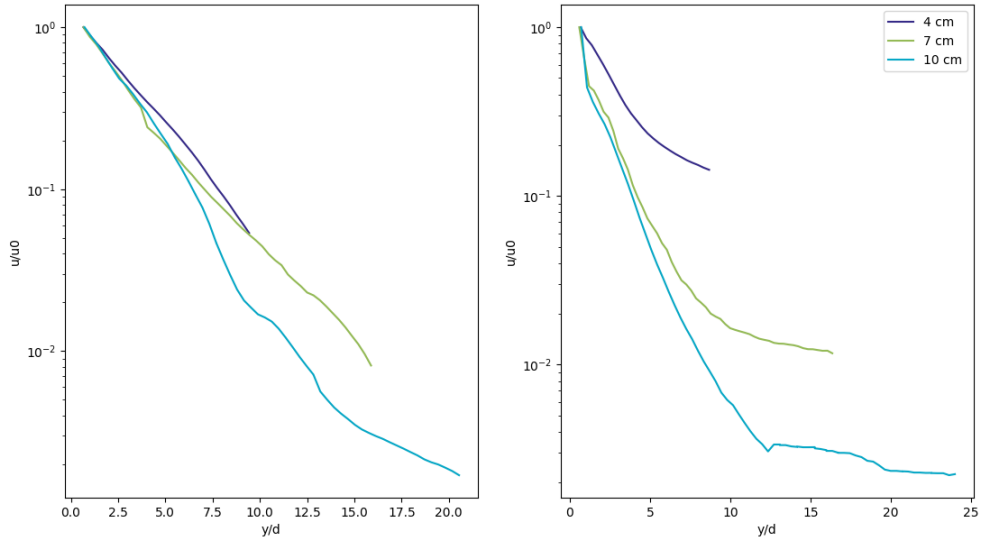

Figure 5.19: (Left) Velocity profiles with roughest surface, varying the height; L=1.1 Kg, Ω =23.4 rpm. (Right) Velocity profiles with smooth surface, varying the height; L= 1.1 Kg, Ω=23.4 rpm.

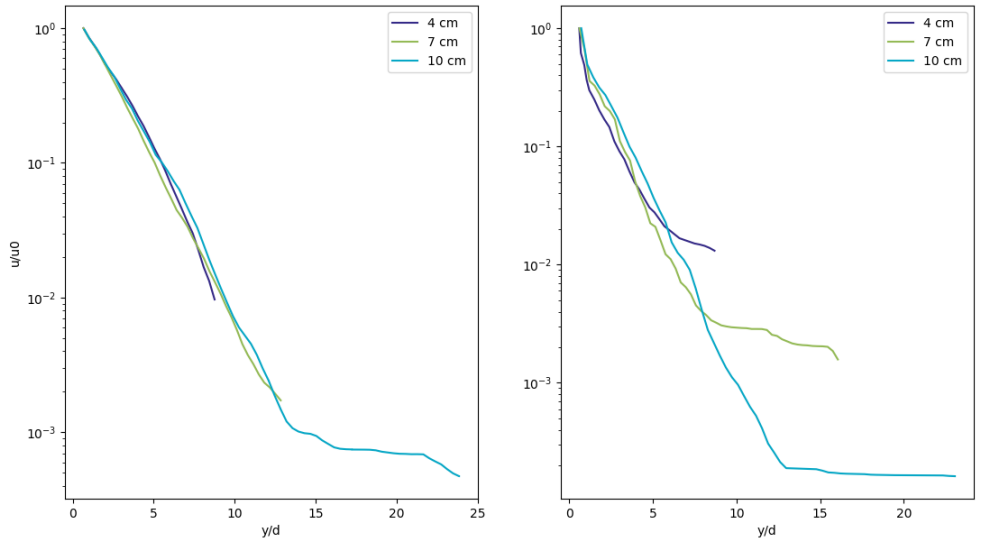

Figure 5.20: (Left) Velocity profiles with roughest surface, varying the height; L=5.5 Kg, Ω =23.4 rpm. (Right) Velocity profiles with smooth surface, varying the height; L=5.5 Kg, Ω=23.4 rpm

Successively, the decay coefficients and the slip velocity are compared, for the three surfaces, in the figures 5.21 to 5.25. The procedure is the same described in the analysis of the tests on the first surface.

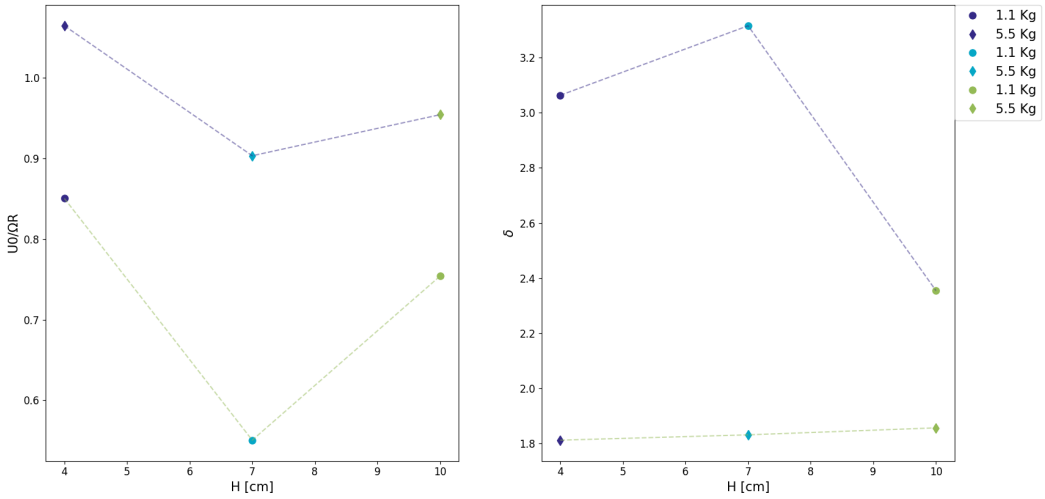

Figure 5.21: (Left) Slip Velocity and exponential decay coefficient (Right) with roughest surface, varying height and load. Ω =23.4 rpm.

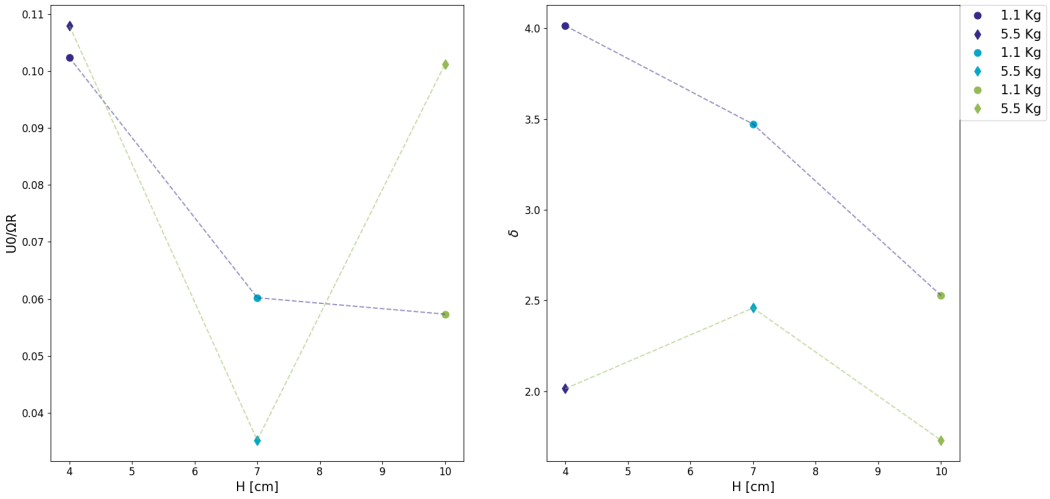

Figure 5.22: (Left) Slip Velocity and exponential decay coefficient (Right) with smooth surface, varying height and load. Ω =23.4 rpm.

In the first two figures, the effect of velocities and load on the two surfaces is displayed. Respectively, figure 5.21 shows the results with the roughest surface, whereas in figure 5.22 the results with the smooth surface are displayed. In the case

of the roughest surface, the trend is well established: increasing the load on top, the slip velocity is increased. Instead, concerning the decay coefficient, the trend is the opposite: Increasing the load on top, the coefficient of the exponential decay of the velocity profile decreases. This consideration is illustrated also in the previous analysis, since it is well established that the profiles get lower increasing the load. This effect consists in a reduction of the width of the shear band. The same thing can be said by the right part of figure 5.22: also for the smooth surface, the increase of the load decreases the decay coefficient. On the other hand, in both cases it is possible to notice that the effect of the height of the granular material is not consistent with the previous considerations about the similarity with the load. In fact, the coefficients are widely distributed without any trend in both cases, for both curves, even if it is expected that they decrease with the increasing of the height. Instead, it can be noticed that increasing the load, the differences between their values are lower. Therefore, it is possible to say that the effect of the load is dominating over height and velocity effects. Moreover, it is not possible to assess the effect of the load on the slip velocity for the smooth surface, since the values does not follow a trend. It is possible to carry out a final comparison between the slip velocity and decay coefficient for the three different surfaces.

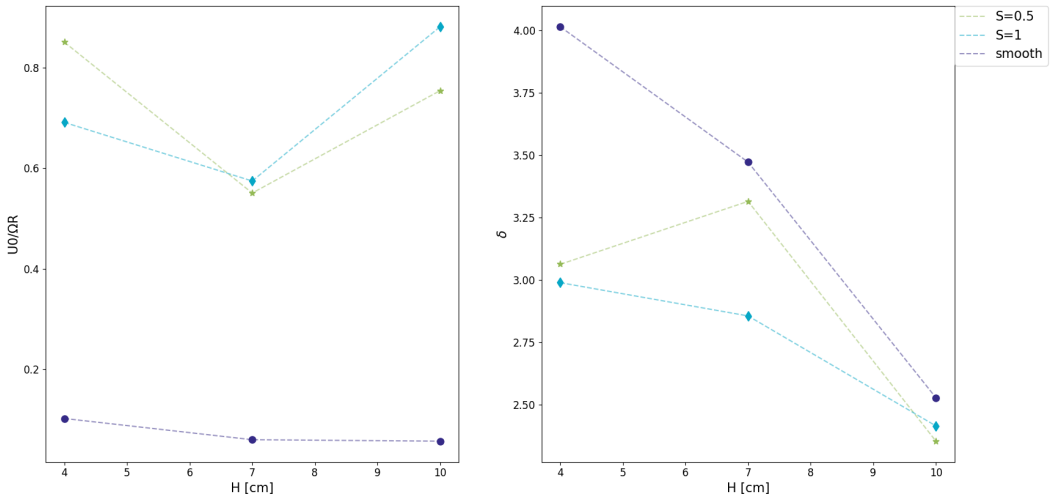

Figure 5.23: (Left) Slip Velocity and exponential decay coefficient (Right) with three surfaces, varying height; L=1.1 Kg, Ω =23.4 rpm.

In figure 5.23, the slip velocity and the coefficient of exponential decay for any

case are displayed. In all the cases, the load on the top is 1.1 Kg and the rotational velocity is 23.4 rpm: In this way, just the effect of the surface roughness is underlined. It is possible to notice for the left part of figure 5.23 that there is a notable difference between the slip velocity in rough and smooth surfaces: in the latter case, the most of the momentum given by the rotational surface is wasted; in fact the highest velocity of the particles is 10 % of the angular velocity. In the case of rough surfaces, instead, at least 60 % of angular velocity is conserved. Another aspect is that the slip velocity in smooth surface case is lightly dependent on the height of the granular solid: nevertheless, considering figure 5.22, it is possible to notice that the dependence on the load is the same than the other cases, since the ratio between maximum and minimum value is about 60%. In the other hand, it is possible to figure out the trend of the rough surfaces: increasing the height of the granular material, and so the load over the base, the slip velocity is higher. Therefore, the roughest surface is more effective in the transfer of momentum when the base on the load is higher. From the right part of figure 5.23, it is noticed that the decay coefficient is dependent on the roughness of the surface: the coefficients of the smooth surface case are higher than the coefficients of the rough surfaces in any condition. Moreover, the coefficients of the roughest surface are higher than the ones of the heterogeneous surface in any case, except in the last one where they are nearly equal. Therefore, it is possible to say that the surfaces with homogeneous roughness causes an higher exponential decay compared to the first surface. The dependence between exponential decay and the slip velocity is not well defined: it seems that if the slip velocity is higher, the waste of momentum is higher, in the case of the smooth surface. In this case, in particular, it is possible to notice that in these conditions (load and angular velocity) the slip velocity and the decay coefficient decrease with the increase of the base load. Instead, for the other curves, it is not possible to identify a common trend. Moreover, it is possible to compare the velocity profiles in the same conditions of the figure 5.23 cases, which are reported in figure 5.24 and 5.25.

In figure 5.24, it is possible to notice that the shape of the profiles is exponential in all the cases, since all the curves are nearly linear if represented in a logarithmic scale. For the first two heights (figures at the left) the decay is at least of two orders of magnitude, whereas for the smallest height the decay is 1 order of magnitude, in fact

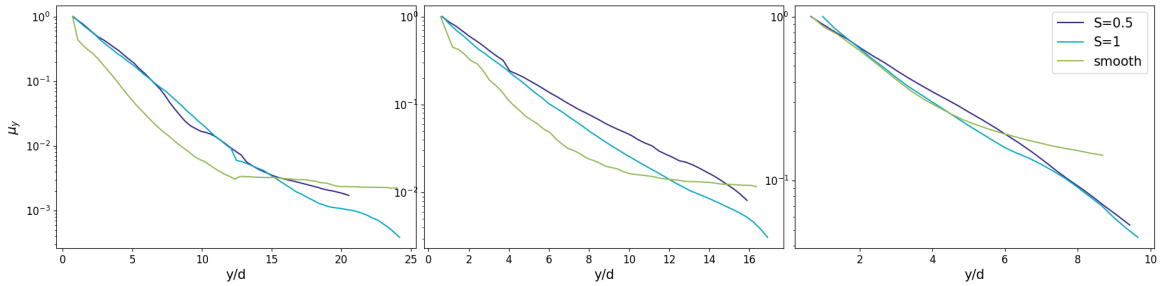

Figure 5.24: Velocity profiles with three surfaces in logarithmic scale, varying the height: 10 cm (Left), 7 cm (Center) and 4 cm (Right). L=1.1 Kg, Ω =23.4 rpm.

in this case the profiles are close to linearity. The most evident thing is that there is a notable difference between the velocity profiles. In fact, in a linear scale (figure 5.25), the profile of the smooth surface is lower than the other profiles, and so the shear band in notably smaller.

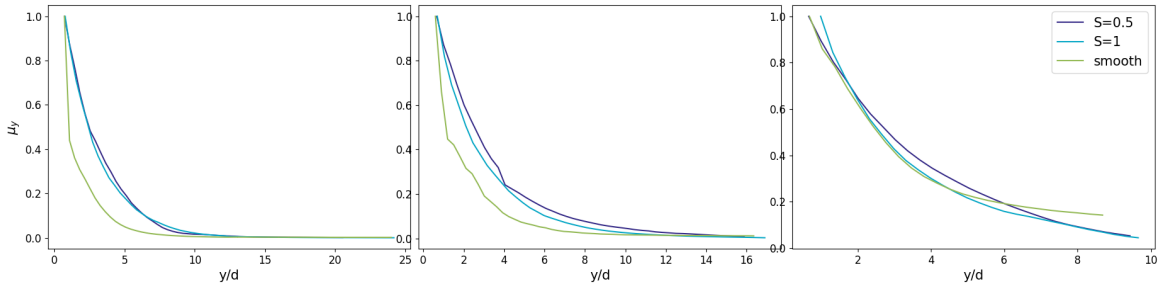

Figure 5.25: Velocity profiles with three surfaces, varying the height: 10 cm (Left), 7 cm (Center) and 4 cm (Right). L=1.1 Kg, Ω =23.4 rpm.

This means that the shape of the profiles of the rough surface cases look similar in any case, whereas the smooth surface profiles are more curved in the logarithmic scale. In particular, the difference is less remarkable in the last case, for the smallest height, since the profiles are less developed. Moreover, it is noticed from the rightest figure that for all the curves the flattening of the profile in logarithmic scale: in smooth case, the flattened part of the curve is well defined, whereas in the roughest case the curve flattens close to the top. Nevertheless, comparing the three curves, in cases 1 and 2 the medium roughness surface shows the lowest values of velocity, so the decay of velocity mostly effective. In conclusion, it is possible to say that the smooth surface notably reduces the shear band, whereas the difference between the roughest and the medium roughness surface is negligible. Especially, the shapes of the curves in logarithmic scale are dependent on the surface, which means that the

difference in shear band size is well defined. Considering figure 5.23, it is supposed that the poor transfer of momentum between the rotational surface and the spheres in contact (represented by the low values of the slip velocity) is linked to the further loss of momentum, which takes place in a smaller number of particle layers than in the other cases.

5.2 Wall Friction

Several tests are carried out, see Table 5.3, in order to examine how the flow of the particles is affected by the wall friction. The characteristic variables are the rotational velocity of the bottom surface, the load over the top surface and the height of the analysis window. In particular, for any height of the window of measurement, 3 different masses are loaded and 3 velocities are tested for any case. As explained in section 4.6, the measurements with the slowest velocity are not considered. In Table 5.3 the tests carried out are rapidly resumed.

Table 5.3: Tests for the wall friction coefficient

Test	*Height of the window* (mm)
1 to 3	15
4 to 6	30
7 to 9	70

5.2.1 Normal stress

In figure 5.26, the measured stresses normal to the wall are displayed, varying the height of the analysis window and the load over the top surface. In order to be more clear, the displayed stresses are just those measured when the rotational velocity of the bottom surface is Ω=23.4 rpm. It can be observed that increasing the load, the normal stress increases, since the higher curve is obtained on the 5.5 Kg load test. This result agrees with the expectations, since, considering the granular material, increasing the normal stress, the radial stress increases as well, as explained in section 1.3. In fact, considering the stress state of the granular material by wall's point of view, the normal stress coincides with the radial stress just indicated. Secondly, it is noticed that the stress decreases with the increase of the height of the analysis window. This is expected, since both the theories illustrated in the section 1.3 indicate that the stresses increase by the increase of the distance to the top surface, if y is less than a critical value in Janssen equation. In order to establish which is the most suitable theory, the normal stress is calculated with a hydrostatic approach 5.2.1.

$$\sigma_r = \rho_b g(h - y) + L/A \tag{5.2.1}$$

where ρ_b is the poured density of the granular material, h is the height of the granular material and y is the height of the analysis window; L is the load over the top surface (in terms of force) and A is the surface of the top surface. It is possible to notice that the two observations agree, since the increasing of the height of the particles above the level of the window analysis cause an increase of the mass over that point. Therefore, the trend of the curves is well described by the hydrostatic model: this result was expected, since the height of the granular solid bed is shallow.

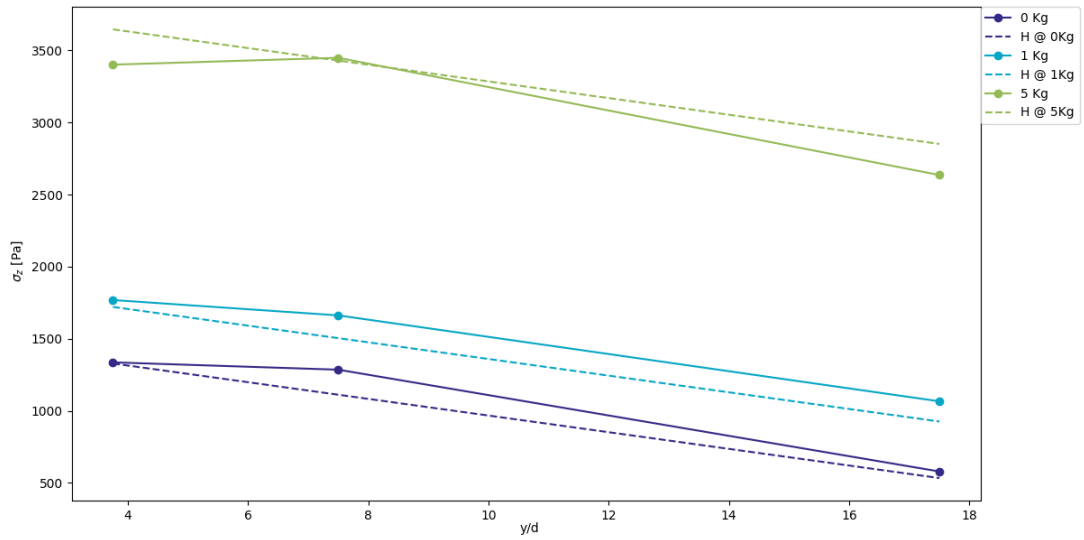

Figure 5.26: Normal stresses and hydrostatic profiles.

5.2.2 Horizontal effective wall friction coefficient

Successively, the effective wall friction is calculated, as indicated in equation 4.6.2 in section 4.6, as the ratio between the normal stress and the tangential stress. By the way, it is possible to obtain two different coefficients, considering the horizontal and the vertical tangential stresses. Concerning the horizontal effective wall friction, figures 5.27 and 5.28 represents the obtained results. In figure 5.27, it is possible to see that the coefficient decreases when the load on the top surface increases. This result was expected, since in figure 5.26 it is known that the normal stress increases and,

referring to equation 4.6.2, it is the denominator variable. Therefore, supposing that the tangential horizontal force is slightly affected by the increase of load, the effective friction coefficient decreases. Considering the orientation of the measurement system, this means that, increasing the load, the friction between the wall and the particles is lower. Moreover, the trend based on the analysis window is not well established: the difference between the lower and the medium window varies between the different cases and the velocities.

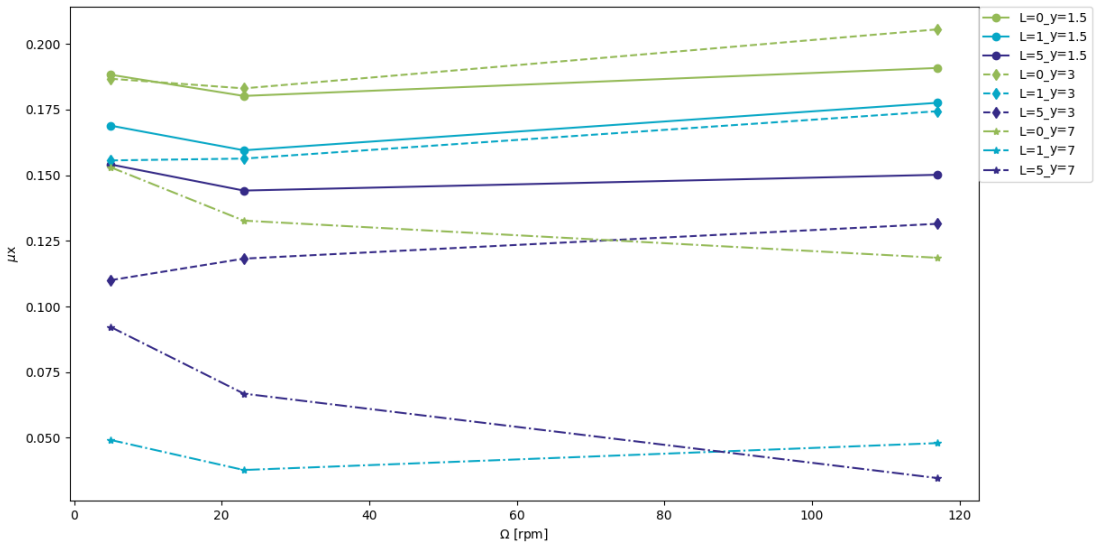

Figure 5.27: Horizontal effective wall friction coefficient

Anyway, it is possible to notice some typical trends: the difference between the measurements at constant load generally increases with the increase of the rotational velocity. In addition, the difference between the two lowest analysis window and the highest one increases where the velocity increases. In particular, in the two lowest windows the coefficient is higher, while in the highest one the coefficient is lower, in any of the presented cases. Furthermore, comparing with figure 5.26, the decrease of the normal force with the increase of the height is too low to be the only responsible of this trend. Therefore, it is possible to assume that the tangential force is varying as well: in particular, it increases if the height decreases. This trend agrees with the fact that, if the velocity of the granular material is higher, the effective friction between the wall and the particles increases.

In order to verify the relation between the shear rate and the effective wall friction,

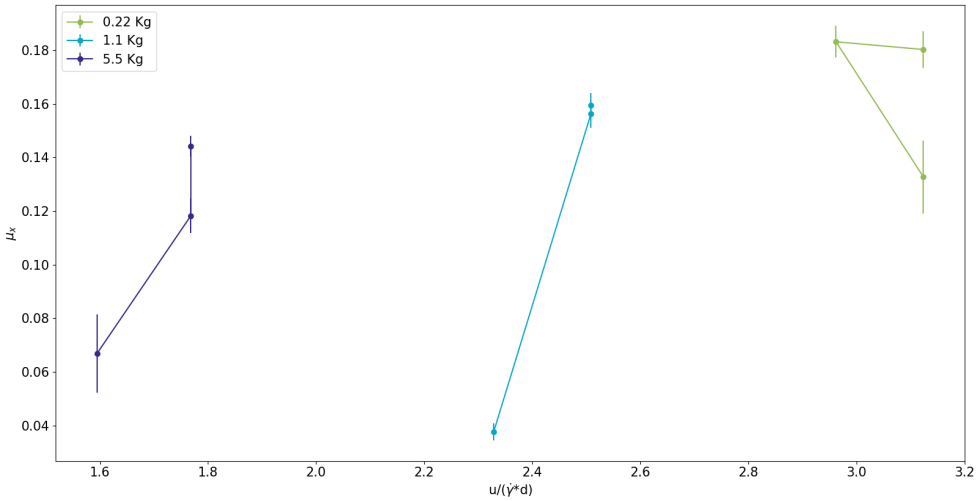

Figure 5.28: Horizontal effective wall friction coefficient varying load and height of the analysis window

in figure 5.28 the coefficient is plotted versus a non-dimensional parameter. This sliding parameter, the ratio of the horizontal velocity and the product of the shear rate and the diameter of the particles, was found to scale the friction coefficent properly in the reference work [4]. It is representative of the rheology of the granular material. Only the values calculated with rotational velocity equal to 23.4 rpm are considered. In this case, the error bars representing the standard error to mean calculated on the friction coefficient are plotted as well. Anyway, the calculated errors are low, then they do not affect the results relevantly. In order to carry out this comparison, the velocity profiles of the particles, coming from the analysis in section 5 are considered. Three points are plotted for each curve, since each points represents one of the analysis windows at constant load. As reported in the reference publications [1], it is expected that the effective friction coefficient is dependent on the shear localization. In particular, increasing the load over the top surface, the shear zone is localized at a lower height: therefore, measuring the coefficient in the same window, it is expected that it decreases where the load increases. From a different point of view, for lower values of the friction coefficient, lower values of the shear band width are expected. At the same time, considering the results displayed in the first part of section 5, it is shown that the width of the shear band decreases with the increasing of the load over the top surface. Considering figure 5.28, these considerations are not complied

with: the trend between the friction coefficient and the shear rate is not well defined. Therefore, it is not possible to assume that the former is function of the latter. A better choice for the scaling factor of the friction coefficient would be probably the granular temperature, as reported in the reference publication [3]. Nevertheless further tests are needed to verify this supposition.

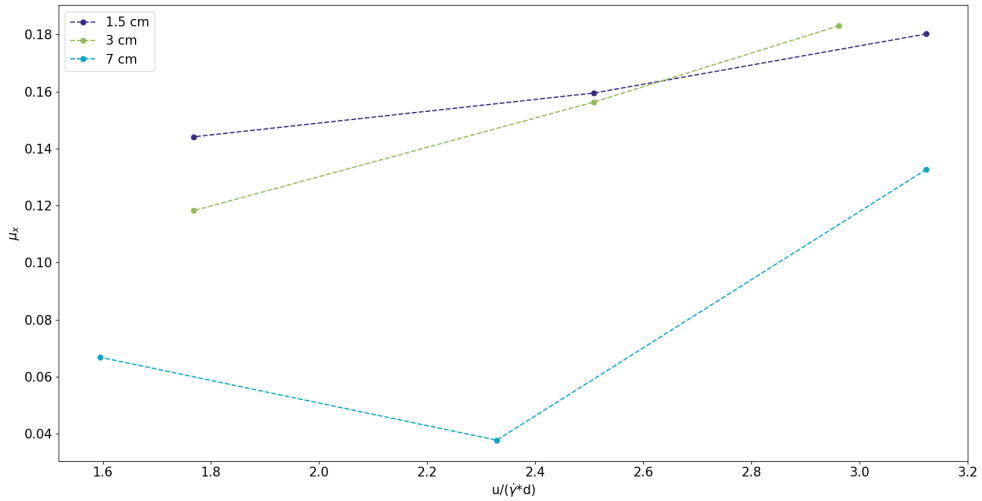

Figure 5.29: Horizontal effective wall friction coefficient at different heights

In Figure 5.29 it is particularly clear that the horizontal friction coefficient varies along the height of the granular bed. This is an important results, since there were no experimental tests that verified this assumption in a cylindrical configuration. This concept was firstly supposed by Mr. Richard [17], and it was worked out from the study of a gravity flow of granular material down chutes. As it is described in that letter, the effective horizontal wall friction coefficient weakens with with depth. In figure 5.29, in fact, it is possible to notice that the values of 1.5 cm curve are in 2 out of 3 cases the highest ones. In the last case, 3 cm is the highest value, whereas the highest analysis window (7 cm curve) shows in any case the lowest value. It is possible to notice that these values are affected by the load as well, since it was shown in first part of section 5 that the load affects the shear band width. Nevertheless, the effect of the load (and so the effect on the shear band width) in not univocally determined, so the effective wall friction coefficient does not scale with this parameter.

5.2.3 Vertical wall friction coefficient

In conclusion, in figure 5.30 the vertical effective wall friction coefficients are presented. In analogy with equation 4.6.2, these coefficients are calculated as the ratio of the vertical tangential forces and the normal forces. Considering the experimental apparatus, no forces are acting actively on the vertical direction, so the only implied forces are the gravity and an opposite forces dependent on the granular material flow.

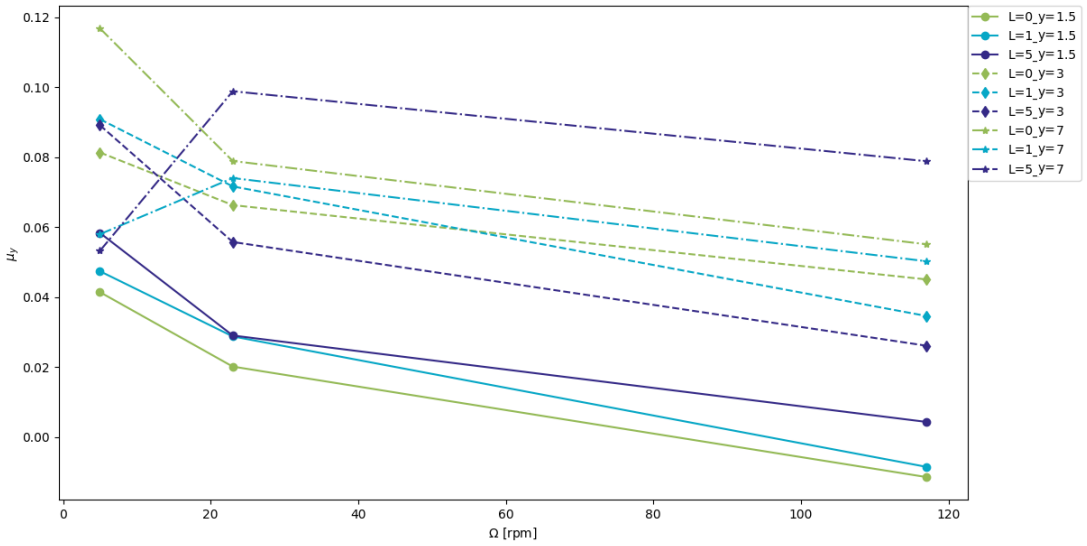

Figure 5.30: Effective vertical wall friction coefficient

In the figure 5.30, it is possible to notice that increasing the height of the analysis window the coefficient decreases. On the other hand, it is seen that increasing the load on the top surface, the friction coefficient does not show a univoquous trend. According to the system of reference of the sensors, the increase of the vertical tangential forces corresponds to a higher magnitude of the forces due to the flow, since the gravity has a negative contribution. Therefore, it is possible to assume that in the lower window, the effect of the vertical friction is less relevant, since the particles are partially sustained by the flow itself. On the other side, in the higher window the granular material is in a creeping zone, so the wall vertical friction is more relevant, since it is the only force that counteracts the gravity. It is even possible to assume, comparing the values on the friction coefficient from figures 5.27 and 5.30,

that in the creeping zone of the flow the magnitude of the vertical tangential forces is higher than the ones of the horizontal one, since in that zone the particles are more affected by the action of the vertical forces.

CHAPTER 6

Segregation

6.1 State of art

The phenomenon of segregation affects many industrial applications of the granular solids. When it is required to obtain a homogeneous mixing of two granular materials which differentiates by some physical characteristics, the segregation makes the mixing process less effective. In fact, this phenomenon causes differences of concentration of the solids between different parts of a mixture. Segregation may occur due to differences in one or more solid properties, such as size, density, shape, surface roughness and friction. However, the two most effective drivers of particle segregation are size differences and density differences. Though there are a few studies dealing with the coupled effect of size and density, typically the effects of these two properties are considered independently to gain a better understanding of the segregation process. In this work, it is considered the case of segregation solely due to density differences. Experiments as well as simulations [21] for vibrated beds show that heavy particles, while starting from a completely segregated state, concentrate near the centres of convection rolls of the system. Mixtures with a larger density ratio are segregated more completely and the granular temperature of the heavy particles is found to be higher than that of the light particles. In flowing systems,

instead, segregation results in changes in the local rheology and consequently the flow. The segregation flux also depends on the local rheology. Thus, the flow and segregation are coupled, and a complete description requires a rheological model for mixtures. The flow of the motion of the high-density particles can be understood in terms of the buoyancy and drag forces acting on it. The buoyancy force is given by Archimedes principle, with an effective volume associated with the particle, which depends upon the local packing fraction. The buoyancy arises primarily from normal forces acting on the particle, and tangential forces have a negligible contribution. The drag forces on a sphere sinking in a granular solid can be calculated with a modified Stokes law, and they depend on the apparent viscosity of the medium. Specifically, particles lighter than the surrounding mixture of particles experience a buoyancy force greater than their weight and rise, while particles denser than the surrounding mixture sink. [19] In vibrated systems, several factors have been shown to play important roles in the segregation process, including convection, gravity, interstitial air, and granular temperature (essentially, the kinetic energy associated with velocity variances). In sheared flows, similar mechanisms have been shown to influence the segregation processes, including variations in particle concentration. In sparse sheared flows, kinetic theory has been used successfully to model and predict segregation in simulations and experiments. The segregation predictions may represent segregation according to several competing elements: gravity, granular temperature, pressure, and diffusion "forces". For example, gravity segregates denser particles downward (in the direction of gravity) relative to less dense particles while a gradient of granular temperature segregates denser particles to lower granular temperature. [6] Therefore, in order to define how denser particles segregate it is needed to carry out some specific tests.

6.2 Segregation test and model

Since the shear bands location and the vertical profile of the wall friction have been determined, it is possible to test some additional applications of this experimental apparatus. In this frame, the density-driven segregation is investigated. With this purpose, some ceramic spheres are placed over the glass spheres. The volume fraction

of the added spheres is 0.5 %, so it is possible to assume that they do not affect the flow. The shape and the dimension of the two kinds of particles are the same, so the only driving force of the segregation is the difference of density. In particular, the density of the glass beams is 2500 kg/m^3 while the density of the ceramic spheres is 3670 kg/m^3. In order to simplify the identification of the ceramic particles, they are covered with a fuchsia spray. In addition, as it is described in section 2, a LED ribbon is placed in the hollow space of the internal cylinder, in order to make the spheres more visible. The bottom surface rotates to provide the motion of the granular material: the chosen rotational velocity is 23.4 rpm. Concerning the other settings of the test, the mass on the top surface is 1.1 Kg and 11 cm is the total height of the granular material (glass and ceramic spheres): therefore, the velocity profiles and the shear bands of this configuration had already been studied. A GoPro Camera is placed in front of the external cylinder, in the same way of the HS camera described in section 2, and the Time Lapse setting is used. Therefore, one photo of the frontal surface of the experimental apparatus is taken every minute. This measurement time is chosen because it is expected that the characteristic time of the phenomenon is much greater than this, in fact this analysis is carried out for 6 hours. In a second time, the pictures are cut and a smaller part of the picture is considered in order to minimize the effect of the curvature of the surface in the picture. In fact, any picture is successively divided in 11 layers, any layer is 1 cm high: counting the ceramic particles in any layers in each picture, it is possible to work out the profile of coloured particles in time. It is required to cut the images because they show a curved surface in 2D: in the curving parts of the image it is not possible to identify the correct height of the particles. For simplicity, the counting procedure is run manually, taking note of the particles in any layer for any image. Secondly, an average number of glass spheres in any layer is calculated and so it is possible to identify how the concentration of ceramic spheres evolves in time and along the height of the cylinder. In order to decrease the noise on the measurement, data are binned in intervals of 10, 15 and 30 minutes. As greater is the binning time, as smoother is the concentration profile.

In any case, no significative difference can be identified on the different profiles: the ceramic particles sink during time, so their concentration in the lower layers increase, as can be noticed by Figure 6.1. In this case, the 30 minutes binning have been

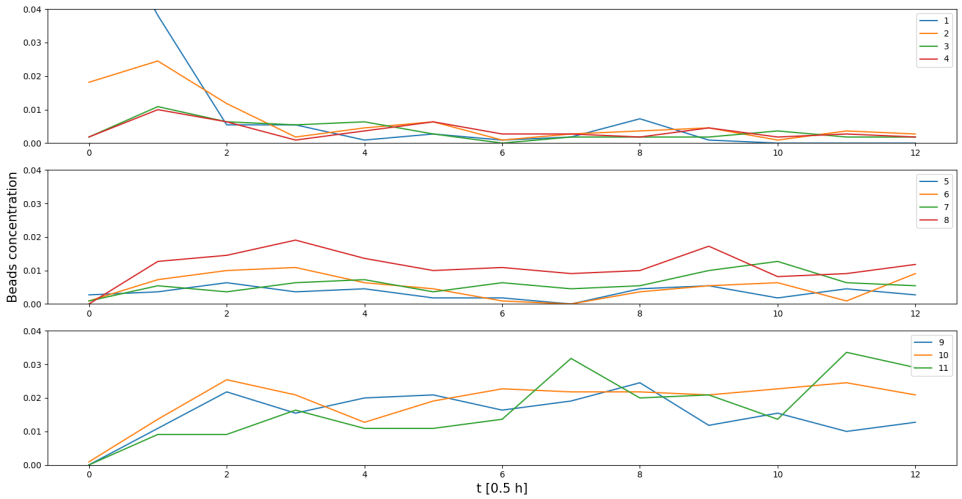

Figure 6.1: Profiles of concentration of ceramic particles in time for all the layers. Label refers to the layer, from 1 the top layer to 11 the bottom layer.

applied. Nevertheless, the percolation of the denser particles is not the only effect that can be recognized, since at the end of the test the particles are not completely sink to the bottom of the cylinder. So, it is possible to suppose that the particles show a diffusive phenomenon as well. Moreover, most of the variations of the concentration profiles occurs initially: successively, the variations on the concentration are generally not relevant. Therefore, it is possible to split the segregation of the denser particles in two states: an initial transitory state and a successive steady state. In the first state, the concentration of the ceramic beads in the upper layers decreases rapidly, while the presence of the ceramic beams in the lower layers gradually increases. Secondly, in the last 3 hours 30 minutes of the test, the concentration of the particles on the layers does not vary anymore. The time when the system switches from one state to the other is identified by comparing the profiles of the concentration of particles along the height calculated over different intervals of time: when the profile is constant, the state of the particles is steady. Starting from this qualitative analysis of the concentration profiles, it is possible to describe the segregation phenomenon with a segregation model which considers the effect of percolation, which represents the sinking of the denser particles, and the effect of diffusion, which justifies the presence of particles in upper layers even at steady state.

$$\frac{\partial \phi}{\partial t} + \frac{\partial q(y)\phi(1-\phi)}{\partial y} = \frac{\partial D(y)\frac{\partial \phi}{\partial y}}{\partial y} \tag{6.2.1}$$

ϕ is the volumetric fraction of ceramic spheres over the glass beads while q and D quantifies the velocity of segregation and diffusion, respectively; y is the vertical coordinate. Both the segregation and diffusion coefficients are assumed to be dependent on the vertical coordinate, and consequently on the shear rate. The analysis is carried out on the stationary state of the segregation, so the variation in time of the terms is disregarded. Therefore, equation 6.2.1 becomes

$$\frac{\partial [q(y)\phi(1-\phi) - D(y)\frac{\partial \phi}{\partial y}]}{\partial y} = 0 \tag{6.2.2}$$

where

$$\begin{aligned} q(y) &= -C_q \dot{\gamma} d \\ D(y) &= C_d \dot{\gamma} d^2 \end{aligned} \tag{6.2.3}$$

The definition of the percolation coefficient q comes from the paper by May [10], whereas the diffusion coefficient D is taken from the Xiao's paper [20]. The shear rate $\dot{\gamma}$ is calculated as the ratio $\frac{dv}{dy}$, where v is defined as in chapter 5, so its equation is $\dot{\gamma} = \frac{V0}{\delta} e^{-\frac{y}{\delta}}$. C_q and C_d are two parameters that quantify the dependency between the shear rate and the coefficients of percolation and diffusion and they are related to difference of density between the two materials; d is the diameter of the spheres. Both the works assume that the parameters are constant along the height of the granular material. Defining some boundary conditions, it is possible to solve the derivative equation 6.2.1. Since the mass fraction of the ceramic spheres is low, (0.5%) it is possible to assume that the case is very diluted. Therefore, the approximation $q(y)\phi(1-\phi) = q(y)\phi$ is valid. Since the beads cannot go lower than the bottom surface (y=h) and higher than the top surface (y=0), the sum of the fluxes (segregation and diffusion) is 0 in the whole domain.

So, equation 6.2.2 becomes

$$q(y)\phi(y) - D(y)\frac{\partial \phi(y)}{\partial y} = k \tag{6.2.4}$$

and the value of that constant is 0, according to the boundary conditions. Then, isolating the derivative term it is possible to solve equation 6.2.4 and to work out an expression for the segregation term:

$$\phi = \phi_0 e^{-\frac{C_q}{C_f}\frac{y}{d}} \tag{6.2.5}$$

From equation 6.2.5, it is possible to notice that the profile of volumetric fraction over the height of the cylinder is exponential, and it agrees with the shape of the profile shown in Figure 6.2. Representing the results in a logarithmic scale, the ratio $\frac{C_q}{C_d}$ is the coefficient of the linear dependence between volumetric fraction and height. In Figure 6.2, it is possible to notice that the equation approximates the data significantly. In order to determine the two coefficients, successive tests and the solution of the model in the transient state are required. It is possible to notice that the effect of the shear rate is neglected, since the term is simplified in the ratio between the two coefficients.

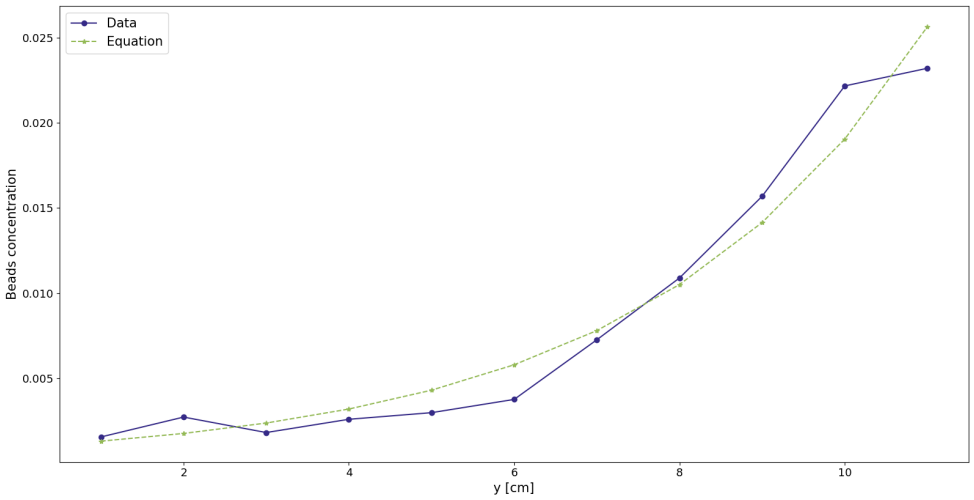

Figure 6.2: Concentration of ceramic beads at steady state

Small errors could potentially result from particles that are not at the wall but visible in gaps between particles at the wall and are therefore not well lighted.However, the misidentified particles are fewer than 5% of the total particles identified, and this error is minimized by spatial and temporal averaging, so it only causes slight fluctuation in the resulting velocity field, but not any systematic error.

Nevertheless, future tests will be needed to determine the parameters of the equation and to solve the model also in the transient unsteady part. In addition, it will be necessary to determine how the difference of density between the two kinds of spheres affect their segregation by using some sphere made of different materials. Other future perspectives will be the increase of the fraction of the ceramic beams, to determine the difference between the diluted cases and the concentrated cases. Anyway, it is possible to say that this experimental configuration is suitable to the analysis of the segregation phenomenon.

CHAPTER 7

Conclusions and Perspectives

The aim of this thesis is to explore the capabilities of the experimental apparatus used in this work on the study of the confined granular material flow. The most important topic is the experimental verification of the friction weakening. From the obtained results, it can be said that the assumption of the constant wall friction coefficient is not valid, both for horizontal and vertical cases. Nevertheless, the coefficient does not scale with the shear band width, so it is necessary to look for a different sliding parameter. Moreover, in the characterization of the rheology of the granular solid in this configuration, some interesting results were found. In fact, the effect of the rotational velocity of the bottom surface is negligible in the shallower cases of the granular beds, whereas for the thickest beds the width of the shear band is slightly smaller when the rotational velocity is higher. Concerning the effect of the load on the top surface, it is verified that, increasing the load, the width of the shear bands decreases notably. Regarding the effect of the height of the granular bed, it is noticed that it is similar to the effect of the load. In fact, increasing the height, the width of the shear bands decreases. Summing the effect of load and height, it is found that the effect of the load is dominant, therefore when the highest load is applied on the top surface the velocity profiles are similar even if the height changes, and so it is for the width of the shear bands. The roughness of the surfaces does not influence the

other effects when it is coupled with them, therefore all the previous considerations are verified. When the sole effect of roughness is tested, the smooth surface shows the smallest shear bands, whereas the difference between the rough surfaces is negligible. Finally, it is verified that this experimental apparatus could be used for the analysis of the segregation phenomenon. In fact, the proposed steady state model agrees with the experimental data. Nevertheless, it is needed to analyse the transient state to determine the values of the model parameters. At the same time, it will be possible to vary the operative conditions in order to determine their effect on the segregation and to test also the size-driven segregation. Further perspectives are the analysis of the flattening of the velocity profiles, since additional tests are necessary to determine the causes of this particular behaviour of the curves in their terminal section. The results about the friction weakening will be deepened, modifying the operative conditions in order to obtain a comprehensive model that explains the effect of the rheology on the wall friction and to eventually find a sliding parameter able to scale the coefficient.

Appendix A

```
import os, sys
from numpy import *
import openpiv.tools
import openpiv.process
import openpiv.scaling
import openpiv.validation
import openpiv.filters
from matplotlib.pyplot import *

def treatframes(im1,im2,dt,sc):
        ws=64
        ov=48
        frame_a = openpiv.tools.imread(im1).astype(int32)
        frame_b = openpiv.tools.imread(im2).astype(int32)

        u,v,sig2noise = openpiv.process.extended_search_area_piv
        (frame_a,frame_b,window_size=ws,overlap=ov,dt=dt,
        search_area_size = ws,sig2noise_method='peak2peak')

        x,y = openpiv.process.get_coordinates
        (image_size=frame_a.shape,window_size=ws,overlap=ov)
```

```
        u,v,mask = openpiv.validation.sig2noise_val
        (u,v,sig2noise,threshold=1.3)

        u,v = openpiv.filters.replace_outliers
        (u,v,method='localmean',max_iter=10,kernel_size=2)

        x,y,u,v = openpiv.scaling.uniform(x,y,u,v,scaling_factor= sc)
        return x,y,u,v

outf='testn2_1000'
scaling=10.25
card='test2/testn2_1000/testn2_1000'
dt=1./1000.
N=5000
sk=1
u0=0.
v0=0.
NN=0

for i in range(0,N,sk):
        im1=card+'\%04i.tif'\%(i+1)
        im2=card+'\%04i.tif'\%(i+1+sk)
        x,y,u,v = treatframes(im1,im2,dt*sk,scaling)
        u=u+u0
        v=v+v0
        u0=u
        v0=v
        NN+=1
        u=u/float(NN)
        v=v/float(NN)
```

```
openpiv.tools.save(x,y,u,v,outf+'.txt')
figure()
subplot(311),quiver(x,y,u,v)
subplot(312),plot(y,u,'+')
subplot(313),plot(y,v,'+')
show()
```

Bibliography

[1] R. Artoni and P. Richard. Effective wall friction in wall-bounded 3d dense granular flows. *Physical Review Letters*, 2015.

[2] R. Artoni and P. Richard. Torsional shear flow of granular materials : shear localization and minimum energy principle. *Computational Particle Mechanics*, 2016.

[3] R. Artoni and P. Richard. Shear localization and effective wall friction in a wall bounded granular flow. *EPJ Web of Conferences*, 2017.

[4] R. Artoni, A. C. Santomaso, M. Go', and P. Canu. Scaling laws for the slip velocity in dense granular flows. *Physical Review Letters*, 2012.

[5] B. Chakraboty and R. Behringer. Jamming of granular matter. *Encyclopedia of Complexity and System Science*, 2009.

[6] Y. Fan and K. Hill. Shear-induced segregation of particles by material density. *Physical Review*, 2015.

[7] S. Franklin and M. Shattuck. *Handbook of granular materials*. CRC Press, 2016.

[8] R. Holdich. *Fundamentals of Particle Technology.* Midland Information Technology and Publishing, 2002.

[9] J. Jenkins and M. Richman. Boundary conditions for plane flows of smooth, nearly elastic, circular disks. *Journal of Fluid Mechanics*, 1986.

[10] L. May, L. Golick, K. Phillips, M. Shearer, and K. Daniels. Shear-driven size segregation of granular materials: Modeling and experiment. *Physical Review*, 2010.

[11] G. MiDi. On dense granular flows. *The European Physical Journal E*, 2004.

[12] R. Nedderman. *Handbook of granular materials*. Cambridge University Press, 1992.

[13] A. Orlando and H. Shen. Effect of particle size and boundary conditions on the shear stress in an annular shear cell. *Granular Matter*, 2012.

[14] O. Poliquen and F. Chevoir. Dense flows of dry granular materials. *Comptes Rendus Physique*, 2002.

[15] M. Raffel, C. Willert, and J. Kompenhaus. *Particle image velocimetry. A practical guide*. Springer, 1998.

[16] M. Rhodes. *Introduction to particle technology*. Wiley and sons, 2008.

[17] P. Richard, A. Valance, J.-F. Metayer, D. Sanchez, J. Crassous, M. Louge, and R. Delannay. Rheology of confined granular flows: Scale invariance, glass transition, and friction weakening. *Physical Review Letters*, 2008.

[18] D. Schulze. *Flow Properties of Powders and Bulk Solid*. Springer, 2008.

[19] A. Tripathi and D. Khakhar. Density difference-driven segregation in a dense granular flow. *Journal of Fluid Mechanic*, 2013.

[20] H. Xiao, P. Umbanhowar, J. Ottino, and R. Lueptow. Modeling density segregation in flowing bidisperse granular materials. *Proceedings Royal Society*, 2016.

[21] S. Yang. Density effect on mixing and segregation processes in a vibrated granular mixture. *Powder Technology*, 2006.

Acknowledgements

Je tiens à remercier vivement toutes le personnel IFSTTAR - Site de Bouguenais de m'avoir accueilli durant ce stage. Je veux exprimer ma reconnaissance pour votre aide dans mon travail, ainsi que pour tout les activités ludique organisées et pour les délicieux plats de la cantine. En particulier, je remercie Madame Nicole Airieau pour sa gentillesse, sa cordialité et sa disponibilité; Monsieur Jean Marc Paul pour son travail patient et précis et pour ses solutions pratiques et Monsieur Patrick Richard pour ses sages conseils. Je remercie tout particuliérement Monsieur Riccardo Artoni pour tout le travail qu'il a fait avec moi, pour toutes les choses que il m'a appris, pour sa sympathie et son enthousiasme, pour avoir rendu possible cette expérience. Enfin, je veux exprimer ma reconnaissance à Monsieur Andrea Claudio Santomaso pour m'avoir proposé ce projet et pour son patient travail de supervision de mon project de fin d'études.